

Airplane Propeller Principles

By

WILBUR C. NELSON

Professor of Aeronautical Engineering
University of Michigan

NEW YORK

JOHN WILEY & SONS, INC.

CHAPMAN & HALL, LTD.

LONDON

COPYRIGHT, 1944
BY
WILBUR C. NELSON

All Rights Reserved

*This book or any part thereof must not
be reproduced in any form without
the written permission of the publisher.*

THIRD PRINTING, OCTOBER, 1948

PRINTED IN THE UNITED STATES OF AMERICA

PREFACE

A major contribution to the creation of high performance aircraft during the last decade has been the rapid advance in airplane propeller design. Propeller design is rather complex both because of the aerodynamic, mechanical, and structural considerations involved and because of the close relationship of the propeller to the performance of the engine and the complete airplane. It is therefore the purpose of this book to present an elementary treatment of these principles.

Since 1936 the author has been engaged in some phase of propeller work, and during the summer of 1941 it was his privilege to conduct an extensive series of lectures for a group of graduate engineers of the Aeroproducts Division of the General Motors Corporation, orienting them in the field of airplane propeller design. This material was subsequently used in mimeographed form for the course in airplane propellers at Iowa State College, and it is the basis of this publication.

Emphasis has been placed throughout upon the basic principles underlying the design and operation of the modern airplane propeller, rather than upon specific design data. The aerodynamic and structural analyses are developed sufficiently to prepare the capable student for additional specialization should the need arise. A liberal use of references should point the way to further exploration of the subject. An adequate background in elementary aerodynamics and structural analysis on the part of the reader is assumed, although the use of higher mathematics is limited to the graphical integration of certain integral relationships.

Grateful acknowledgment is made to the airplane propeller manufacturers, the Army Air Force, and the National Advisory Committee for Aeronautics for the release of illustrations and various technical data. The author's colleagues both at Iowa State College and in the propeller industry have given generously of their time in checking portions of the manuscript. Particular thanks are due to Professor Milton J. Thompson of the University of Texas for reviewing the entire manuscript, to Mr. Oliver P. Harwood for completing the original drawings, and to Mrs. Myra Thompson for typing the manuscript.

WILBUR C. NELSON.

*Ames, Iowa
November, 1943*

CONTENTS

CHAPTER	PAGE
1. PROPELLER BLADE ACTION THEORY	1
2. AERODYNAMIC PROPELLER TESTS.	18
3. BLADE DESIGN AND STRESS ANALYSIS	36
4. HUB DESIGN AND STRESS ANALYSIS	77
5. EFFECT OF THE PROPELLER ON AIRPLANE PERFORM- ANCE	97
APPENDIX	123
INDEX	127

CHAPTER 1

PROPELLER BLADE ACTION THEORY

Definition and Terminology

An airplane propeller may be defined as a device for producing thrust at all normal forward velocities of the airplane.¹ This definition emphasizes the prime output which is thrust. The propeller designer must create a safe mechanism which will produce a maximum of thrust under all conditions. The combination of airplane, engine, and propeller is interrelated so that the thrust must be evaluated with different combinations of engine rpm, engine torque, and airplane velocity. In conventional airplanes the propeller may be rightly termed an air screw since it rotates and advances through the atmosphere in much the same manner as a screw advancing in a solid medium. This type of propeller, it will be seen later, has definite limitations; a suitable propeller for the higher velocities and altitudes of the future might well be a jet-reaction device. In this text we shall concern ourselves primarily with the air-screw type on conventional aircraft.

It is necessary first to consider a system of classification and terminology. Airplane propellers may be divided into three major classifications:

a. Fixed pitch. Those in which the construction is essentially one piece and in which the pitch (or blade angle) cannot be changed after the propeller is built.

b. Adjustable pitch. Those in which the blades may be loosened in the hub and adjusted to the desired pitch on the ground, after which the blades are again clamped securely to the hub.

c. Controllable pitch. Those in which the blade pitch is controlled manually or automatically during flight.

A typical adjustable-pitch propeller is shown in Fig. 1-1 with the various portions titled. In a fixed-pitch wood propeller the central portion is termed the hub boss and has a steel hub bolted to it. A controllable-pitch design would allow the blades to rotate in the hub sockets through some mechanical control.

¹ By normal velocities is meant the range from zero to maximum velocity in level flight.

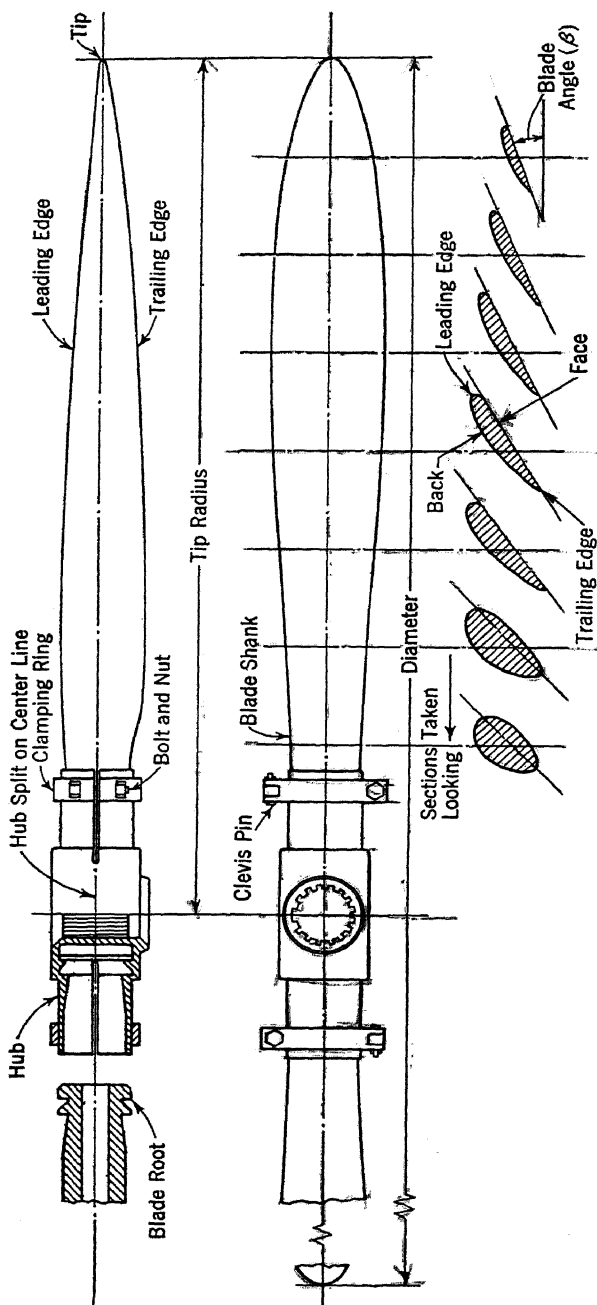


Fig. 1-1. Adjustable-pitch propeller.

Geometric pitch is the advance per revolution of a propeller blade element moving along a helix whose angle equals the propeller blade angle.

Effective pitch is the distance the airplane advances along its flight path for one revolution of the propeller.

$$p = \pi d \tan \beta \quad [1]$$

where p = the geometric pitch in feet.

d = the diameter in feet at the reference element (usually three-quarter radius).

β = the blade angle at the reference element.

It will also be seen from Fig. 1·2 that

$$p_e = \pi d \tan \phi \quad [2]$$

where p_e = the effective pitch in feet.

$\tan \phi$ = advance per revolution divided by πd .

The difference between geometric and effective pitch is termed slip and will, of course, vary with the forward velocity of the airplane.

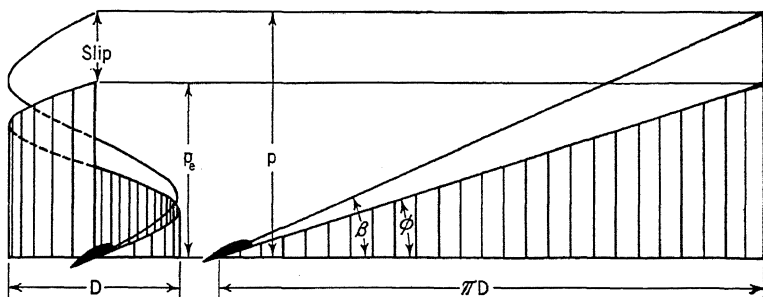


FIG. 1·2. Geometric pitch and effective pitch relationships.

Propeller blade settings are usually designated in the United States by giving the blade angle at the three-quarter radius, instead of calculating the geometric pitch. The term increase pitch or decrease pitch is commonly used, however, instead of increase or decrease blade angle. A complete collection of propeller terminology is included in the Appendix.

Momentum Theory

Many theories of propeller blade action have been advanced and applied of which one of the simplest in its concepts and most useful

qualitatively is the momentum theory.² In this theory the propeller is treated as a disk producing a uniformly distributed thrust created by a pressure differential between the front and back of the disk. A stream tube encloses the affected streamlines which are considered continuous through the disk. Air is assumed a perfect fluid with no viscosity or compressibility effects.

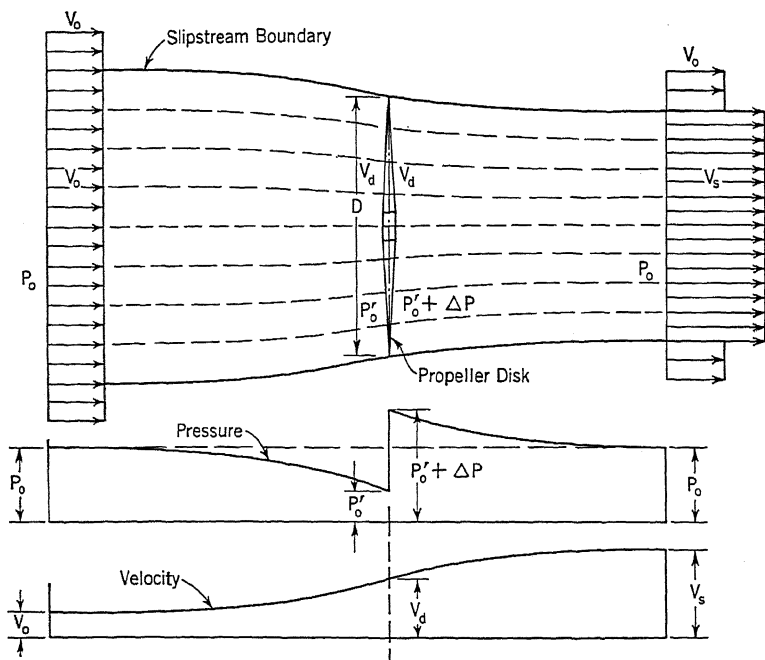


FIG. 1-3. Momentum theory relationships.

The general relationships³ are presented in Fig. 1-3. The unaffected air has the velocity V_0 and pressure p_0 . The velocity increases to V_d at the disk and reaches a final value of V_s in the slipstream. The pressure drops to p'_0 in front of the disk, receives an increment Δp at the disk, and finally returns to its original value p_0 in the slipstream.

² W. J. M. Rankine, "On the Mechanical Principles of the Action of Propellers," *Trans. Inst. Naval Architects* (1865), p. 13.

R. E. Froude, "On the Part Played in Propulsion by Differences of Fluid Pressure," *Trans. Inst. Naval Architects* (1889), p. 390.

³ The propeller disk is considered stationary in a moving body of air. This is the opposite of actual conditions, but for analytical purposes the relative motion is the same.

The thrust T may be evaluated by equating it to the increased axial momentum per unit time.

$T = \text{mass per unit time through the disk} \times \text{velocity increase}$

$$T = A\rho V_d(V_s - V_0) \quad [3]$$

where A is the disk area and equals $\pi D^2/4$.

ρ is the mass density of air.

The thrust may also be expressed as $A\Delta p$ where Δp is the difference in total pressure head along the stream tube between the back and front of the disk.⁴

$\Delta p = \text{final pressure head} - \text{initial pressure head}$

$$\Delta p = [p_0 + \frac{1}{2}\rho V_s^2] - [p_0 + \frac{1}{2}\rho V_0^2]$$

$$\Delta p = \frac{1}{2}\rho(V_s^2 - V_0^2) \quad [4]$$

then

$$T = \frac{A\rho}{2}(V_s^2 - V_0^2) \quad [5]$$

A comparison of equations 3 and 5 for thrust will show that

$$V_d = \frac{V_s + V_0}{2}$$

and therefore half of the final slipstream velocity increment is imparted before the propeller disk.

An evaluation of the ideal efficiency η is also interesting.

$$\eta = \frac{\text{Output}}{\text{Input}} = \frac{\text{Thrust} \times \text{Velocity}}{\text{Total work done}}$$

The total work done by the propeller equals the kinetic energy increase in the flow.

$$\text{K.E. increase} = (\frac{1}{2}A\rho V_d)(V_s^2 - V_0^2)$$

Then

$$\begin{aligned} \eta &= \frac{TV_0}{\frac{1}{4}A\rho(V_s + V_0)(V_s^2 - V_0^2)} \\ &= \frac{A\rho(V_s^2 - V_0^2) \cdot 2V_0}{A\rho(V_s + V_0)(V_s^2 - V_0^2)} \\ &= \frac{2V_0}{V_s + V_0} \end{aligned}$$

⁴By Bernoulli's theorem the total energy $p_0 + (\rho V_0^2/2)$ is a constant along a given stream line. This equation cannot be applied across the disk, however, because energy is added at that point.

or finally

$$= \frac{2}{1 + V_s/V_0} \quad [6]$$

The final value for efficiency given by equation 6 may then be combined with the preceding expression 5 for thrust, resulting in the following relationship when V_s is eliminated.

$$\frac{T}{2\rho V_0^2 A} = \frac{1 - \eta}{\eta^2}$$

Figure 1-4 is a plot of the ideal and actual efficiency versus the dimensionless ratio of $T/(\frac{1}{2}\rho V_0^2 A)$. In a qualitative sense the ideal efficiency curve tells us that we may expect:

- A drop in efficiency with an increase in thrust.
- A drop in efficiency with a decrease in forward velocity.
- A drop in efficiency with a decrease in propeller disk area.

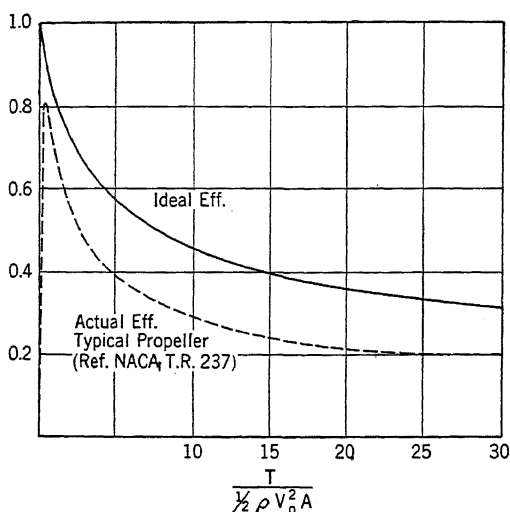


FIG. 1-4. Actual and ideal efficiency variation.

From a design viewpoint the efficiency losses of the last item which would be found in a small-diameter, high slipstream-velocity propeller are to be avoided whenever possible. Test data as given by the actual efficiency curve bear out the trends indicated up to the velocity for maximum efficiency. However, the momentum theory neglects several important items that limit its application: aerodynamic drag of the blades, energy loss in the slipstream rotation, compressibility losses, blade interference, and losses from the periodic thrust variation due to a finite

PROPELLER BLADE ACTION THEORY

number of blades. These losses mean that power is still required to rotate the propeller even at zero thrust, and hence the actual efficiency curve drops to zero as the ideal efficiency approaches unity. It should also be noted that it is impossible to introduce propeller or engine torque into this analysis.

Airfoil Theory and Test Data

In order to overcome some of the preceding disadvantages it is necessary to turn to the blade element theory,⁵ which considers the propeller blade as a rotating wing and sums up the forces acting upon each individual blade section to obtain the resultant thrust and torque per blade for a given operating condition. A working knowledge of both airfoil theory and test data is essential in order to apply this analysis. Several excellent books have been published treating airfoil theory and discussing available test data⁶ so that no attempt will be made to present more than a brief summary of typical test results and the main variables involved.

Figure 1.5 gives the results of a Clark-Y airfoil test conducted by the NACA. The absolute system of coefficients is used as defined by the following equations in which L is the lift in pounds, D is the drag in pounds, S denotes wing area in square feet, V is the velocity in feet per second, ρ is air density in mass units and equals 0.002378 slugs/ft³ at sea level standard conditions, and $q = \rho V^2/2$ the impact pressure in pounds per square foot.

$$L = \frac{C_L S \rho V^2}{2} = C_L S q \quad [7]$$

$$D = \frac{C_D S \rho V^2}{2} = C_D S q \quad [8]$$

C.P. = Center of pressure of resultant force on airfoil in per cent chord from the leading edge

A complete dimensional analysis⁷ yields the following equation for the dynamic reaction of a viscous and compressible fluid upon a body.

$$R = S V^2 \rho f_1 \left(\frac{VL}{\nu} \right) f_2 \left(\frac{V}{c} \right) f_3 \left(\frac{Lg}{V^2} \right) \quad [9]$$

⁵ William Froude, "The Elementary Relation between Pitch, Slip, and Propulsive Efficiency," *Trans. Inst. Naval Architects* (1878). Also independently developed by Drzewiecki in 1885 and finally summarized as "Théorie Générale de l'Helice Propulsive," Gauthier-Villars of Paris (1920).

⁶ Clark B. Millikan, "Aerodynamics of the Airplane," John Wiley & Sons (1941).

E. P. Warner, "Airplane Design," McGraw-Hill (1936).

⁷ Cowley and Levy, "Aeronautics in Theory and Experiment," Longmans, Green and Co. (1918), Chapter IV.

In this expression L is a representative linear dimension, ν is the kinematic coefficient of viscosity for the fluid, g is the acceleration due to gravity, and c is the velocity of sound or rate of travel of a pressure wave in the fluid. The first factor is the Reynolds number and necessi-

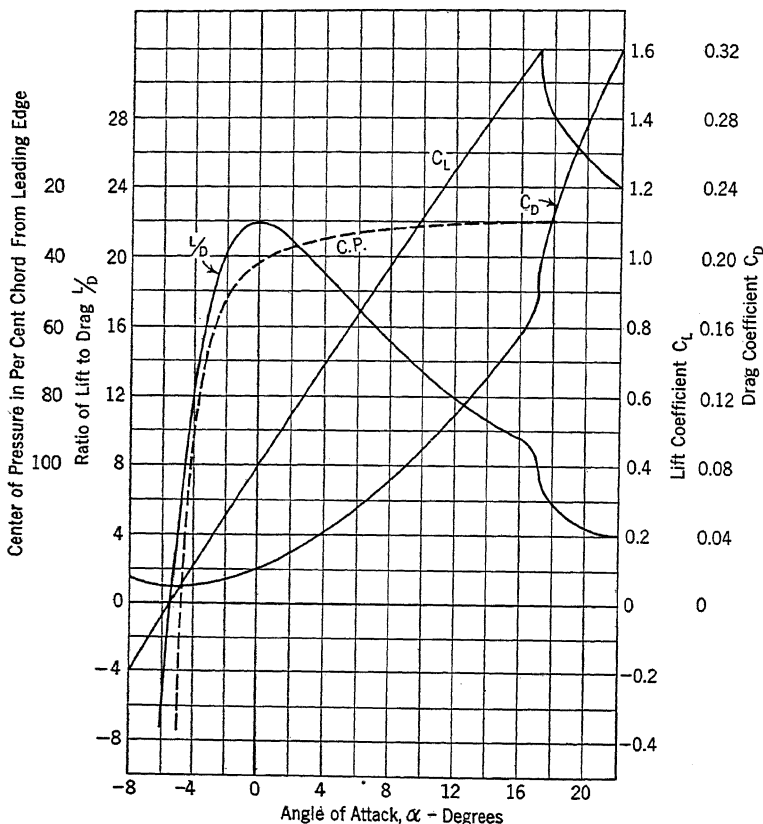


Fig. 1-5. Clark-Y airfoil test data: aspect ratio 6; Reynolds number 6,000,000. (NACA Tech. Rept. 502.)

tates corrections which must be applied to model test data to adapt it to actual full-scale conditions. The second factor is Mach's number and represents the compressibility effect created as the flow velocity approaches the velocity of sound. Both of the above factors are very important for high-velocity airplanes and high propeller tip speeds and they will be discussed under propeller tests. The reciprocal of the third item is commonly known as Froude's number. It is important chiefly in marine work and can be considered constant for air. For a specific test condition it is therefore possible to express the reaction as a test

coefficient multiplied by $S\rho V^2/2$, keeping in mind the effect of Reynolds number and Mach's number.

Another important variable in airfoil test data is the wing planform. Its effect may be evaluated by means of the Lanchester-Prandtl wing theory which expresses the induced drag and the related downwash angle in terms of C_L and the aspect ratio \mathcal{R} ⁸ as follows.

$$C_{Di} = \frac{C_L^2}{\pi \mathcal{R}} \quad [10]$$

$$\alpha_i = \frac{\gamma}{\pi \mathcal{R}} \text{ (in radian measure)} \quad [11]$$

The aspect ratio then reflects changes in planform, and by means of these formulas airfoil data may be corrected for such changes with excellent results.⁹

Variations in thickness or camber of the airfoil require separate tests to isolate their effect. Figures 1-6 and 1-7 are NACA wind tunnel test results on a series of RAF-6 airfoils in which the thickness and camber were varied.¹⁰ The RAF-6 and Clark Y are the most commonly used propeller airfoil sections and will be discussed under blade design.

Simple Blade Element Theory

In the blade element theory, the propeller blade is considered as a rotating airfoil, with each element following a helical path and reacting as an ordinary airfoil section. The airflow is treated as two-dimensional with no mutual interaction between blade sections and no radial flow due to slipstream contraction.

Consider an element dr as given in Fig. 1-8. It is located a distance r from the center of rotation. Its rotational velocity will be $2\pi nr$ and when combined with the forward velocity V , the section will be operating with a resultant velocity V_R at an angle of attack, α . The lift acting upon the element may be expressed as

$$dL = C_L \cdot \frac{1}{2}\rho V_R^2 \cdot dA = C_L \cdot \frac{1}{2}\rho V_R^2 \cdot b \, dr$$

Introducing the angle γ where $\tan \gamma = D/L$, the corresponding resultant force on the airfoil section is

$$dR = \frac{dL}{\cos \gamma} = \frac{\frac{1}{2}\rho V_R^2 \cdot b \, dr \cdot C_L}{\cos \gamma}$$

⁸ \mathcal{R} = span²/wing area.

⁹ L. Prandtl, "Applications of Modern Hydrodynamics to Aeronautics," *NACA Tech. Rept. 116* (1921).

¹⁰ E. N. Jacobs, "Characteristics of Propeller Sections Tested in the Variable Density Wind Tunnel," *NACA Tech. Rept. 259* (1927).

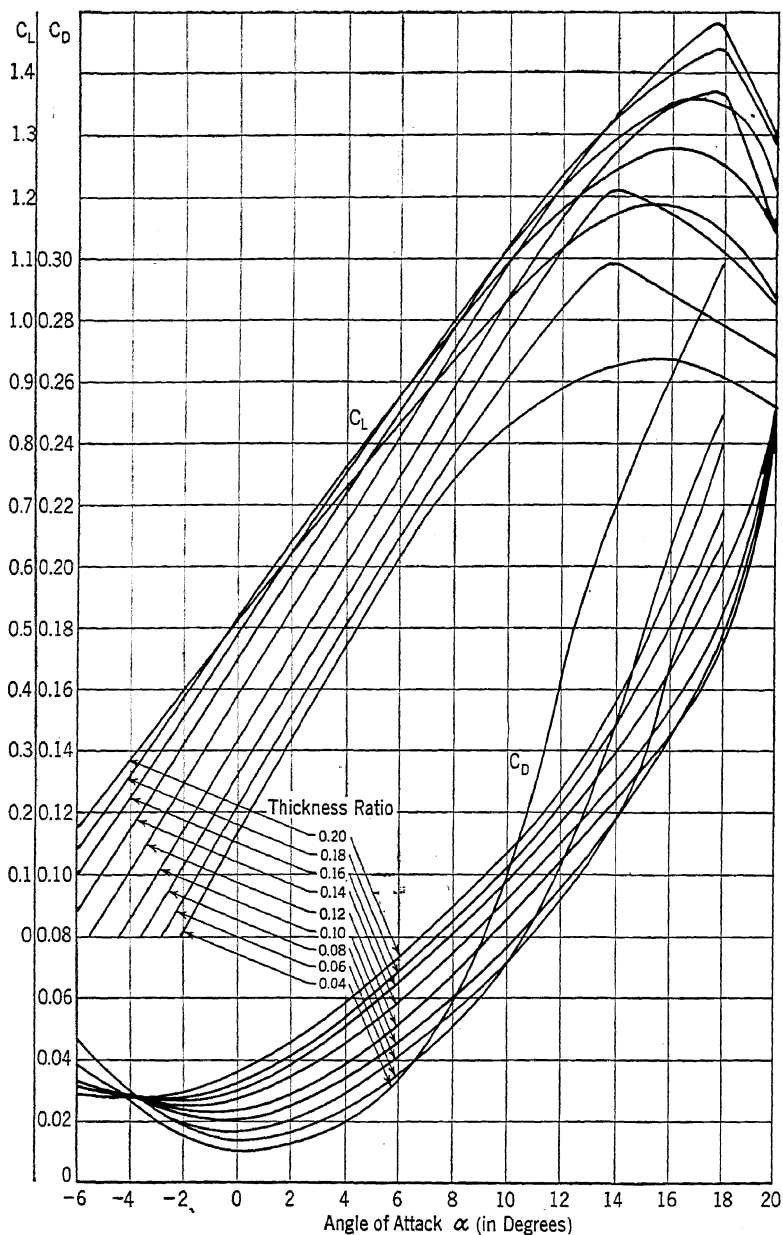


FIG. 1-6. RAF-6 propeller section aerodynamic data for aspect ratio 6.

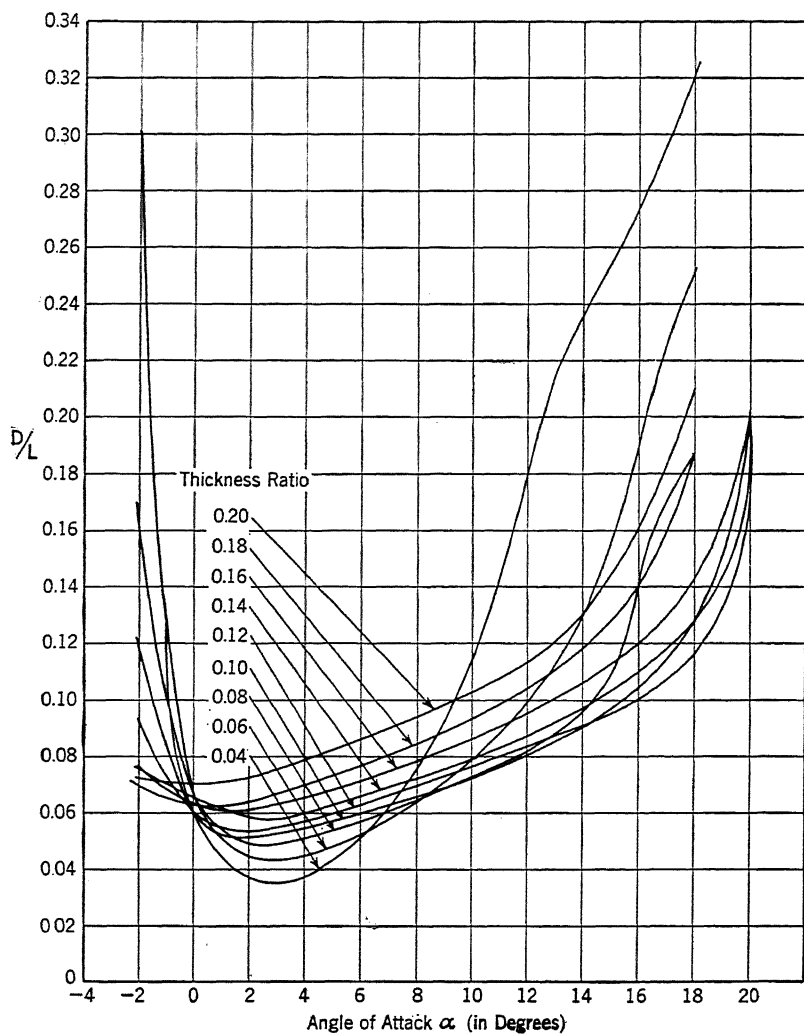


FIG. 1-7. RAF-6 propeller section aerodynamic data for aspect ratio 6.

The thrust component dT may be calculated as a component of dR .

$$dT = dR \cdot \cos(\phi + \gamma)$$

$$dT = \frac{1}{2}\rho V_R^2 \cdot b \, dr \cdot C_L \left[\frac{\cos(\phi + \gamma)}{\cos \gamma} \right]$$

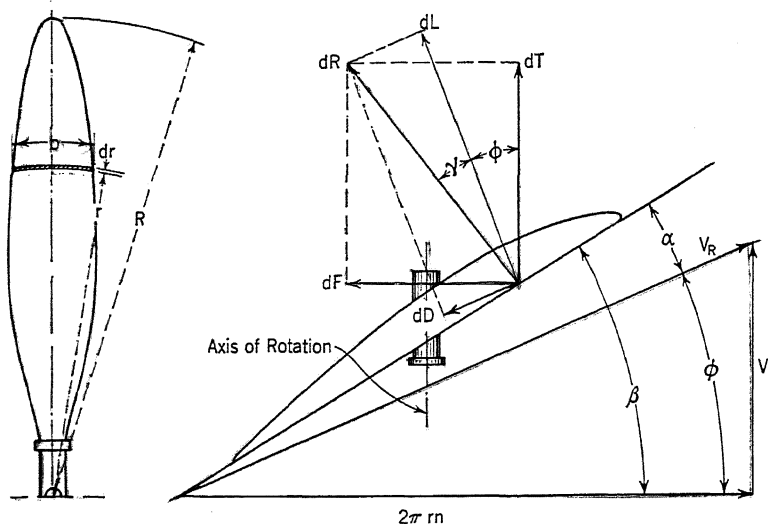


FIG. 1-8. Blade element theory relationships.

By substituting $V_R = V/\sin \phi$,

$$dT = \frac{1}{2}\rho V^2 \cdot b \, dr \cdot C_L \left[\frac{\cos(\phi + \gamma)}{\sin^2 \phi \cos \gamma} \right] \quad [12]$$

The above expression will give the thrust loading in pounds per unit length and may be plotted versus radius and integrated to give the total thrust per blade. Similarly, the torque component is

$$\begin{aligned} dQ &= r \cdot dF \\ &= \frac{1}{2}\rho V^2 \cdot b r \, dr \cdot C_L \left[\frac{\sin(\phi + \gamma)}{\cos \gamma \sin^2 \phi} \right] \end{aligned} \quad [13]$$

Once the total thrust T and total torque Q are determined, the brake horsepower required to rotate the propeller and the efficiency η under the given design condition may be calculated.

$$\eta = \frac{\text{Output}}{\text{Input}} = \frac{TV}{2\pi nQ}$$

It is interesting to analyze the efficiency of a specific blade element on the basis of the above theory. If the element is taken at the three-quarter radius, it will be representative of the entire blade action.

$$\begin{aligned}\eta &= \frac{\text{Power output}}{\text{Power input}} = \frac{dT \cdot V}{dQ \cdot 2\pi n} \\ &= \frac{dR \cos(\phi + \gamma) \cdot V}{dR \sin(\phi + \gamma) \cdot 2\pi n r} \\ &\quad \frac{\tan \phi}{\tan(\phi + \gamma)}\end{aligned}\quad [14]$$

The efficiency of an element is therefore dependent only upon the angles ϕ and γ . If the above expression is differentiated with respect to ϕ and equated to zero in order to find the value of ϕ corresponding to maximum efficiency, the angle ϕ is found to be $45^\circ - (\gamma/2)$. The efficiency η as determined by equation 14 is plotted versus ϕ in Fig. 1-9

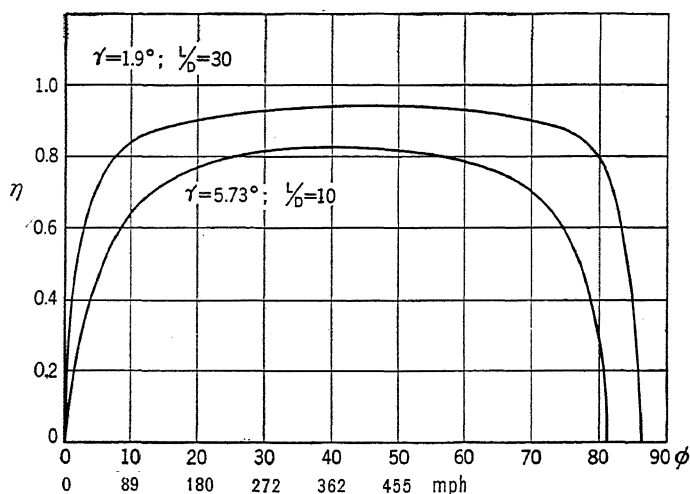


FIG. 1-9. Simple blade element efficiency variation.

for two extreme values of γ . The angle ϕ is also converted to forward velocity, assuming a limiting rotational tip speed of 1000 fps and basing the efficiency upon the three-quarter radius blade element, i.e., $\tan \phi = V/0.75\sqrt{10^6 - V^2}$.

The higher efficiency of thin sections with a high L/D as compared with thick sections with a low L/D is evident over the entire range. It will be noted that the low drag sections have a comparatively greater advantage at the slower velocities of climb. The angle ϕ is

approximately equal to β for the design condition so that the abscissa may also be regarded as the reference blade angle β . NACA tests have shown that the efficiency of a typical propeller blade does approach a maximum near a 35° blade angle at the three-quarter radius.¹¹

A solution for thrust and torque under a given set of design conditions may be readily accomplished. Figure 1-10 is a typical adjustable-pitch aluminum-alloy blade drawing. Let us take this blade and analyze it for the condition of 100 mph forward velocity and 2000 rpm as a two-bladed propeller. The following table lists the essential steps for such a calculation.

SIMPLE BLADE ELEMENT ANALYSIS OF PROPELLER BLADE OF FIG. 1-10

100 mph Velocity 2000 rpm Crankshaft Rotation

Station	18 in.	24 in.	30 in.	36 in.	42 in.	Ref.
1 r/R	0.375	0.50	0.625	0.75	0.875	Fig. 1-10
2 r (ft)	1.5	2.0	2.5	3.0	3.5	"
3 b (ft)	0.572	0.607	0.588	0.529	0.422	"
4 h/b	0.173	0.123	0.103	0.091	0.087	"
5 β	38.1°	31.65°	26.3°	22.4°	19.5°	"
6 $2\pi rn$ (ft/sec)	314	418	523	627	732	
7 $\tan \phi = V/2\pi rn$	0.467	0.352	0.281	0.234	0.201	
8 ϕ	25.03°	19.4°	15.7°	13.18°	11.36°	
9 $\alpha = \beta - \phi$	13.06°	12.35°	10.64°	9.22°	8.14°	
10 γ	6.05°	4.85°	4.25°	4.0°	3.75°	Fig. 1-7
11 $\cos \gamma$	0.994	0.996	0.997	0.997	0.997	
12 C_L	1.23	1.24	1.05	0.95	0.87	Fig. 1-6
13 $\sin \phi$	0.425	0.332	0.270	0.228	0.197	
14 $\phi + \gamma$	31.08°	24.15°	19.95°	17.18°	15.11°	
15 $\cos (\phi + \gamma)$	0.857	0.912	0.939	0.955	0.965	
16 dT/dr (lb/ft)	86.3	160	211	236	234	Eq. 12
17 $\sin (\phi + \gamma)$	0.516	0.409	0.341	0.295	0.260	
18 dQ/dr (ft-lb/ft)	78.0	144	191	219	221	Eq. 13

Once calculated, the thrust and torque loadings may be plotted versus radius as in Fig. 1-11 and integrated graphically to give the total thrust and torque on the blade. In the present instance this results in a thrust of 1040 lb and a torque of 918 ft-lb for the complete propeller.¹²

¹¹ Theodorsen, Stickley, and Brevoort, "Characteristics of Six Propellers Including the High Speed Range," *NACA Tech. Rept. 594* (1937).

¹² An alternate method of solution consists of plotting the elementary lift and drag vectors to scale at their respective stations and resolving the thrust and torque components graphically.

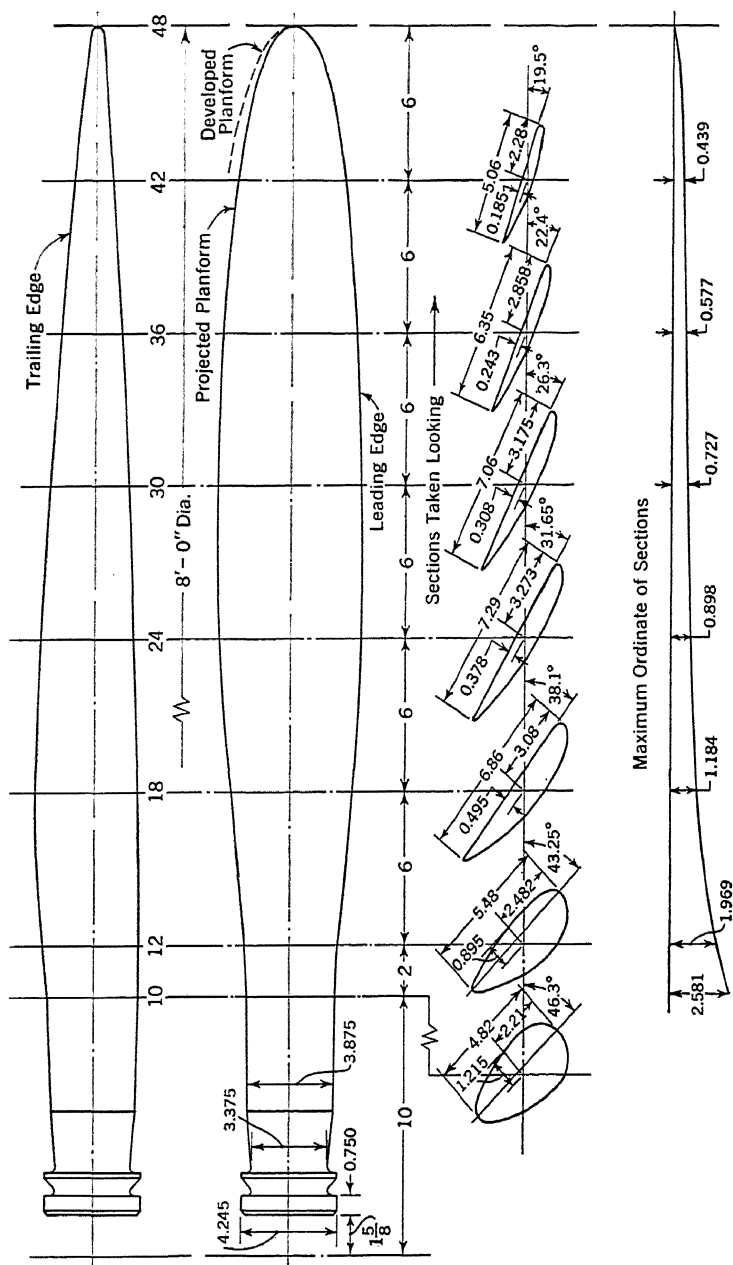


Fig. 1-10. Adjustable-pitch, solid aluminum-alloy propeller blade drawing.

The hub drag tends to drop the thrust loading curve to slight negative values at the hub and to maintain the torque loading at small positive values, but the effect is secondary in this type of analysis.

Results obtained by this method of calculation must be used with discretion due to the many variables involved.¹³ Modified empirically by a seasoned designer, the simple blade element theory is a decidedly useful tool. Above all, it presents a clear picture of the fundamental

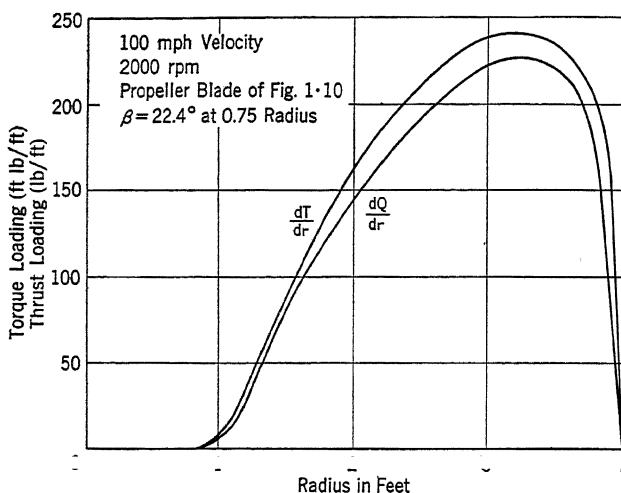


FIG. 1-11. Thrust and torque loading.

blade action and forms a basis of explanation for most problems in propeller performance.

The inaccuracies of the calculations are closely related to the original assumptions previously stated. When wind tunnel airfoil test data are used, the effect of blade interference, radial inflow at the blade tip, and tip losses are neglected. A closer approximation would be obtained by using airfoil characteristics as actually measured on a rotating propeller.

Many modifications of the simple blade element theory have been devised to correct for some of the preceding factors. The combined momentum and blade element theory adds an empirical increment to the forward velocity at the blade element to account for the increase in velocity in front of the propeller disk discussed under the momentum theory. A multiplane interference correction may be obtained by using wind tunnel test data on a cascade series of airfoils, resulting in a modified lift coefficient and angle of attack. An additional refinement using

¹³ W. F. Durand and E. P. Lesley, "Comparison of Model Propeller Tests with Airfoil Theory," *NACA Tech. Rept. 196* (1924).

the multiplane interference correction applied to airfoil characteristics calculated from actual propeller tests has been developed by F. E. Weick. The vortex theory of propeller analysis by H. Glauert applies the principles of airfoil theory to the simple blade element analysis, and corrections are made to the flow past the blade element for both rotational and axial interference. All these methods have been extensively developed with varied results.¹⁴

PROBLEMS

1. If the blade angle β at the three-quarter radius of a 12-ft diameter propeller is 45° , what is the slip at 1850 rpm and a forward velocity of 100 mph? 200 mph? 300 mph? (Note: $\tan \phi = V/2\pi rn = p_c/2\pi r$.)

2. The thrust of a propeller 10 ft in diameter is 300 lb when the airplane velocity is 100 mph at sea level. Assuming that the thrust is due entirely to the change in momentum per unit time of the propeller stream tube, find the slipstream velocity V_s and calculate the ideal efficiency.

3. If the propeller diameter of problem 2 were reduced to 9 ft, what would be the new slipstream velocity and ideal efficiency?

4. Develop the expression for dQ , the elemental torque component of the simple blade element theory.

5. Prove that the maximum efficiency of a blade element in the simple blade element theory occurs at a value of $\phi = 45^\circ - (\gamma/2)$.

6. Compute the thrust and torque of the propeller in Fig. 1-10 by means of the simple blade element theory at a forward velocity of 150 mph and 2000 rpm. Check the result using Fig. 2-3.

¹⁴ Fred E. Weick, "Airplane Propeller Design," McGraw-Hill (1930), pp. 51-81.

H. Glauert, "Aerodynamic Theory: Vol. IV, Airplane Propellers," Julius Springer (1935).

For an extensive bibliography on propeller theory and design refer to the *Journal of the Aeronautical Sciences*, "Aeronautical Review Section," Vol. 8, No. 12 (October, 1941).

CHAPTER 2

AERODYNAMIC PROPELLER TESTS

Wind Tunnel Testing

In order to supplement lengthy theoretical calculations of the type discussed in the preceding chapter and to determine as precisely as possible the performance of a particular design, many series of propeller tests have been conducted in research wind tunnels equipped for this purpose both in the United States and abroad.

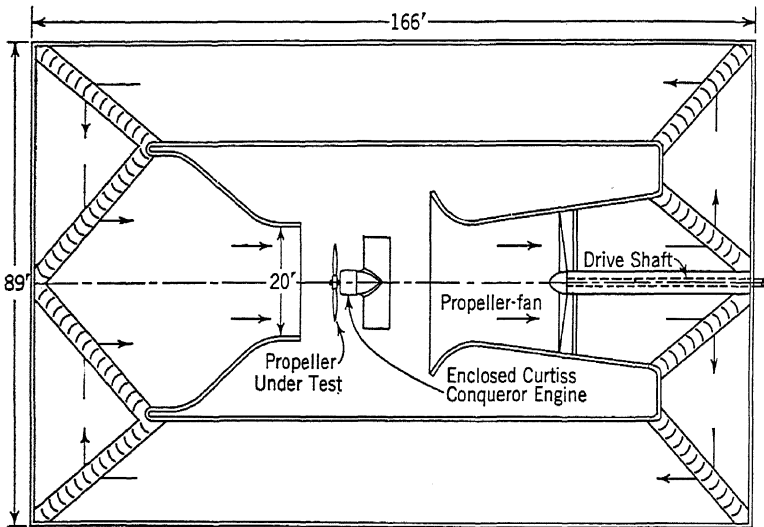


FIG. 2-1. Planform of NACA 20-ft propeller research tunnel.

The NACA Langley Field full-scale propeller research wind tunnel has been the source of much test data. It is an open-jet, double-return type with a 20-ft diameter air stream at the test section. A 28-ft diameter propeller fan driven by an 1800-horsepower electric motor creates wind velocities up to 115 mph at the test section. The plan view is given in Fig. 2-1.¹

Propeller-nacelle combinations are mounted on the balance platform, and the thrust and torque reactions are measured at various air speeds for a given propeller rpm. Figure 2-2 shows a typical installation. The

¹ F. E. Weick and D. H. Wood, "The Twenty-Foot Propeller Research Tunnel of the NACA," *NACA Tech. Rept. 300* (1928).

propeller is driven by a Curtiss Conqueror liquid-cooled aviation engine which is mounted in a cradle-type torque dynamometer and enclosed in the nacelle.

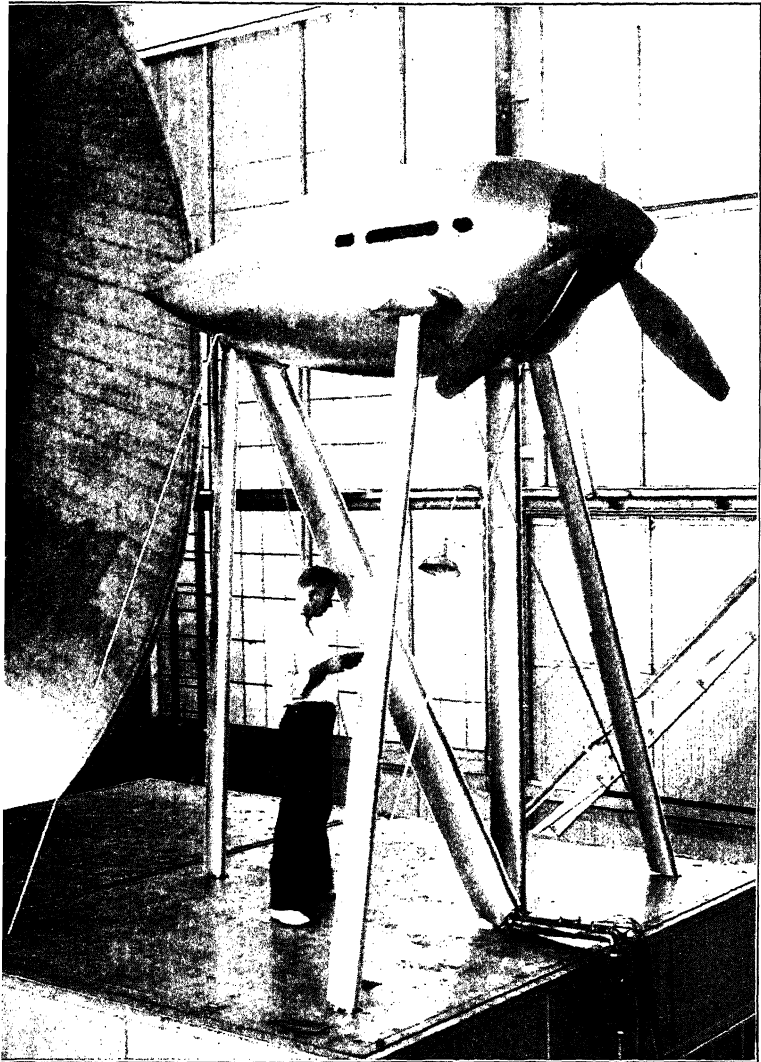


FIG. 2-2. NACA propeller research tunnel test installation. (*Official photograph, National Advisory Committee for Aeronautics.*)

Practically any wind tunnel may be used for propeller testing, provided it is equipped with the necessary apparatus in the test section to

rotate the propeller and measure the thrust, rpm, and torque. In the United States, Stanford University and the California Institute of Technology have conducted extensive propeller investigations in their research wind tunnels. Great Britain has several propeller research tunnels at the National Physical Laboratory, and research is also carried out at the various centers of continental Europe.

Flight Testing

Flight testing a propeller holds forth definite advantages in that the propulsive unit is tested under actual operating conditions, and corrections are minimized. Unfortunately, an accurate means of measuring all the necessary quantities during flight has yet to be placed in general use. Torque meters actuated by the torque reaction on the sun gear in an engine gear reduction unit or by the torque reaction on the propeller hub have been designed and tested with good results.² However, an accurate means of measuring the propeller thrust is not yet available. The most promising method appears to be the use of a hydraulic diaphragm backing the engine thrust bearing. When these two instruments become available for flight test measurements, an entire new field of valuable data should be forthcoming.

It is possible to calculate propeller thrust from the measured airplane velocity and rates of climb at various power outputs. Essentially this means equating the power available from the propeller to the power required by the airplane in level flight and climbing attitudes. The drag of the airplane must be calculated from wind tunnel tests or from actual glide tests on the airplane, and the accuracy of both methods is open to question because of the many variables. This type of calculation is exceedingly difficult and cannot be relied upon to isolate the effect of minor design changes on the propeller. It is therefore necessary to rely mainly upon the results of propeller wind tunnel testing for the prediction of propeller performance.

Performance Curves

In systematizing the results of any test program, the first question arising is that of test coefficients. Reference to the simple blade element vector relationships of Fig. 1-8 will show that the dimensionless parameter V/nD for a given blade angle β is analogous to the angle of attack α in airfoil tests. It is therefore customary to plot thrust and torque ver-

² O. W. Schey, "Measurement of Engine Power in Flight," *Journal of the Aeronautical Sciences*, Vol. 5, No. 9 (July, 1938), p. 364.

McClain, Lewis, and Buck, "Flight Testing With An Engine Torque Indicator," *SAE Journal* (February, 1938).

sus V/nD for a given setting, where the pitch setting is usually expressed as the blade angle β at the three-quarter radius. V/nD is frequently denoted by the symbol J .

When the blade element analysis of Chapter 1 is carried out for a series of forward velocities at a constant rpm, the resulting performance

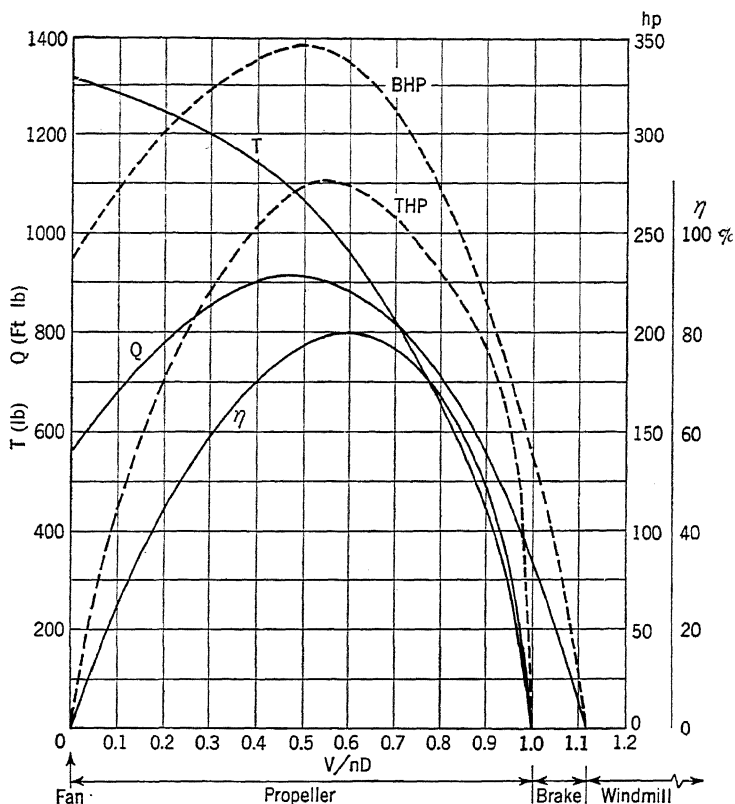


FIG. 2-3. Performance curves: 2000 rpm crankshaft rotation; blade angle 22.4° at 0.75 radius (for propeller of Fig. 1-10); simple blade element calculations.

curves may be plotted as shown in Fig. 2-3 with either velocity or V/nD as the abscissa. Similar results would also be obtained from wind tunnel tests in which the thrust and torque were measured at various wind velocities, maintaining the propeller rpm constant.

The efficiency η which is evaluated as $TV/2\pi nQ$ becomes a derived curve passing through zero at zero forward velocity (fan state) and then again at some higher value of velocity corresponding to zero thrust and dependent primarily upon the blade angle. The latter condition can be

readily visualized by reference to the blade element vectors of Fig. 2-4. At some velocity above zero the resultant airfoil force on the entire blade at a fixed pitch must pass through a zero thrust component point because the angle of attack becomes negative at higher values of V/nD . As some profile drag always remains at zero lift, the zero torque condition will then occur at some higher value of V/nD when the resultant force on the airfoil has become negative. At a still higher value of V/nD ,

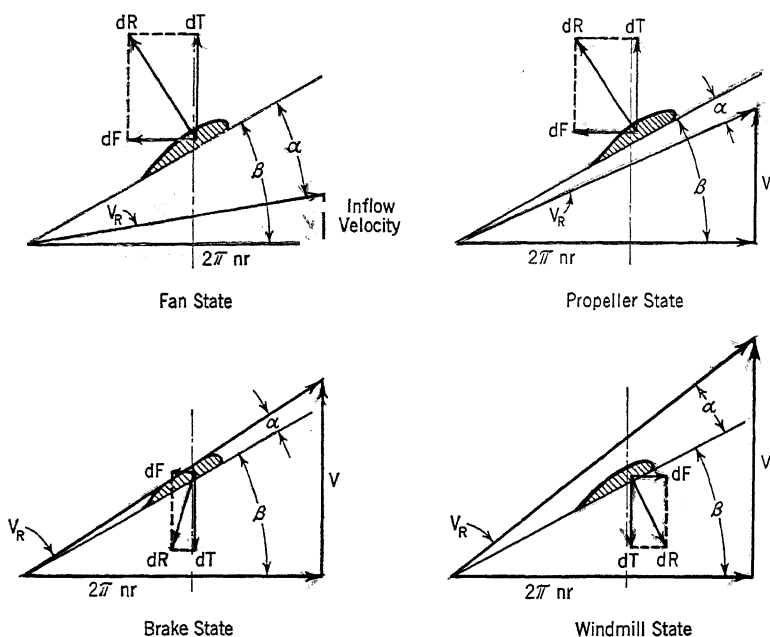


FIG. 2-4. Blade element relationships under various operating conditions.

the thrust and torque are both negative, and the propeller is rotated by the resultant aerodynamic force resulting in the windmill state. The propeller range exists throughout the region of positive thrust. An intermediate condition between the propeller range and windmill range is the brake state, where the propeller actually furnishes additional drag to the airplane. The thrust horsepower and brake horsepower are also derived curves passing through zero at the respective zero values of velocity, thrust, and torque.

$$\text{Thrust horsepower} = \frac{TV}{550}$$

$$\text{Brake horsepower} = \frac{2\pi nQ}{550}$$

[1]

With an increasing V/nD ratio the propeller is therefore operating successively in the fan, propeller, brake, and windmill regimes. The vector relationships for a typical blade element under these various conditions are given in Fig. 2-4. Note that the inflow velocity $(V_s - V_0)/2$ discussed under the momentum theory does create a certain flow past the propeller even though the forward velocity is zero. This inflow velocity becomes proportionately smaller as the forward velocity of the airplane increases and is neglected in the simple blade element analysis of Fig. 2-3.

The majority of propeller operations are, of course, conducted in the true propeller state. Static thrust which occurs at the fan state is an important factor in the evaluation of airplane takeoff ability. Braking and windmilling action can readily be encountered in an airplane dive and windmilling may become a dangerous engine overspeed condition if not carefully controlled. These factors will be discussed further in Chapters 4 and 5.

Thrust, Torque, and Power Coefficients

In order to apply the results of Fig. 2-3 to geometrically similar propellers with different engine installations, it is necessary to reduce the thrust and torque to some form of coefficient.³ Examining the simple blade element expression for thrust

$$dT = \frac{1}{2}\rho V^2 \cdot b \, dr \cdot C_L \left[\frac{\cos(\phi + \gamma)}{\sin^2 \phi \cos \gamma} \right]$$

it will be seen that

$$T = \text{Constant} \cdot \rho V^2 D^2 = T_c \cdot \rho V^2 D^2 \quad [2]$$

for a given V/nD ratio, since both b and r vary directly with diameter for geometrically similar propellers and the angles ϕ and γ and C_L are dependent directly upon V/nD . Likewise

$$Q = Q_c \cdot \rho V^2 D^3 \quad [3]$$

As velocity and V/nD approach zero both T_c and Q_c approach infinity, and their application becomes difficult and meaningless for this region where accurate calculations must be made. They may therefore be

³ G. Eiffel, "The Resistance of the Air and Aviation," translated by J. C. Hunsaker, Houghton, Mifflin & Co. (1913). See Chapter II of the supplement dated July, 1912, for a description of Eiffel's basic work on propeller experiments and his discussion of test coefficients.

modified to form a new coefficient by multiplying by the proper power of V/nD to eliminate the velocity.

$$C_T = T_c \frac{V^3}{nD} = \frac{T}{\rho n^2 D^4} \quad [4]$$

$$C_Q = Q_c \left(\frac{V}{nD} \right)^2 = \frac{Q}{\rho n^2 D^5} \quad [5]$$

The power coefficient C_P may be derived from C_Q , using the relationship that power is directly proportional to torque multiplied by rpm.

$$C_P = \frac{2\pi n \cdot Q}{\rho n^3 D^5} = \frac{P}{\rho n^3 D^5} \quad [6]$$

The efficiency may now be expressed in terms of C_P and C_T .

$$\begin{aligned} &= \frac{TV}{2\pi n \cdot Q} = \frac{C_T \rho n^2 D^4 \cdot V}{C_P \rho n^3 D^5} \\ &= \frac{C_T}{C_P} \left(\frac{V}{nD} \right) \end{aligned} \quad [7]$$

The performance curves of Fig. 2-3 may be replotted in terms of the coefficients C_T and C_P as shown in Fig. 2-5. It should be noted that C_T , C_Q , and C_P are dimensionless coefficients so that consistent units must be employed to give the proper results. In the United States the foot-pound-second system is used. The calculations follow for 100 mph as developed in the previous chapter.

$$\frac{V}{nD} = \frac{100 \times 1.467}{\left(\frac{2000}{60} \right)^8} = \frac{100 \times 1.467}{33.3 \times 8} = 0.550$$

$$C_T = \frac{1040}{0.002378(33.3)^2(8)^4} = \frac{1040}{0.002378 \times 1110 \times 4100} = 0.0962$$

$$C_P = \frac{2\pi \times 33.3 \times 918}{0.002378(33.3)^3(8)^5} = \frac{2\pi \times 33.3 \times 918}{0.002378 \times 36,920 \times 32,780} = 0.0667$$

Figure 2-5 is analogous to the plot of C_L and C_D versus α for an airfoil as given in Fig. 1-5. A series of wind tunnel tests or theoretical calculations would yield a set of C_T and C_P curves for each blade angle. By including a sufficient range of blade angles to cover all normal operating conditions a complete picture of propeller performance is obtained. Power coefficient curves of this type taken from NACA tests are shown in Figs. 2-6 and 2-7. These tests were made in the NACA propeller

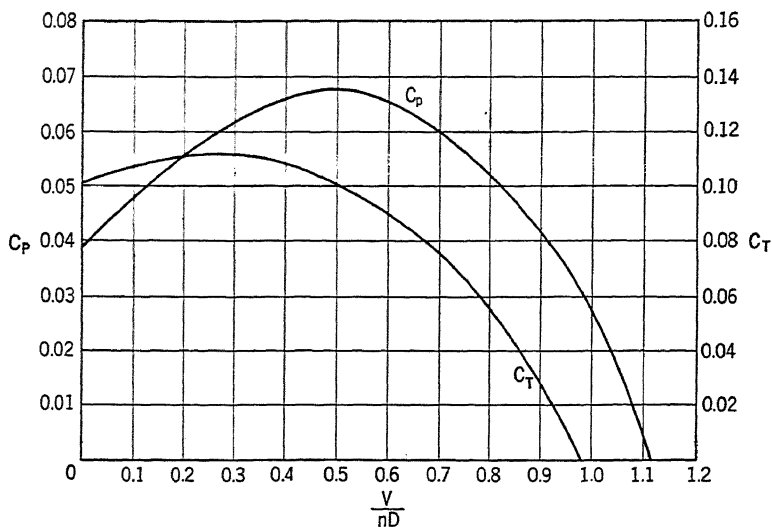


FIG. 2-5. Thrust and power coefficient curves: blade angle 22.4° at 0.75 radius (for propeller of Fig. 1-10); simple blade element calculations.

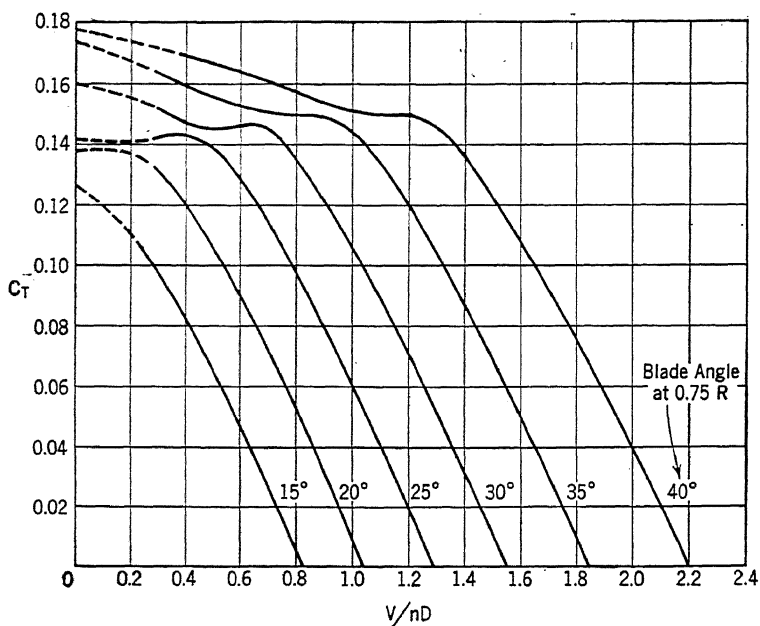


FIG. 2-6. Thrust coefficient curves for propeller 5868-9, three blades, radial engine nacelle. (NACA Tech. Rept. 642.)

research tunnel on a 10-ft diameter, three-bladed aluminum-alloy propeller of Clark-Y section mounted on a radial engine nacelle.⁴ An evalu-

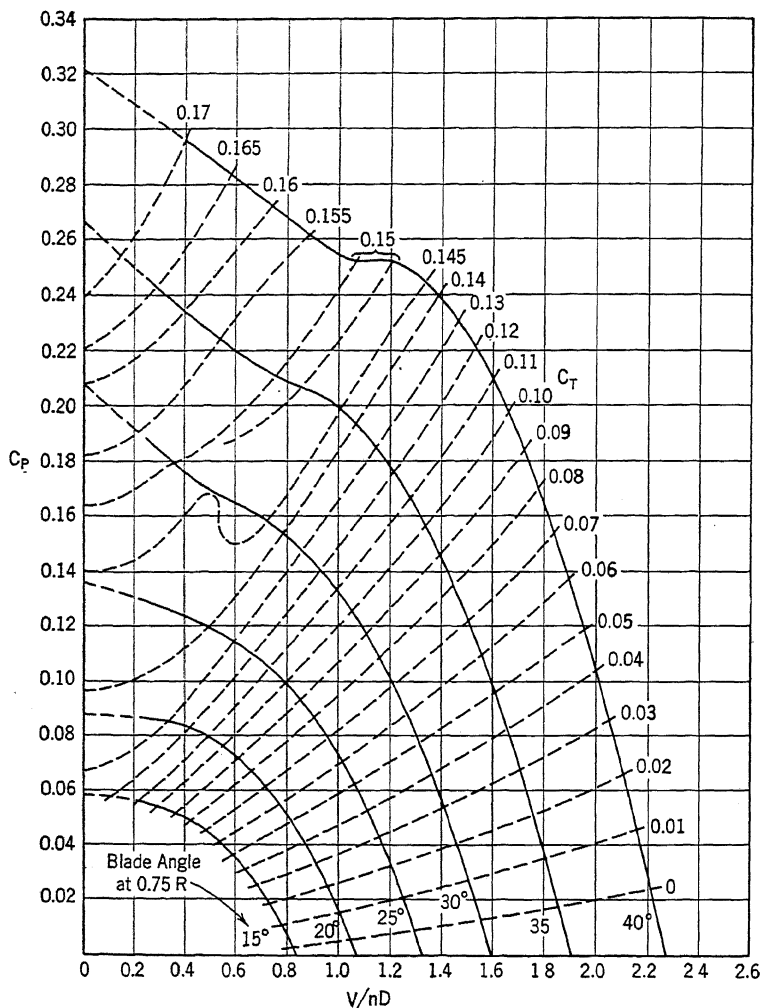


FIG. 2-7. Power coefficient curves for propeller 5868-9, three blades, radial engine nacelle. (NACA Tech. Rept. 642.)

ation of thrust and propulsive efficiency for any given set of flight conditions may be made by means of these charts. The quantities P , ρ ,

⁴ Biermann and Hartman, "Tests of Five Full-Scale Propellers in the Presence of a Radial and a Liquid-Cooled Engine Nacelle," NACA Tech. Rept. 642 (1938).

n , D , V which are known in constant-speed operation determine C_P , β , and C_T in Fig. 2-7. The thrust may then be calculated from equation 4 and the efficiency from equation 7. Thrust and efficiency calculations for both a fixed-pitch and constant-speed propeller are discussed in detail in Chapter 5.

Speed-Power Coefficient

Since many propeller problems involve a determination of the diameter, a coefficient excluding this factor would be most helpful. For such design purposes Weick⁵ has developed a speed-power coefficient C_s by modifying the power coefficient C_P as follows.

$$K = \frac{(V/nD)^5}{C_P}$$

$$K = \frac{V^5}{\beta^5} \left(\frac{\rho n^3 D^5}{P} \right) = \frac{\rho V^5}{P n^2}$$

$$K^{1/5} = V \left(\frac{\rho}{P n^2} \right)^{1/5} \quad [8]$$

In engineering units⁶

$$C_s = \frac{0.638 (\text{mph}) \sigma^{1/5}}{(\text{rpm})^{2/5} (\text{bhp})^{1/5}} \quad [9]$$

Design Chart

The efficiency η and V/nD may then be plotted versus C_s for various blade angles in the form of a propeller design chart. The NACA test results of Fig. 2-6 and Fig. 2-7 are plotted in this form in Fig. 2-8. The line of maximum efficiency for C_s indicates the blade angle necessary to obtain the maximum efficiency for any given value of C_s . Efficiency values thus obtained will fall on the envelope of the efficiency curve.

By use of the design chart a propeller diameter and blade angle may be selected to fit any design condition, where the engine power and rpm are known and the forward velocity known or estimated. The basic procedure follows.

- a. Calculate C_s for the operating condition considered critical.
- b. Choose a blade angle at which the propeller operates on the desired portion of its efficiency curve.

⁵ F. E. Weick, "Working Charts for the Selection of Aluminum Alloy Propellers of a Standard Form to Operate with Various Aircraft Engines and Bodies," *NACA Tech. Rept. 350* (1930).

⁶ $\sigma = \rho/\rho_0$ for altitude operation. See Appendix for variation of σ and $\sigma^{1/5}$ with altitude. Exponential values of rpm and bhp are also given in the Appendix.

- c. Find V/nD for the blade angle selected and C_s calculated.
 d. Solve for the diameter using the value determined for V/nD .

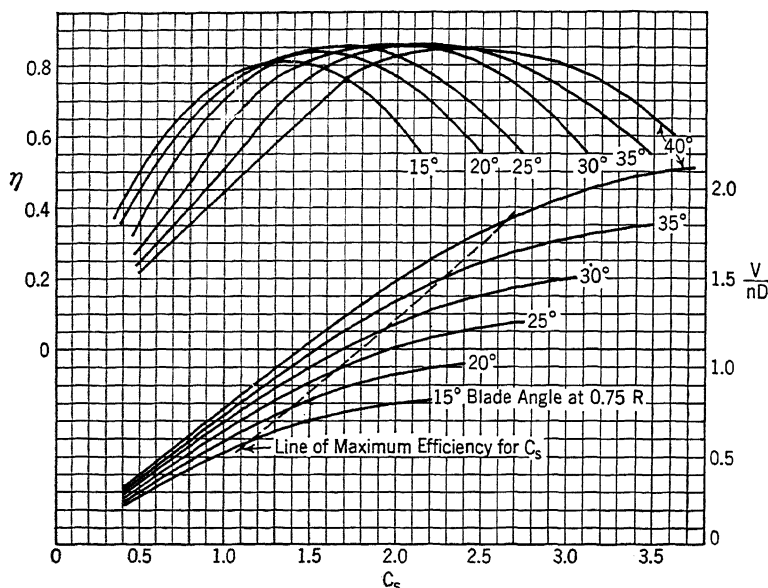


FIG. 2-8. Design chart for propeller 5868-9, three blades, radial engine nacelle. (NACA Tech. Rept. 642.)

Effective Thrust and Propulsive Efficiency

The efficiency given in the design chart of Fig. 2-8 is termed the *propulsive efficiency* and may be defined as follows.

$$\begin{aligned}\eta &= \frac{[T' - (D - D_0)]V}{2\pi nQ} \\ &= \frac{(T' - \Delta D)V}{2\pi nQ}\end{aligned}\quad [10]$$

where $D - D_0$ is the increased drag of the nacelle-wing combination due to the propeller slipstream effect, and T' is the propeller shaft tension. The factor $T' - \Delta D$ is termed the effective thrust and is used also in determining the thrust coefficient C_T of Figs. 2-6 and 2-7. Due consideration of this factor will show that it is a most useful way of expressing propeller thrust and efficiency because it evaluates only the net thrust which the propeller creates when acting on a given installation. Corrections must then be made to apply the test results to other installations where the supporting structure is different.

Various other expressions of efficiency may be derived by evaluating the thrust in a different fashion. If the thrust is not penalized for the added body drag an *apparent efficiency* is obtained which is appreciably higher than the propulsive efficiency. A *net efficiency* is obtained by subtracting from the thrust the total drag of the entire installation. This efficiency is, of course, lower than the propulsive efficiency. There is also the efficiency of the isolated propeller with no adjacent body.

All these alternate forms of efficiency may be useful when attempting to isolate some effect on propeller performance, but they should be handled with care. NACA design charts and test data are usually published on the basis of effective thrust and propulsive efficiency. The chief difficulty of the propeller designer and aerodynamicist is then to find a tested installation similar to the one under consideration or to find some logical method of correcting existing data to apply to the design in question.

The effect of the surrounding configuration of airplane structure on both thrust and torque may be quite pronounced. Many tests have been conducted in order to find the position of best efficiency for the propeller on a given installation and in the hope of securing some modification factor to account for different installations.⁷ Extreme care must be taken when using any given set of test data in order to ascertain its adaptability to the proposed design calculations or to modify it by studying related tests. Large variations in the airplane structure aft of the propeller or the introduction of a prominent obstruction forward of the propeller, as in a pusher propeller mounted closely behind a cabin, will greatly affect the performance, and comparable test data must be obtained for accurate calculations. *NACA Tech. Rept. 680* indicates that the propulsive efficiency is not appreciably affected by changes in a radial engine nacelle diameter when the diameter is less than one-third the propeller diameter. With larger nacelle diameters the propulsive efficiency decreases rapidly with increase in body size. Spinners mounted on the hub of tractor propellers have created a decided increase in efficiency, especially when they are made large enough to fair in with the rest of the nacelle.⁸ A correctly designed spinner should reduce the drag of the hub and blade shanks and act to reduce the nacelle drag.

⁷ D. H. Wood, "Tests of Nacelle-Propeller Combinations in Various Positions with Reference to Wings," *NACA Tech. Rept. 436* (1932); also *NACA Tech. Repts. 415* (1932), *462* (1933), *505* (1934), *506* (1934), *507* (1934), *564* (1936), *569* (1936).

⁸ Biermann and Hartman, "Tests of Five Full-Scale Propellers in the Presence of a Radial and Liquid-Cooled Engine Nacelle, Including Tests of Two Spinners," *NACA Tech. Rept. 642* (1938).

Torque-Speed Coefficient

The concept of propulsive efficiency is most useful when considering airplane performance in climb and level flight. For the condition of takeoff a direct evaluation of propeller thrust is desirable. To assist in this type of calculation Hartmann has developed a method of analysis based upon known engine characteristics.⁹

It is possible to obtain a coefficient containing only torque and velocity if the torque coefficient C_Q is modified.

$$K = C_Q \left(\frac{nD}{V} \right)^2 = \frac{Q}{\rho n^2 D^5} \left(\frac{nD}{V} \right)$$

$$C_{QS} = \left(\frac{1}{K} \right)^{1/2} = V \left(\frac{\rho D^3}{Q} \right)^{1/2} \quad [11]$$

Since the engine torque Q is approximately constant for a given throttle setting, C_{QS} is directly proportional to velocity for a given engine, propeller, and altitude. Q may be calculated from the rated engine power using the relationship $\text{bhp} = 2\pi nQ/550$. C_{QS} is called the torque-speed coefficient. Also,

$$\frac{C_T}{C_Q} = \frac{T\rho n^2 D^5}{Q\rho n^2 D^4} = \frac{TD}{Q} \quad [12]$$

The ratio C_T/C_Q is therefore directly proportional to thrust for a given propeller and engine throttle setting. A plot of C_T/C_Q versus C_{QS} becomes essentially a curve of thrust versus velocity for each blade angle which is very useful in takeoff calculations. Figure 2-9 is a plot of the above coefficients for a typical propeller installation. Note that the larger blade angles give less thrust at the lower velocities owing primarily to the stalled condition of the blade as shown in Fig. 2-4 for the fan state.

Compressibility Effects

As the forward velocity of a conventional airfoil approaches the speed of sound, the lift declines rapidly and drag increases abruptly. Since pressure waves cannot be propagated faster than the velocity of sound, a shock wave is formed at the airfoil leading edge at sonic velocities, and the pressure distribution is radically altered. This compressibility effect

⁹ E. P. Hartman, "Working Charts for the Determination of Propeller Thrust at Various Air Speeds," *NACA Tech. Rept. 481* (1934).

is more pronounced with thick airfoils and sets in at lower velocities. The local velocity at the leading edge is critical.

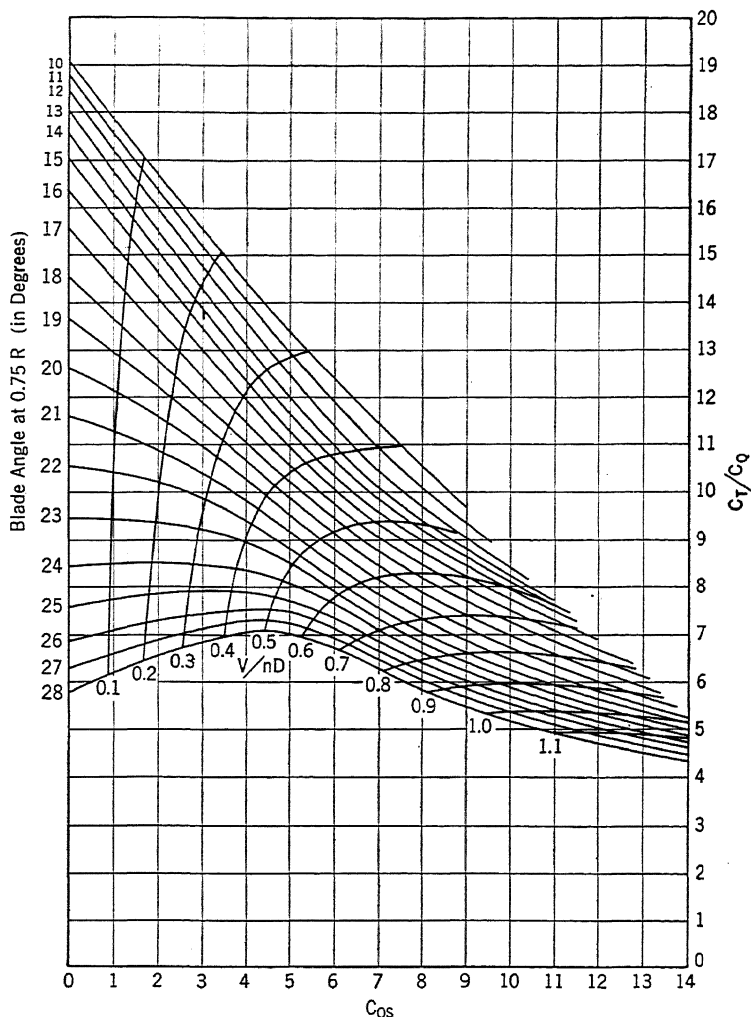


FIG. 2-9. Propeller performance chart for a 9-ft diameter, adjustable-pitch, metal propeller mounted on a cabin fuselage with J-5 engine and NACA engine cowling. (NACA Tech. Rept. 481.)

The preceding phenomenon is reflected in the propeller's performance by a modification of the thrust and power coefficients and a decrease in efficiency accompanied by an increase in noise as the tip speed approaches the speed of sound. A series of curves based upon wind tunnel

and flight test data is given in Fig. 2-10 for the variation in propulsive efficiency with tip speed for thin metal blades.¹⁰ In using this chart the V/nD for maximum efficiency may be determined from the design chart for the propeller under consideration. The 1.4 V/nD line may well represent an upper limit to be used for higher values of V/nD . The correction factor may then be applied directly to the design chart efficiency.

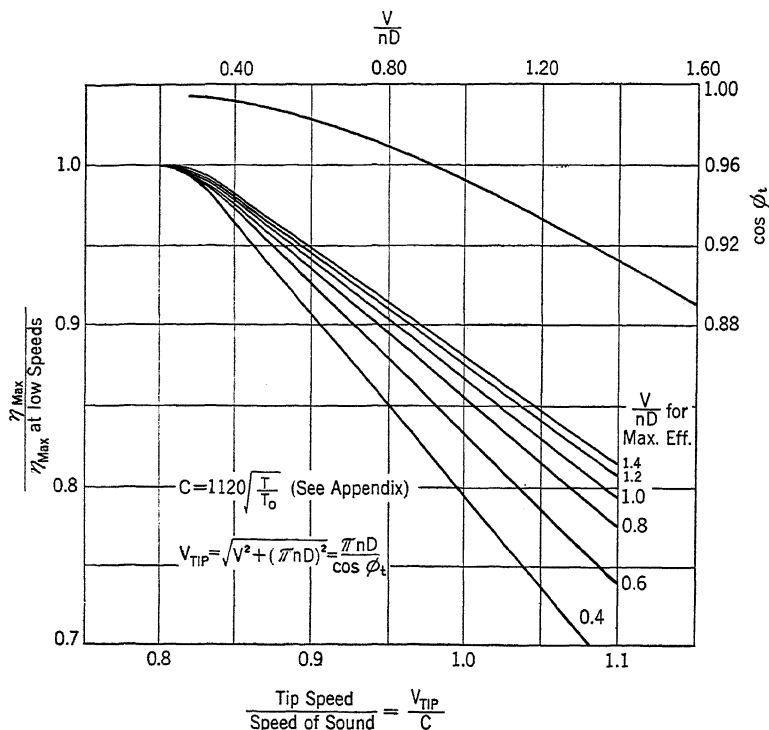


FIG. 2-10. Efficiency variation with tip speed for thin metal blades.

Several limiting factors are present to aggravate the tip speed problem. Propeller tip speed is, of course, a helical velocity formed by the resultant of the rotational and forward velocities.

$$V_{\text{tip}} = \sqrt{V^2 + (\pi n D)^2} = \frac{\pi n D}{\cos \phi_t} \quad [13]$$

where $\tan \phi_t = V/\pi n D$.

With the extremely fast military airplanes now in use, the forward velocity V is appreciably in excess of 400 mph and therefore limits the

¹⁰ H. M. McCoy, "A Discussion of Propeller Efficiency," *Journal of the Aeronautical Sciences*, Vol. 6, No. 6 (April, 1939), p. 220.

value of nD in order to retain V_{tip} at a low enough value to avoid large compressibility losses. Inasmuch as the velocity of sound c is directly proportional to the square root of the absolute temperature, a further limitation is introduced in high-altitude operation. At 35,000 ft the critical tip speed is 87 per cent of its sea-level value (see altitude curve in Appendix). The lower tip speeds necessitated by high-speed, high-altitude operations must then be accomplished by limitations on the diameter and by a high gear reduction drive in the engine.

Recent test data have shown that the effect of tip speed should not be generalized and that each blade design must be treated individually whenever possible in order to obtain the highest degree of accuracy.¹¹ The effect of angle of attack is predominant. At the higher angles, corresponding to the high thrust coefficients of takeoff, compressibility losses may occur at tip speeds as low as $0.55c$.

As stated previously, the compressibility effect occurs at lower velocities with thick sections. Hence the circular shank sections on propellers operating at high forward velocities are more critical than the thin tip sections and demand special treatment such as blade cuffs or spinners to alleviate this condition. (Refer to Fig. 3-8.) In this connection it should be noted that thin metal blades are not only superior to wood blades at low velocities because of their high L/D ratio but also at high forward and rotational velocities because of their delayed compressibility effects.

Application of Test Data

One of the chief difficulties of the propeller designer is to find test data applicable to the design under consideration. If an identical nacelle-propeller combination has not been tested, the only alternative is to modify the available test data in as logical a fashion as possible to apply to the new design. The most complete analysis of this type yet published, and one which is extensively used in the propeller industry, has been made by Thomas, Caldwell, and Rhines.¹² In their approach to this problem they introduce a series of correction factors based upon such model and full-scale test data as are available. These factors correct for variations in blade width, blade section, blade thickness, tip speed, and body interference. Where appropriate test data are lacking and the utmost accuracy is desired, this method should be applied.

¹¹ Biermann and Hartman, "The Effect of Compressibility on Eight Full-Scale Propellers Operating in the Take-off and Climbing Range," *NACA Tech. Rept. 639* (1938).

¹² Thomas, Caldwell, and Rhines, "Practical Airscrew Performance Calculations," *Journal of the Royal Aeronautical Society* (January, 1938), pp. 1-86.

An important parameter introduced in the Thomas, Caldwell, and Rhines analysis is the *activity factor*. This factor evaluates the distribution of blade area along the radius and expresses the ability of a blade to absorb power. It is a non-dimensional function of the planform and may be expressed as follows.

$$\text{A.F.} = \frac{100,000}{16} \int_{0.2}^{1.0} \frac{b}{D} \left(\frac{r}{R}\right)^3 d\left(\frac{r}{R}\right) \quad [14]$$

where A.F. = activity factor.

b = blade width at radius r .

R = propeller radius.

D = propeller diameter.

In making comparisons between different propellers, this factor is much more indicative of power absorption than a simple ratio of blade area to total disk area. It may be evaluated for any propeller by graphical integration over the limits indicated. The constant 100,000/16 merely gives the activity factor a convenient magnitude. Numerical values normally range from 60 to 110 per blade.

One question arising in applying propeller test data to airplane performance calculations is the effect of inclination of the propeller thrust axis due to varying attitude of the airplane. For angles of yaw up to 10° the maximum efficiency is reduced only slightly so that corrections are not normally needed.¹³

Data Needed

One of the most urgent needs at the present time is adequate test data at the maximum velocities now being attained in recent airplane designs. Studies based on existing airfoil test data indicate that propeller efficiencies appreciably in excess of 40 per cent do not appear possible at forward velocities above 500 mph at 20,000 ft. Compressibility effects predominate under these conditions and research is therefore needed at high forward speeds in the wind tunnel. Accurate flight test data compiled with a thrust and torque meter would be an acceptable substitute or auxiliary to such wind tunnel testing.

More extensive tests are also needed on the effects of variation in blade width, blade section, blade diameter, tip speed, and nacelle interference. Rapidly increasing demands have been placed upon the propeller, and its critical nature on the larger powerplant installations make it reasonable to expect that much more test data are being accumulated by the NACA and other research laboratories.

¹³ Lesley, Worley, and Moy, "Air Propellers in Yaw," *NACA Tech. Rept. 597* (1937).

PROBLEMS

1. A $\frac{1}{4}$ -scale model propeller operating at full-scale velocity and tip speed in an atmospheric wind tunnel will require what fraction of the full-scale power? Its thrust will be what fraction of the full-scale thrust?
2. From Fig. 2-3 prepare a plot of V/nD and η versus C_s . (Note that this is the basis for the preparation of a design chart such as Fig. 2-8.)
3. Calculate the static thrust at sea level of a bi-motored airplane equipped with a constant-speed, 10-ft diameter propeller installation as given in Fig. 2-7 if the engines are rated at 1200 bhp and 3000 rpm (geared down 16 : 11) for takeoff. At what blade angle will the propellers be operating?
4. Calculate and plot total thrust and blade angle versus velocity from 0-200 mph for the airplane of problem 3 under sea-level conditions.
5. If the airplane of problem 3 were taking off at 10,000 ft altitude with engine power unchanged, what would be the variation in thrust and blade angle?
6. Determine the diameter and blade angle necessary for a propeller installation as given in Fig. 2-8 to operate at maximum efficiency under the following conditions: airplane cruising velocity of 240 mph, 5000 ft altitude, engine power output 1000 bhp at 2850 rpm (geared down 3 : 2). What is the chart efficiency? (Neglect compressibility losses.)
7. Use Fig. 2-10 and correct the chart efficiency of problem 6 for tip speed and altitude effects.
8. Select the necessary diameter and blade angle to fulfil the conditions of problem 6 and avoid compressibility effects. Compare chart efficiency with problem 7.
9. Prepare a plot of thrust versus velocity from 0-100 mph at sea level for a cabin airplane with a propeller installation as given in Fig. 2-9. The propeller is an 8-ft diameter, adjustable-pitch type and is set at a blade angle of 20° at the 0.75 radius. The engine is rated 350 bhp at 2400 rpm, and is operating at full throttle.
10. Assume the critical sea-level tip speed of an aluminum-alloy propeller to be 900 fps and calculate the per cent reduction in rotational tip speed (πnD) to avoid compressibility losses necessitated by changing the installation from an airplane whose maximum velocity is 200 mph at sea level to an airplane whose maximum velocity is 450 mph at 40,000 ft.
11. Evaluate the activity factor of the propeller of Fig. 1-10.

CHAPTER 3

BLADE DESIGN AND STRESS ANALYSIS

Materials

Any study of propeller blade design must of necessity include a comparison of suitable materials because of the dominant influence of material properties upon the actual design. The earliest propellers were built of wood, and a great number are still so constructed. Various other materials have since been introduced and there are now propeller blades constructed of wood, aluminum alloy, magnesium, steel, and impregnated wood. A good propeller blade material must have high resistance to corrosion and abrasion in order to maintain its shape and strength under widely varying operating conditions. Intense vibratory loads created by the powerplant impulses and aerodynamic disturbances demand a material of high fatigue strength and preferably high internal damping. The large amount of centrifugal force present necessitates a material that also combines high tensile strength with a minimum of weight.

The following table lists comparative values of various qualities and significant ratios for the above materials. Corrosion resistance is omitted

PROPELLER BLADE MATERIAL PROPERTIES

Material	Abrasion Resistance	Specific Weight (lb/cu in.)	Ultimate Tensile Strength (lb/sq in.)	Fatigue Strength (lb/sq in.)	Ultimate Tensile Strength <u>Specific</u> Weight	Fatigue Strength <u>Specific</u> • Weight
Wood (bireh)	Poor	0.025	6,000	6,000	240,000	240,000
Aluminum-alloy forging (25ST.)	Poor	0.100	62,000	14,000	620,000	140,000
Steel-alloy forg- ing (SAE 4330)	Good	0.283	150,000	78,000	530,000	276,000
Magnesium forging	Poor	0.062	42,000	18,000	677,000	290,000
Compressed im- pregnated wood	Fair	0.047	35-60,000	745,000 min
Micarta	Poor	0.050	10,000	9,000	200,000	180,000

as it is primarily dependent upon the protective coating employed. A comparison of this type is very interesting. Although each material has its own peculiar disadvantages, it will be noted that steel presents a very good picture for potential development. Its difficulties as compared with other materials might be said to lie in its manufacturing problems at the present time.

Wood Propellers

Wood propellers are usually fixed pitch and are formed from glued laminations which may vary from $\frac{1}{2}$ to 1 in. in thickness. Oak, birch, and walnut are most commonly used. Laminations are generally cut to planform and then glued together with casein or animal glues. After a setting period of approximately seven days the propeller is roughed out by hand or by a duplicating cutter to within $\frac{1}{8}$ in. of the finished surface. Following an additional aging period the blades are worked to a final template fit. Final operations include a smooth sanding. A brass strip is usually attached to the leading edge from the 50 per cent radius to the tip with wood screws and copper rivets to prevent excessive abrasion in this critical area. A linen sheath is commonly fitted over the tip for additional strength. The metal tipping is vented by several drilled holes near the blade tip to prevent excessive moisture accumulation and resulting unbalance. One coat of clear varnish is applied before tipping and at least two coats after. The propeller is balanced after each major operation, and final balance is obtained by adjusting the amount of solder on the leading edge brass strip at the rivet heads.¹ A typical cross section of glued-up laminae is shown in Fig. 3-1.

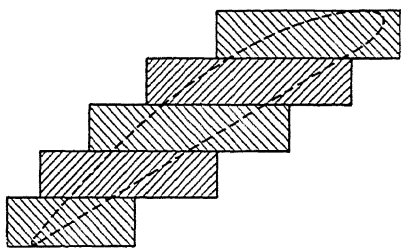


FIG. 3-1. Laminated wood propeller section prior to shaping.

Individual wood blades with steel-encased shank portions are also manufactured and used in adjustable-pitch hubs. The shank portion is composed of a phenol-resin impregnated wood to avoid shrinkage and slipping between the wood and steel. A blade of this type is shown in Fig. 3-2.

¹ For a more detailed account of wood propeller fabrication methods refer to *Civil Aeronautics Authority Manual 14*, "Aircraft Propeller Airworthiness," Superintendent of Documents, Washington, D. C. (1938). Also G. W. Trayer, "Wood in Aircraft Construction," National Lumber Manufacturers Association (1930).

The outstanding advantage of wood propellers lies in their economy of manufacture. Low retail cost makes them an ideal propeller for the light airplane market. High internal damping of wood and its high fatigue strength-weight ratio are also favorable properties. There are, however, certain inherent disadvantages. Wood splits easily along the grain under longitudinal shear. It also tends to warp under varying moisture conditions. Furthermore, because the blade sections must be

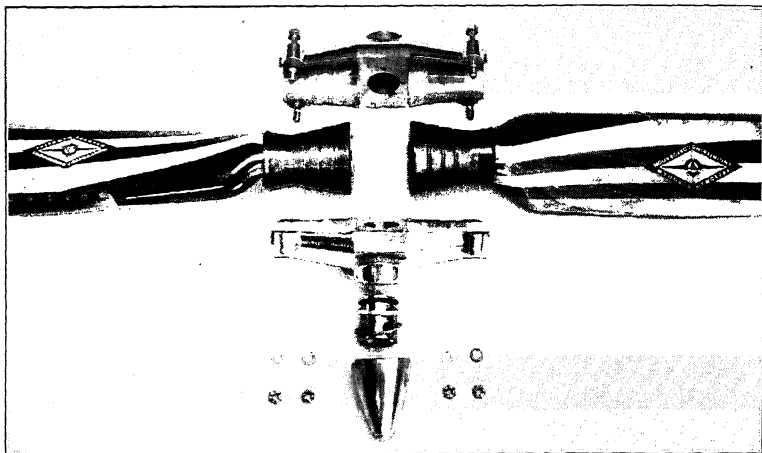


Fig. 3-2. Adjustable-pitch propeller with wood blades. (Courtesy Freedman Burnham Engineering Corp.)

relatively thick owing to its low tensile strength-weight ratio, a lower propulsive efficiency results.

Aluminum-Alloy Propellers

Aluminum-alloy blades are machined by profiling cutters from forgings after which they are heat-treated and then finished by grinding and buffing. The complete propeller may be forged in one piece, or the blades may be forged separately for use in adjustable and controllable-pitch propellers. The one-piece propeller has a splined steel sleeve pressed and keyed into position at the center for attachment to the engine crankshaft. A propeller of this type is shown in Fig. 3-3.

Blade forgings for the larger propellers are pierced radially for a considerable distance at the shank to save weight and provide a more efficient structure. Aluminum alloy 25ST is generally used for this type of blade although improved alloys with higher strength properties and increased abrasion resistance have been recently introduced. Blades operating near salt water are given a chromic acid anodic treatment

which forms an oxide on the surface and protects from corrosion. Each blade is finally balanced on an arbor against a master blade or master cylinder to close limits.

Aluminum will erode rapidly under severe operating conditions and also has a low fatigue strength-weight ratio. Pebbles or cinders on the runway are likely to cause dangerous scratches on the blade. Advantages of aluminum are its relative ease of manufacture compared with steel blades and also its capacity for being straightened easily after an accident. Bent blades may be cold-straightened if the bend does not exceed a variation between 20° at 0.15-in. blade thickness to 0° at 1.1-in. thickness. Usually the manufacturer can handle bends 5° in excess of the preceding by heat treatment.



FIG. 3-3. Curtiss one-piece, aluminum-alloy propeller. (Courtesy Curtiss Propeller Division, Curtiss-Wright Corp.)

Single-piece aluminum-alloy propellers are used along with adjustable-pitch designs in the range of 100 to 300 hp. Horsepowers in excess of this usually result in controllable-pitch designs where the competing design is a steel blade.

Aluminum-alloy blades are etched with caustic soda and examined with a magnifying glass for cracks that may occur in service. Periodic inspections are necessary.

Steel Propellers

Steel is used for both solid and hollow blade construction. The alloy is usually SAE 4330 chrome-nickel-molybdenum or a similar high-strength alloy. Owing to its high specific weight, the cross section of a steel blade must either be hollow or of unconventional airfoil design. Typical sections are shown in Fig. 3-6. Solid steel blades are machined from the forging and ground and polished to a final finish. The solid type lacks torsional rigidity in the larger sizes because of its thinness. Curtiss hollow steel blades are formed by atomic-hydrogen welding at the leading and trailing edges of two sheets formed to make the face and back sides. After welding, the blade is heat-treated and ground to final template fit. Figure 3-4 shows the construction of a Curtiss hollow steel blade. Lycoming hollow steel blades are made from a tube which is split, die-formed and electric seam-welded at the leading and trailing

edges. Aeroproducts hollow steel blades are formed by copper brazing a thin camber sheet to a relatively thick forging which forms the face. Copper brazing eliminates the local heating of the welding operation and also makes it possible to provide an internal rib.

In all designs the blades are carefully balanced at each major operation. As a finishing step a protective coating such as chrome plate is added. Compared with aluminum, steel has far greater abrasion resistance, and the protective coating is primarily to prevent surface oxidation. At the present time, both hollow steel and solid aluminum-alloy blades weigh about the same in a 12-ft diameter, three-bladed design. With increasing engine powers, however, the hollow steel designs may

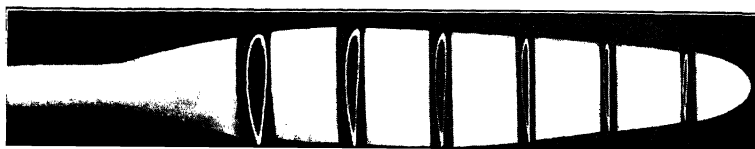


FIG. 3-4. Hollow steel propeller blade. (Courtesy Curtiss Propeller Division, Curtiss-Wright Corp.)

come to the fore in the larger sizes because of their more efficient utilization of material combined with better material properties and the aerodynamic advantages of relatively thin sections.

During manufacture and in the field the steel blade is magnafluxed periodically for any signs of cracks. In this operation a strong magnetic field is set up in the blade while it is coated with a solution containing ferrous particles. These particles collect about a crack and make it visible.

Magnesium Propellers

Magnesium propellers are still an experimental development. Their fabrication is similar to the aluminum-alloy blades. The material has excellent properties with one exception: abrasion and corrosion resistance. As the material will wear away rapidly under the action of water spray, cinders, etc., its fatigue strength is rapidly diminished because of the surface cracks, and a dangerous condition results. Until this condition is improved, the material must of necessity be considered unsuitable.

Impregnated Wood

Impregnated wood has been introduced as a propeller material in this country by the Engineering Research Corporation of Riverdale, Maryland. Their design is licensed under the Schwartz patents and consists

basically of a shank portion of compreg to which is spliced spruce laminations which comprise the outer blade sections. The compreg shank is composed of hardwood veneer strips which have been impregnated with a phenol-formaldehyde resin, compressed to half their original thickness and formed at elevated temperatures. After carving the blade sections to final shape, the entire blade is covered with a fabric gauze, the leading edge encased in a wire mesh, and the entire combination sealed in a hard, tough, cellulose acetate covering. This outer sheathing is applied soft and plastic and bonded to the wood under pressure and temperature.

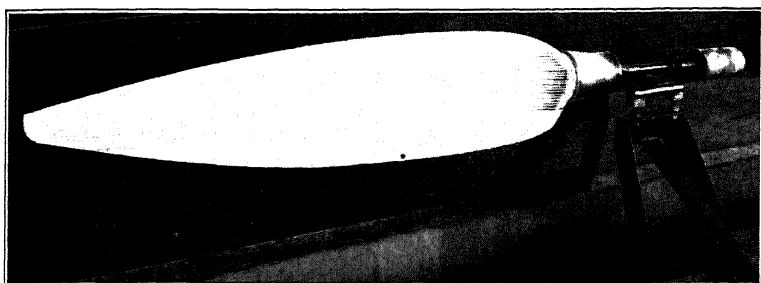


FIG. 3-5. Blade balancing operation. (*Courtesy Engineering and Research Corp.*)

A steel ferrule is screwed onto the compreg shank to facilitate attachment of the blade to the hub.

A blade design of this type eliminates some of the original objections to wood as a blade material. Owing to the lightness of the outboard spruce sections, the center of gravity of each blade is kept in toward the center of rotation, resulting in lowered centrifugal stresses on the shank. A blade balancing operation prior to applying the cellulose acetate covering is shown in Fig. 3-5. The compreg splice at the shank is apparent. Note the master balancing cylinder used. Individual blades may vary appreciably in weight and still be acceptable. Horizontal and vertical balance must be obtained so that the blade shows no tendency to rotate.

Micarta

Micarta blades were introduced by the Westinghouse Electric and Manufacturing Company in 1922. The material consisted of a duck fabric impregnated with a synthetic resin and formed under high pressure and temperature. Certain undesirable characteristics made it unsatisfactory. The abrasion resistance was poor. In addition, the internal working of the material under vibration caused it to char and disintegrate. Micarta soon gave way to aluminum alloy as a blade material and is mentioned here because of its relationship to impregnated wood.

Figure 3-6 provides a résumé of the various blade types discussed and shows their major characteristics for outboard sections.

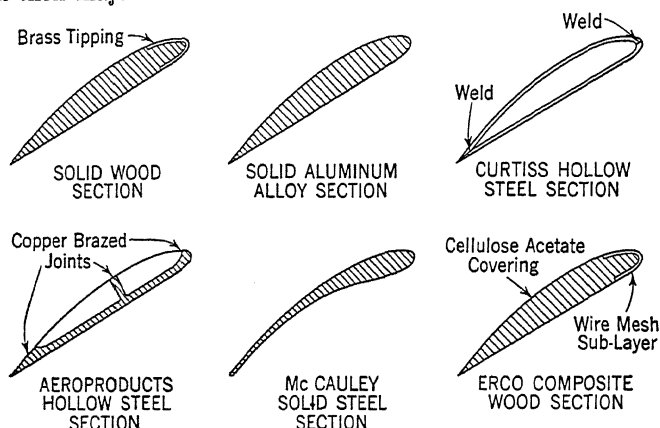


FIG. 3-6. Propeller blade sections of different materials and construction.

Propeller Types

With this brief discussion of materials and processes it is helpful to break down the various existing designs according to type and construction.

- a. Fixed pitch.
 - (1) Laminated wood.
 - (2) Aluminum alloy.
- b. Adjustable pitch.
 - (1) Laminated wood blades with steel shank casing.
 - (2) Aluminum-alloy blades.
 - (3) Impregnated wood blades with steel shank casing.
 - (4) Solid steel blades.
- c. Controllable pitch.
 - (1) Impregnated wood blades with steel shank casing.
 - (2) Aluminum-alloy blades.
 - (3) Hollow steel blades.

Pitch Distribution

After the blade material has been selected, the next problem is to proportion this material in the most efficient manner possible, both structurally and aerodynamically. It is first necessary to determine the proper pitch distribution for the blades.

In a fixed-pitch propeller the blades must be pitched high enough to prevent overspeeding the engine at the maximum forward velocity of the airplane. The distribution usually approximates a uniform geometrical pitch, the only difference being a slightly adjusted blade angle at each station to provide the best angle of attack. The blade angle is such that at the design condition of cruising or maximum velocity the airfoil section is operating near the angle of maximum L/D .

Tests indicate that the distribution of pitch is relatively unimportant under normal conditions and that uniform geometrical pitch will give

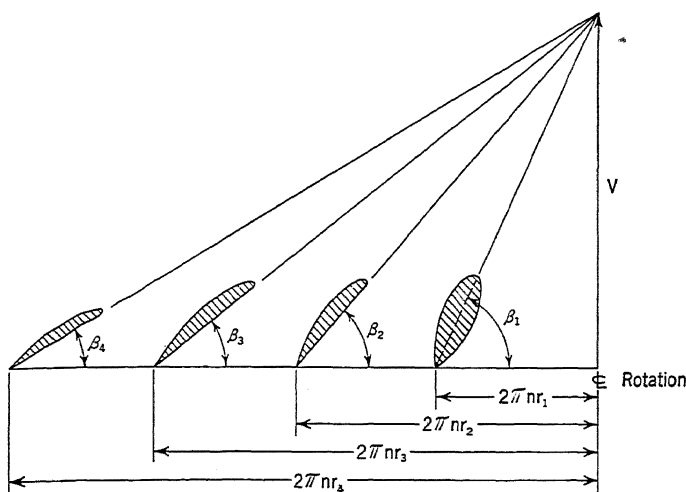


FIG. 3-7. Uniform geometric pitch distribution for design V and n .

about the best efficiency. In adjustable-pitch and controllable-pitch blade designs, the pitch distribution is usually determined for some forward velocity below the design condition. This results in an increase of pitch with radius for the higher velocities, and this effect has proven beneficial to the efficiency.²

Blade Width and Number

Blade width may be considered in terms of a solidity factor which is defined as the ratio of the total untwisted blade area to the total propeller disk area. Another necessary concept is that of disk loading, which is the total power to be absorbed by the propeller divided by the

² Lesley and Reid, "Tests of Five Metal Model Propellers with Various Pitch Distribution," *NACA Tech. Rept. 326* (1929).

Biermann and Hartman, "Tests of Two Full-Scale Propellers with Different Pitch Distribution, at Blade Angles up to 60° ," *NACA Tech. Rept. 658* (1939).

disk area. A high solidity factor is needed in order to obtain a satisfactory propulsive efficiency for high disk loadings and high-altitude operation. This may be obtained by wider blades or by an increased number of blades. When considering blade width variations, it must be remembered that the propeller should not be operating at an effective angle of attack appreciably larger than that for maximum L/D at the design condition. If the blade angle has to be increased to large values to absorb high engine powers at low density ratios the efficiency will be reduced appreciably.

Recent test data indicate that for the same solidity factor the multi-bladed designs are more efficient.³ The simple blade element theory would yield identical results for all propellers having the same solidity factor, whereas the multi-plane interference correction would tend to reduce the efficiency with an increasing number of blades. Actual test data should be used to evaluate the effect of blade width changes. For small changes in blade width the thrust and power coefficients (refer to Figs. 2-6 and 2-7) may be assumed to vary directly with the change in area.

It should be noted here that modern supercharged engine requirements are necessitating much higher solidity factors. Usually in an airplane design the nacelle, fuselage, and landing gear arrangement combined with limiting tip speed at altitude dictate the maximum propeller diameter. The high power output and high-altitude operation of modern engines then demand a very high solidity factor. From density considerations alone the solidity would have to be approximately doubled in order to absorb the sea-level engine power at 20,000 ft without increasing the effective angle of attack. The trend to three- and four-bladed propellers and counter-rotating propellers is a necessary outgrowth of these considerations.

Blade Planform

Blade planform has to a large extent been dictated by structural considerations which require a tapering toward the tip from about the 50 per cent radius to maintain consistent stresses under normal steady load conditions. Marked changes in propeller planform, both at the tip and at the inboard stations, have given comparatively minor variations in the peak efficiency. Fairly wide tip sections are sometimes used to increase the aerodynamic damping of that portion under vibration conditions. The inner third of the radius is usually faired into a circular

³Hartman and Biermann, "The Aerodynamics Characteristic of Full-Scale Propellers Having 2, 3, and 4 Blades of Clark Y and R.A.F. 6 Airfoil Sections," *NACA Tech. Rept. 640* (1938).

section for structural and design reasons. However, the improved cooling of radial air-cooled engines at low forward velocities and the delayed compressibility effect obtained by using airfoil sections at the inner portion of the radius have resulted in the addition of blade cuffs on metal propeller blades designed for high powers and high velocities. These blade cuffs completely fair in the circular sections, as shown in Fig. 3-8.

The blade shank fairs into a boss portion in a fixed-pitch propeller, and the boss is bolted or splined to the engine crankshaft. In the adjustable and controllable-pitch designs, the shank must terminate with some

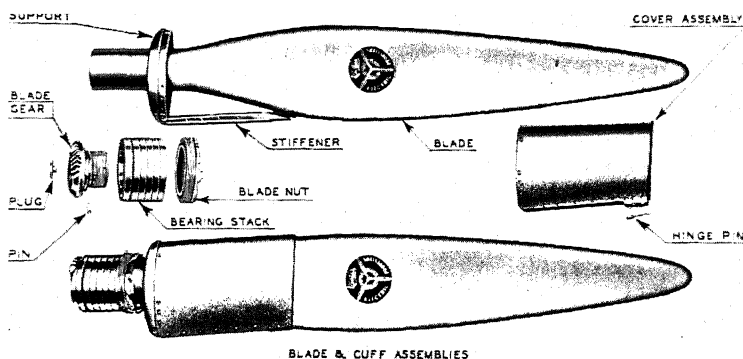


FIG. 3-8. Blade cuff assembly. (Courtesy Curtiss Propeller Division, Curtiss-Wright Corp.)

sort of provision for a shoulder to supply the necessary blade retention such as shown in Fig. 1-1. The various blade retention design features are discussed in Chapter 4.

Thickness Ratio

As the blade element theory would indicate, an increase in blade section thickness with its resultant lower L/D ratio causes a drop in propulsive efficiency.⁴ In general the relatively thin sections employed in metal propellers yield a substantial increase in efficiency when compared with the thicker wood sections.⁵ The original work on thin aluminum-alloy propeller blades had as its goal the realization of that improvement.

Another factor in favor of thin sections is the delayed compressibility effect at high tip speeds. Thinner sections may operate at higher velocities without running into tip losses and a drop in efficiency.

⁴ Refer to Fig. 1-9.

⁵ Biermann and Hartman, "The Aerodynamic Characteristics of Six Full-Scale Propellers Having Different Airfoil Sections," *NACA Tech. Rept. 650* (1939):

The variation in thickness with radius along the blade is normally determined by structural and vibrational considerations once the plan-form is fixed.

Blade Section

The effect of extreme changes in propeller blade section upon propulsive efficiency is not very large.⁶ If the usual flat thrust face is considered, much variation is not possible if the thickness ratio is held constant. The Clark-Y and RAF-6 airfoil sections shown in Fig. 3·9 have been

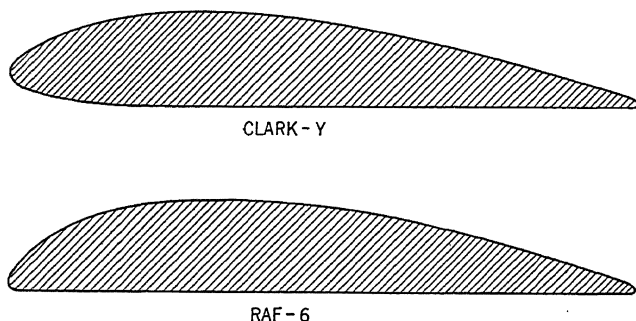


Fig. 3·9. Blade sections.

standard in propeller design in this country for many years. Airfoil tests show that the Clark-Y section has a lower minimum drag and lower maximum lift than the RAF-6 section.⁷ This would indicate that a fixed-pitch propeller with the Clark-Y section would be superior at cruising and high speed, and inferior at takeoff. Propeller tests have substantiated this.⁸ For controllable-pitch propellers where the individual blade sections are not so likely to be stalled during takeoff, the section with the lowest drag would be preferable because of higher peak efficiencies. The new NACA laminar-flow airfoil sections with their extremely low drag will undoubtedly enter the field of propeller design. In 1943 the nature and characteristics of these sections were confidential because of military restrictions.

Blade Form Curves

Figure 3·10 is a plot of the blade form curves for the propeller of Fig. 1·10. It will be noted that the variation in b/D and h/b is such as

⁶ Biermann and Hartman, "The Aerodynamic Characteristics of Six Full-Scale Propellers Having Different Airfoil Sections," *NACA Tech. Rept. 650* (1939).

⁷ John Stack, "The NACA High-Speed Wind Tunnel and Tests of Six Propeller Sections," *NACA Tech. Rept. 463* (1933).

⁸ H. B. Freeman, "Comparison of Full-Scale Propellers Having RAF-6 and Clark Y Airfoil Sections," *NACA Tech. Rept. 378* (1931)*

to form a smooth curve when plotted against per cent radius. The p/D curve is calculated, using the blade angle and radius at each station to obtain p , the geometric pitch. At the reference blade angle of 22.4° a

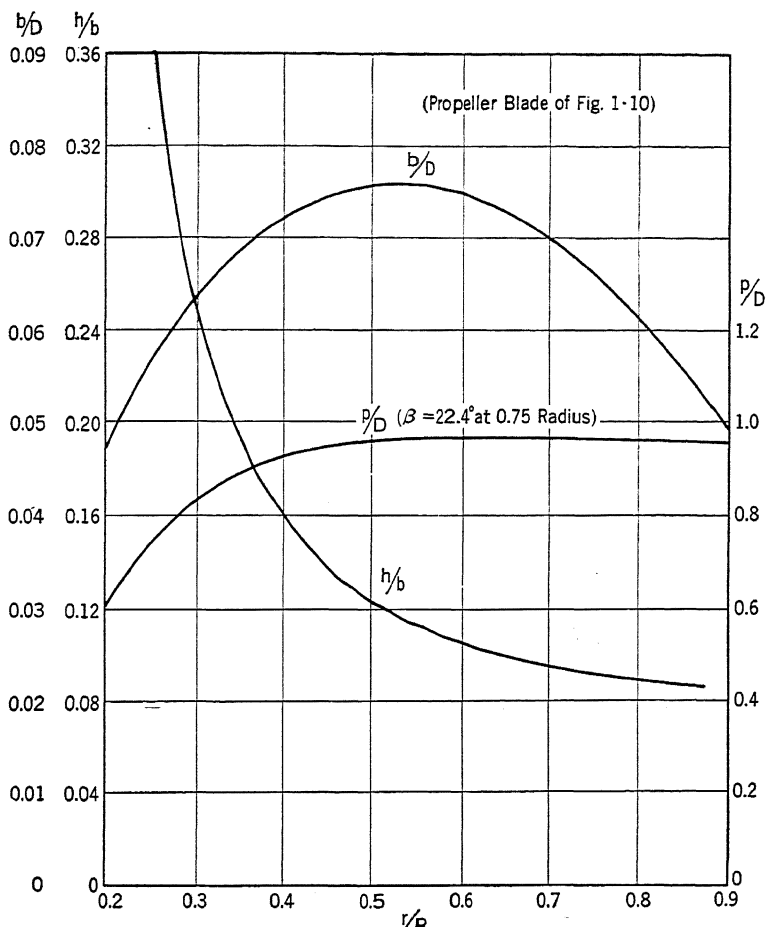


FIG. 3-10. Blade form curves.

fairly uniform pitch distribution is obtained. No well-designed blade will show abrupt changes in section, as these are likely to be stress-concentration points. The section area and maximum and minimum moments of inertia should likewise plot against radius as smooth curves.

Blade Stress Analysis

A propeller blade in operation is essentially a rotating cantilever beam subjected to both steady and vibratory loads. The steady stresses

may be calculated from the known loads, and it is possible to analyze them with a reasonable degree of accuracy. Vibratory loads will be discussed later in the chapter.

The main steady loads acting upon the propeller blade in unaccelerated rectilinear flight are as follows.

- a. Centrifugal force due to rotation.
- b. Thrust and torque air-load bending moments.
- c. Bending moments due to blade tilt.
- d. Aerodynamic blade torque.
- e. Centrifugal blade torque.

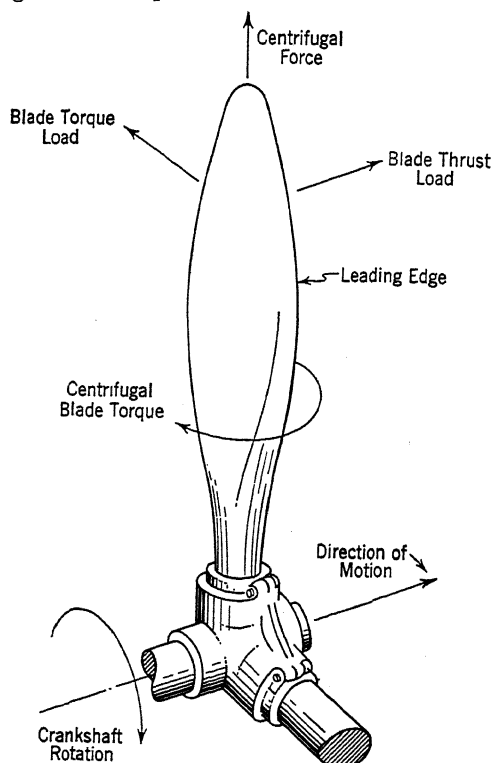


FIG. 3-11. Principal steady loads during operation.

Centrifugal and bending stresses are the principal factors dictating blade strength. Torsion stresses are negligible but an accurate calculation of the torque present is necessary for controllable-pitch propellers, because this is the main load on the pitch-changing mechanism. The preceding loads are indicated in Fig. 3-11.

Critical Loading Conditions

Before evaluating the actual stresses, the condition of maximum load must be considered. This will vary with the type of propeller. The thrust will normally be a maximum at the start of takeoff and will diminish steadily with forward velocity. For a controllable-pitch design with a constant-speed governor, the critical loading condition will then occur at the start of takeoff when the thrust is a maximum and the propeller pitch control is set for maximum rpm, creating the peak centrifugal load. Other flight conditions for this type of propeller will then ordinarily result in lower air loads or centrifugal loads as long as the speed control is effective.

A fixed-pitch or adjustable-pitch propeller has a wide range of rpm at full throttle on the engine, dependent primarily upon the forward velocity of the airplane. The thrust is normally a maximum at the start of takeoff but the rpm is low. At top speed the rpm may be maximum but the thrust is quite low. The climbing condition is usually considered critical because the rpm is then considerably greater than the takeoff rpm, and the thrust is still quite high.

In the following stress analysis the propeller blade of Fig. 1-10 will be analyzed as a two-bladed adjustable-pitch propeller with a critical loading condition of 425-lb thrust per blade at 2000 rpm in climb at 77 mph. This condition would represent an installation of the propeller upon an airplane equipped with a 300-hp engine rated at 2350 rpm and with the propeller pitch set for 145 mph maximum velocity. The actual value of the thrust should be calculated from existing test data, using the methods outlined in Chapter 2. The present case was calculated for $\beta = 18^\circ$ at 0.75 radius, using Fig. 10 of *NACA Tech. Rept. 481*.

Blade Section Characteristics

The blade form curves will require certain calculations for section area and moments of inertia. Empirical formulas have been determined for these factors based upon the section thickness h and section width b . The principal axes of the section are usually practically parallel and perpendicular to the chord line.

For a solid RAF-6 section with a flat thrust face the following formulas will apply.

$$\text{Area} = 0.7380bh.$$

$$I_{\min} = 0.0472bh^3.$$

$$I_{\max} = 0.0446b^3h.$$

$$\text{c.g.} = 0.4210h \text{ above chord.}$$

$$\text{c.g.} = 0.4405b \text{ from leading edge.}$$

For a solid Clark-Y section with a flat thrust face the following formulas will apply.

$$\text{Area} = 0.7245bh.$$

$$I_{\min} = 0.0454bh^3.$$

$$I_{\max} = 0.0418b^3h.$$

$$\text{c.g.} = 0.4160h \text{ above chord.}$$

$$\text{c.g.} = 0.4405b \text{ from leading edge.}$$

For the circular shank sections $I_{\max} = I_{\min} = \pi d^4/64$.

With the critical loading condition evaluated and the blade section properties determined, the steady stresses may then be analyzed. Because of the variation of the moments of inertia and section area with radius, a graphical solution provides the most general method of stress analysis and will therefore be used.⁹

Centrifugal Force Stress

Centrifugal force acting radially outward on the rotating blade causes direct tension. This may be calculated using the formula

$$\Delta \text{ C.F.} = m\omega^2 r \quad [1]$$

where m = mass of a 1-in. long element of blade section.

ω = angular velocity in radians per second ($2\pi n$).

r = radius of section in inches.

The quantity $\Delta \text{ C.F.}$ may be regarded as the centrifugal loading in pounds per inch of blade. This factor is calculated for every 6-in. station and plotted versus radius. The resulting curve may then be integrated from the tip in to give the total centrifugal force acting at each station. This process is essentially an evaluation of the integral

$(2\pi n)^2(\delta/g) \int_R^r A r dr$ for each station; where δ is the density of the material in pounds per cubic inch, A is the blade section area in square inches, and g is the acceleration due to gravity in inches per second per second. By using a specific weight of 0.1 for aluminum alloy, the factor m in equation 1 becomes $(A \times 1 \times 0.1)/386$.

⁹ A tabular, trial-and-error method of steady stress analysis is presented by J. Stuart, "A Tabular Method of Propeller Blade Stress Analysis," *Journal of the Aeronautical Sciences*, Vol. 10, No. 4 (March, 1943), p. 115.

The tension stress $f_{c.f.}$ may be calculated by dividing the total centrifugal force at any section by the section area. A plot of these items

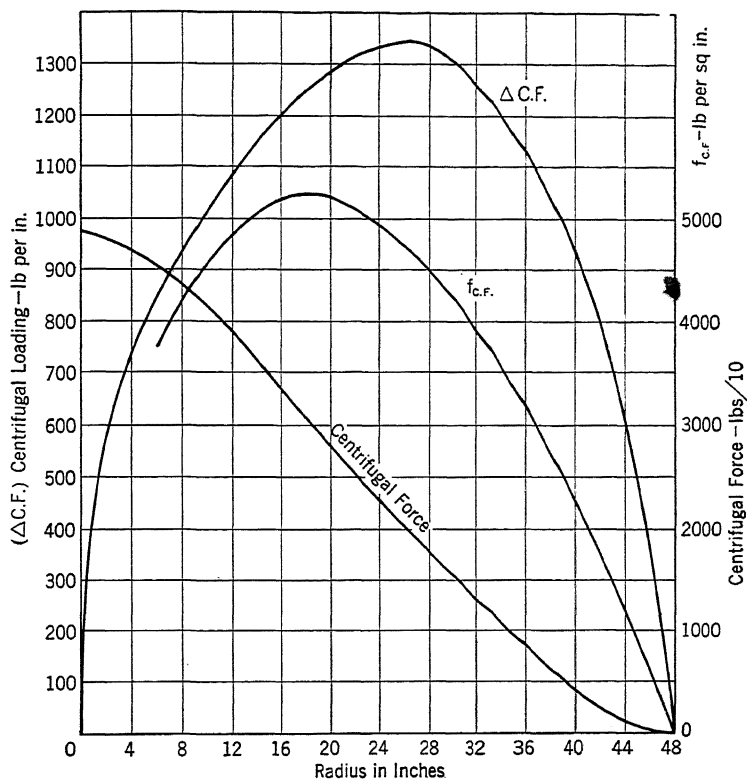


FIG. 3-12. Centrifugal blade loading.

for the propeller of Fig. 1-10 is given in Fig. 3-12 for 2000 rpm. The calculations follow.

CENTRIFUGAL BLADE STRESSES

Station	h (in.)	b (in.)	Area (sq in.)	m (lb-sec ² /in.)	$\Delta C.F.$ (lb per in.)	C.F. (lb)	$f_{c.f.}$ (lb per sq in.)
12	1.969	5.48	7.95	0.002059	1084	38,420	4,835
18	1.184	6.86	6.00	0.001552	1227	31,490	5,250
24	0.898	7.29	4.83	0.001250	1317	23,820	4,935
30	0.727	7.06	3.79	0.000982	1292	15,915	4,200
36	0.577	6.35	2.70	0.000700	1106	8,640	3,200
42	0.439	5.06	1.64	0.000425	783	2,885	1,760

Bending Stress

Bending stresses are more complex and require reference to aerodynamic data in order to obtain the distribution of thrust along the blade. *NACA Tech. Rept. 421* presents sufficient data to determine the thrust distribution for a variety of blades and blade angles. The differences in distribution shown affect but slightly the resultant bending stresses so that one representative curve of thrust distribution for the most conservative condition may be used. Distribution of the blade

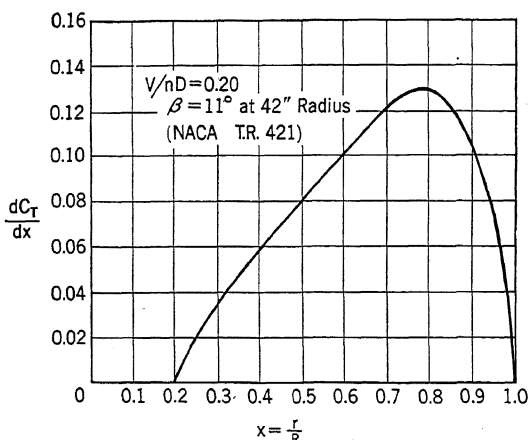


FIG. 3-13. Thrust load distribution.

torque load may be handled in a similar fashion, but torque calculations are ordinarily neglected because the effect on blade stresses is negligible.

Figure 3-13 is a plot from *NACA Tech. Rept. 421* of thrust loading dC_T/dx versus per cent radius at a low V/nD ratio for a typical metal propeller blade and may be used to calculate the actual thrust distribution once the total thrust is determined. The area under this curve represents the total thrust per blade and may therefore be converted into a plot of thrust loading in pounds per inch versus radius in inches.

When the thrust distribution has been determined, the curve of thrust distribution may be graphically integrated from the tip inward to determine the shear at any point on the blade. A second integration will yield the uncorrected bending moment curve. Figure 3-14 contains a plot of these calculations with the thrust loading curve adjusted to give a total thrust of 425 lb. The thrust bending moment causes the blade to deflect forward out of the plane of rotation, and centrifugal force sets

up a restoring moment until equilibrium is obtained. In order to determine the final moment acting it is necessary to estimate a reduced bending moment curve and to calculate the blade deflection under this assumed condition. The centrifugal restoring moment may then be calculated and subtracted from the uncorrected moment to obtain a

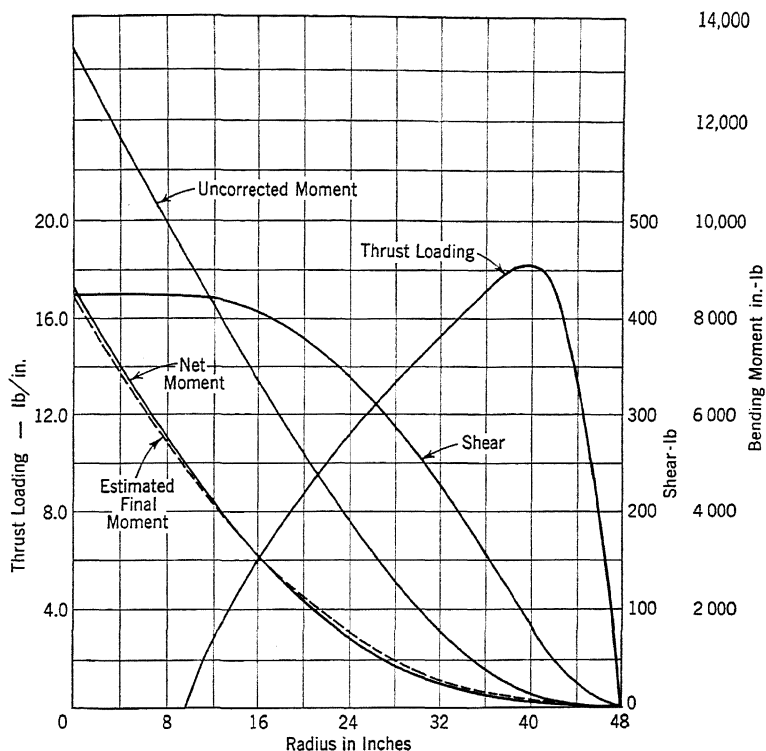


FIG. 3-14. Thrust loading and bending moments.

net moment. If the net moment is reasonably close to the estimated moment the calculations are complete. If not, a new estimated moment must be taken and the calculations repeated until agreement is reached. The estimated moment curve of Fig. 3-14 represents an arbitrary reduction from the uncorrected moment curve. The net moment curve shown will be derived in the next several pages. A tabulation of the uncorrected and estimated moment calculations follows. The factor C_r is a correction factor which, when multiplied by the uncorrected moment, will give the estimated moment value. For blades of this general type it will serve as a first approximation.

ESTIMATED MOMENT CALCULATIONS

Station (in.)	Shear (lb)	Uncorrected Moment (in.-lb)	C_r	Estimated Moment (in.-lb)
12	420	8490	0.515	4370
18	392	6030	0.455	2740
24	338	3820	0.400	1530
30	260	2020	0.355	717
36	159	750	0.350	263
42	55	130	0.400	52

Inasmuch as the propeller blade is essentially a cantilever beam of varying cross section, the deflection under the estimated moment may be obtained by a double graphical integration of the M/EI curve¹⁰ where

M = estimated bending moment in inch-pounds.

E = modulus of elasticity in pounds per square inch (approximately 10,000,000 for aluminum alloys).

I = minimum moment of inertia for blade section in in.⁴

BLADE DEFLECTION CALCULATIONS

Station (in.)	b (in.)	h (in.)	I_{\min} (in. ⁴)	$\frac{M_{\text{est}}}{EI_{\min}}$	Slope (radian)	Deflection (in.)
12	5.48	1.964	1.962	0.000223	0.00104	0.0036
18	6.86	1.184	0.539	0.000509	0.00362	0.0172
24	7.29	0.898	0.249	0.000615	0.00722	0.0496
30	7.06	0.727	0.1282	0.000559	0.01086	0.1036
36	6.35	0.577	0.0577	0.000455	0.01396	0.1788
42	5.06	0.439	0.0202	0.000257	0.01610	0.2696
48	0.01688	0.3696

The above calculations are graphed in Fig. 3-15.

With the forward deflection of all blade sections determined, the restoring moment due to centrifugal force may be calculated by a sum-

¹⁰ Conjugate Beam Method for Beam Deflection. It should be noted that both integrations must be made from the blade root outward. Niles and Newell, "Airplane Structures," Vol. I, John Wiley and Sons (1943), p. 80.

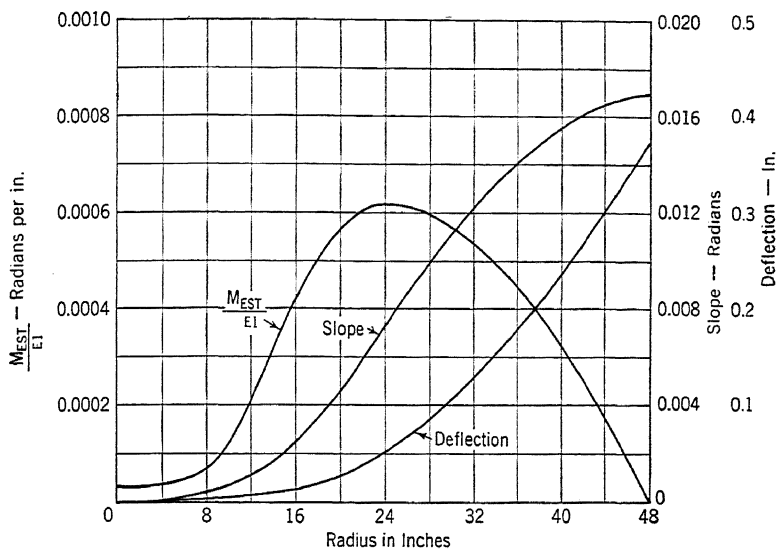


FIG. 3-15. Blade deflection under thrust load.

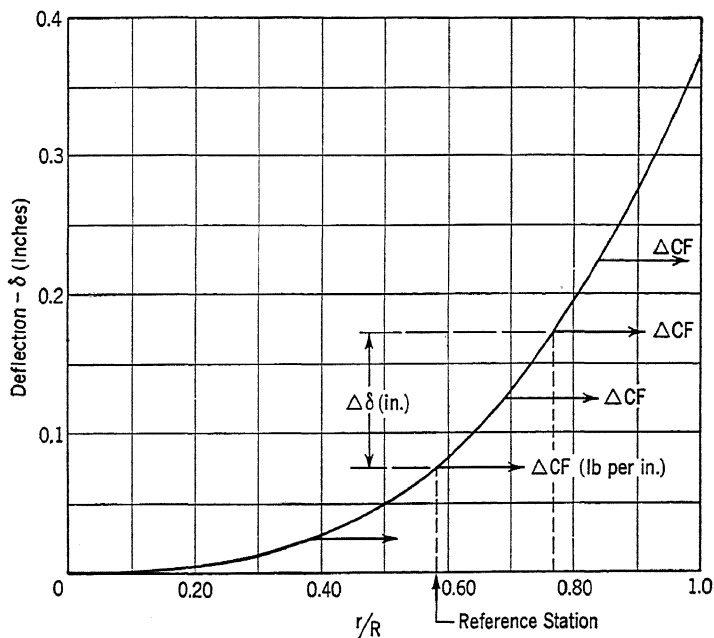


FIG. 3-16. Centrifugal force restoring action.

mation of the increments $\Delta \text{C.F.} \times \Delta \delta$ from each reference station to the tip. $\Delta \text{C.F.}$ is the centrifugal force of some station outboard of the reference station r and $\Delta \delta$ is the blade deflection between the two stations as shown in Fig. 3·16.

Figure 3·17 shows the graphical integration necessary to obtain the centrifugal restoring moment $M_{\text{C.F.}}$ curve. A separate set of computa-

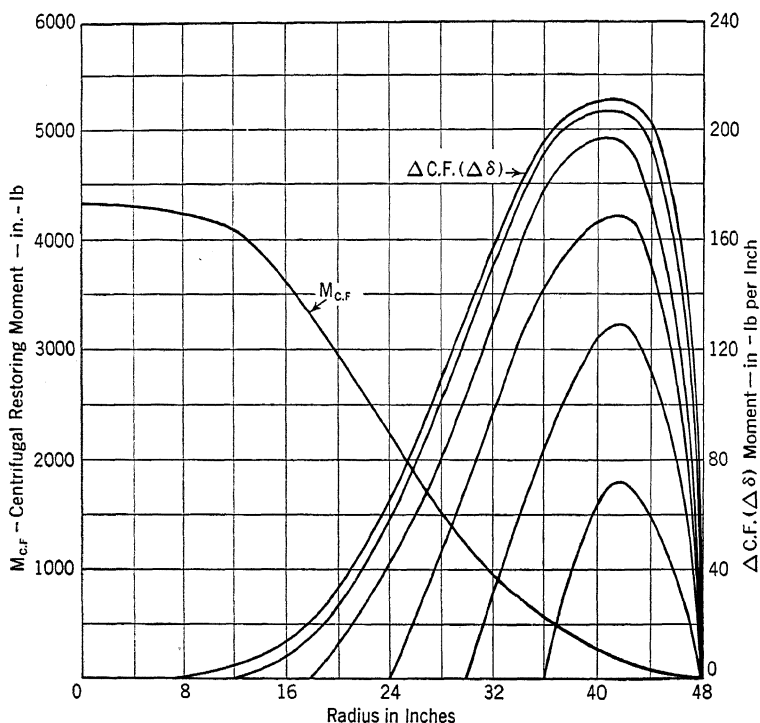


FIG. 3-17. Centrifugal restoring moment due to blade deflection.

tions for each station inboard of the tip yields the $\Delta \text{C.F.} \times \Delta \delta$ curves. The area under these curves is the total centrifugal restoring moment for the reference station, and this value becomes the ordinate of the $M_{\text{C.F.}}$ curve at that point.

The net bending moment is now the uncorrected moment of Fig. 3·14 minus the centrifugal restoring moment of Fig. 3·17. If this net moment does not closely approximate the estimated moment, it will be necessary to make another assumption and repeat. It is usually possible to obtain a good agreement between estimated and net moments with two estimations. In the present instance it would not be necessary to repeat the

calculations. The centrifugal restoring moment calculations follow. In the right-hand column the estimated moment is tabulated for comparison with the net moment.

CENTRIFUGAL RESTORING MOMENT CALCULATIONS

Station	$\Delta\delta$ (in.)	Δ C.F. (lb/in.)	Δ C.F. \times $\Delta\delta$ (in.-lb/in.)	$M_{C.F.}$ (in.-lb)	Uncorrected Moment (in.-lb)	Net Moment (in.-lb)	Estimated Moment (in.-lb)
12	0	1084	0	4131	8490	4359	4370
18	0.0136	1227	16.9				
24	0.0460	1317	60.9				
30	0.1000	1292	129.2				
33	0.1752	1106	193.9				
42	0.2660	783	208.1	3314	6030	2716	2740
18	0	1227	0				
24	0.0324	1317	42.7				
30	0.0864	1292	111.7				
36	0.1616	1106	178.4				
42	0.2524	783	197.5	2334	3820	1486	1530
24	0	1317	0				
30	0.0540	1292	69.9				
36	0.1292	1106	142.7				
42	0.2200	783	172.0				
30	0	1292	0	1348	2020	672	717
36	0.0752	1106	82.9				
42	0.1660	783	129.8				
36	0	1106	0	542	750	208	263
42	0.0908	783	71.1				

In calculating the thrust bending stresses the formula $f_b = My/I$ is used where

M = the net bending moment in inch-pounds.

y = the distance from the neutral axis to the outermost fiber in inches.

I = the minimum moment of inertia (in.⁴).

f_b = bending stress in pounds per square inch.

The thrust force is assumed perpendicular to the chord of the blade section, and the neutral axis parallel to the chord through the section

center of gravity. The blade chord is also assumed to lie in the plane of rotation at all stations. These assumptions result in comparatively small errors and greatly simplify the procedure. They are normally absorbed in the stress analysis by generous margins of safety, as discussed later. Figure 3-18 shows the various relationships.

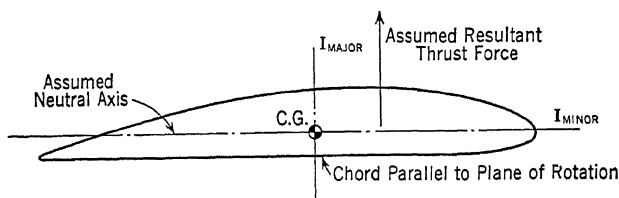


FIG. 3-18. Blade bending stress assumptions.

The blade torque force may be analyzed in the same fashion as thrust bending and added to the preceding results. Owing to the greatly increased blade stiffness about the major axis, it is not necessary to correct for centrifugal restoring moment. The blade torque effect is, however,

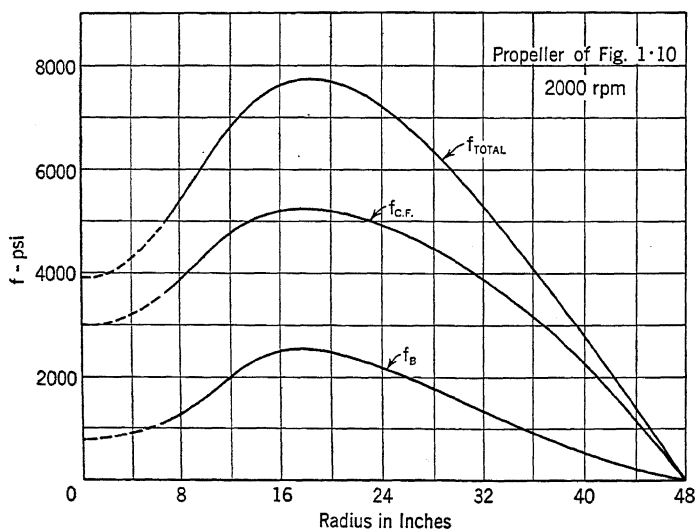


FIG. 3-19. Combined stresses on blade thrust face.

negligible except for the extreme shank portion of the blade and is neglected in this analysis.

Bending stresses caused by the forward thrust loading are compression on the back or camber side of the blade section and tension on the thrust face. When the centrifugal tension load is added to the bending load

the critical tension stress occurs on the thrust face. Figure 3-19 gives a curve of combined stresses on the thrust face. A summary of the calculations follows.

TOTAL STEADY STRESS CALCULATIONS

Station (in.)	I_{\min} (in. ⁴)	y (in.)	M_{net} (in.-lb)	f_b (lb/sq in.)	$f_{\text{C.F.}}$ (lb/sq in.)	f_{total} (lb/sq in.)
12	1.962	0.895	4359	1990	4835	6825
18	0.539	0.498	2716	2510	5250	7760
24	0.249	0.378	1486	2255	4935	7190
30	0.128	0.308	672	1618	4200	5818
36	0.058	0.243	208	876	3200	4076
42	0.020	0.185	40	366	1760	2126

Blade Tilt

The effect of blade tilt would be included in the preceding calculations of net bending moment by modifying the offsets for the centrifugal restoring moment calculations. A small amount of tilt serves to relieve the bending stresses under normal flight conditions, and it has been the practice to use approximately $\frac{1}{2}^\circ$ forward tilt with steel and aluminum-alloy blades in conventional designs. The amount of tilt is essentially a compromise, as it would vary for different flight conditions as the ratio between rpm and thrust varied.

Usually the center of gravity of all blade sections lies on a straight line known as the blade axis, which also coincides with the center of blade rotation in the hub for controllable-pitch propellers. If there is any offset of the center of gravity present, the centrifugal restoring moment must also include this effect.

Torsional Deflections

It is to be expected that some torsional deflection, in addition to the bending deflection, would exist for a propeller blade under the operating loads. This deflection would change the blade angle at each station and therefore affect the calculated performance and stress analysis somewhat. Test data have shown this effect to be negligible for conventional aluminum-alloy blades, and it is therefore probable that no appreciable error is introduced by neglecting it.¹¹

¹¹Hartman and Biermann, "Torsional and Bending Deflection of Full-Scale Aluminum Alloy Propeller Blades Under Normal Operating Conditions," *NACA Tech. Rept. 644* (1938).

Aerodynamic Blade Torque

As previously stated, blade torque forces have a negligible effect on blade stress, but they are the predominant forces acting upon the pitch-changing mechanism. Aerodynamic blade torque is normally very small compared with centrifugal blade torque and is usually disregarded as a torque force. As the aerodynamic center of pressure is ordinarily ahead of the center of rotation (center of gravity) of the blade section, the usual effect is to increase the blade angle. However, with the advent of exceptionally wide blades for high disk loadings, the aerodynamic torque increases rapidly. It may be evaluated by graphically integrating the aerodynamic moment at each section and adding to the result the moment due to the thrust force offset from the center of blade rotation. Aerodynamic blade torque is neglected in the present example.

Centrifugal Blade Torque

Centrifugal blade torque is an appreciable quantity and may be visualized best by considering the blade element as two concentrated masses at the leading and trailing edges. The effect of centrifugal force will be to create both a force perpendicular to the plane and a force in the plane of the blade element. The former causes direct tension, whereas the latter combination tends to reduce the blade angle. This effect is shown in Fig. 3-20. Centrifugal blade torque may be evaluated by means of the following expression.¹²

$$Q_b = \frac{\delta}{g} \omega^2 \int_0^R (I_{\max} - I_{\min}) \sin \beta \cos \beta \cdot dr \quad [2]$$

where δ = density of blade material in pounds per cubic inch.

ω = angular velocity in radians per second.

g = acceleration due to gravity in inches per second per second.

β = blade angle in degrees.

Q_b = centrifugal twisting moment per blade in inch-pounds.

The quantity within the integral sign varies for each blade section and must therefore be plotted versus radius and graphically integrated. The total torque per blade will then be the integral multiplied by the constant. This may be repeated for several different blade angles to determine the maximum value of the blade torque. Figure 3-21 gives the results of calculations made for the blade of Fig. 1-10.

It will be noted that the expression for Q_b is a maximum for any section at a blade angle of 45° , decreasing to zero at 0° and 90° . For con-

¹² Younger and Woods, "Dynamics of Airplanes," John Wiley and Sons (1931), pp. 240-242.

ventional propeller blades the maximum twisting moment usually occurs near a blade angle of 35° at the three-quarter radius. For a 12-ft diameter, aluminum-alloy propeller this quantity approximates 10,000 in.-lb per blade. Once the maximum value is determined or any two widely separated values are obtained, a complete curve of torque versus blade angle may be completed, using the $\sin \beta \cos \beta$ relationship as shown in Fig. 3-22. A curve of this type is important in determining peak loads for the pitch-changing mechanism.

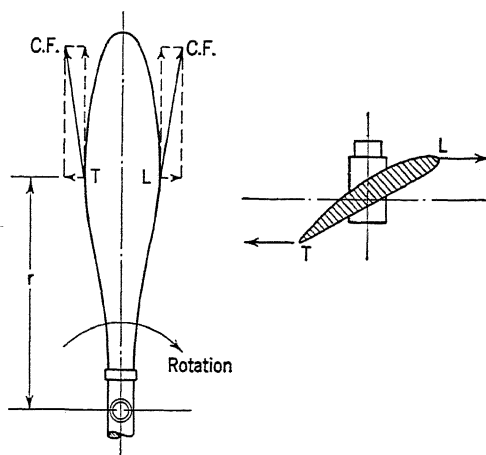


FIG. 3-20. Centrifugal blade torque forces.

Blade Counterweight Action

In order to reduce the centrifugal blade torque effect on the pitch-changing mechanism, the blades are often counterweighted. In the Hamilton Standard constant-speed propeller, the counterweights were incorporated as part of the pitch-changing mechanism, whereas in early Curtiss designs the counterweights were attached rigidly to the blade shank.

Considering the counterweight as a concentrated mass fastened to the blade shank radially outward a distance r and at the length B from the blade axis of rotation as in Fig. 3-23, the following relationships are obtained.

$$\text{C.F.} = \frac{W}{g} \omega^2 \sqrt{r^2 + B^2 \cos^2 \delta}$$

$$F_c = (\text{C.F.}) \cos \psi = \frac{W}{g} \omega^2 \sqrt{r^2 + B^2 \cos^2 \delta} \cdot \frac{B \cos \delta}{\sqrt{r^2 + B^2 \cos^2 \delta}}$$

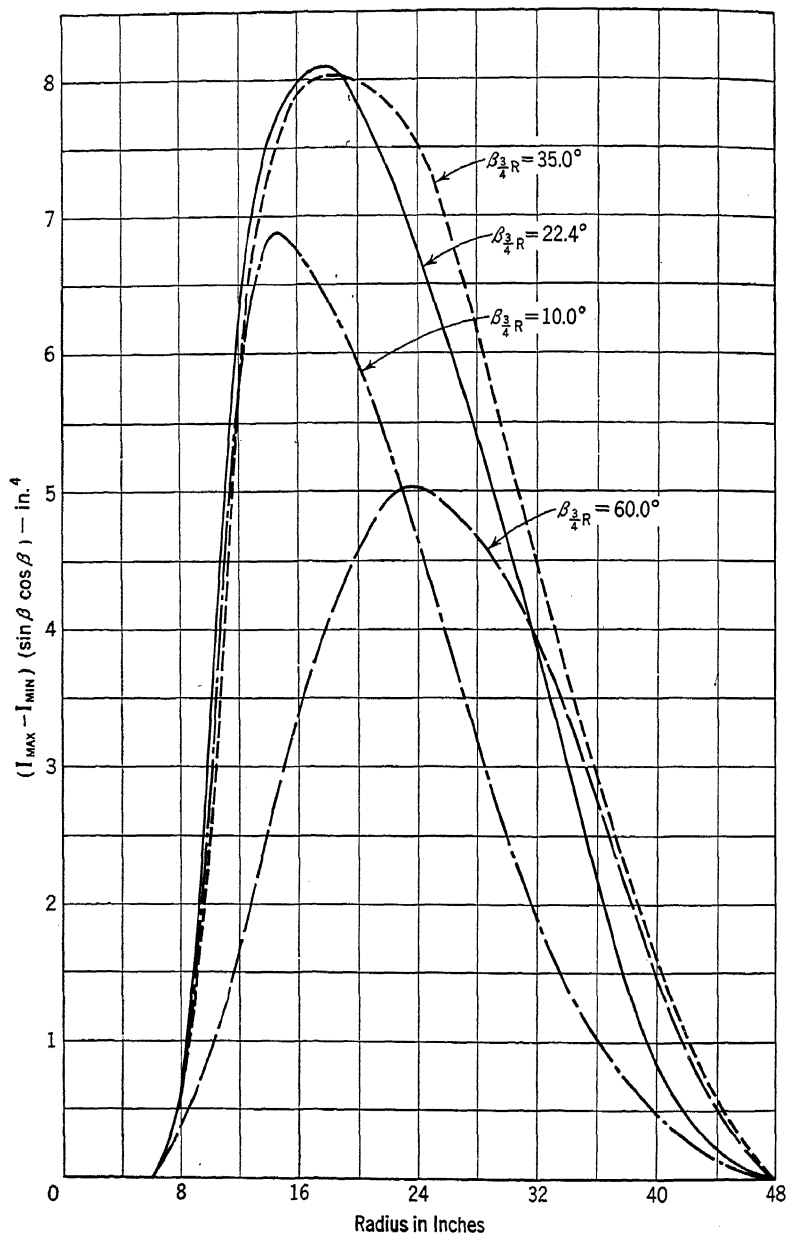


FIG. 3-21. Centrifugal blade torque calculations (propeller of Fig. 1-10).

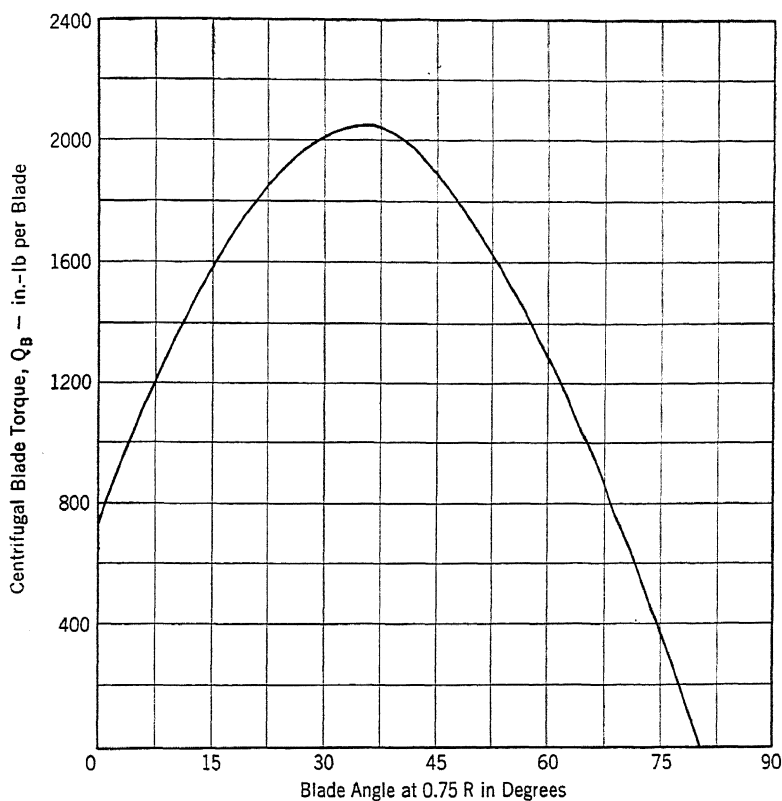


FIG. 3-22. Centrifugal blade torque versus blade angle at 2000 rpm (propeller Fig. 1-10).

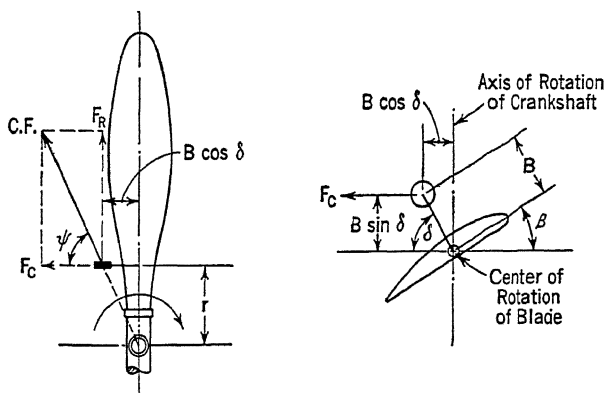


FIG. 3-23. Blade counterweight action.

or

$$F_c = \frac{W}{g} \omega^2 B \cos \delta$$

$$Q_{cx} = F_c \cdot B \sin \delta = \frac{W}{g} \cdot \omega^2 B^2 \cdot \sin \delta \cos \delta \quad [3]$$

where W = weight of counterweight in pounds.

g = acceleration of gravity in inches per second per second.

ω = angular velocity of rotation in radians per second.

B = counterweight arm length in inches.

δ = counterweight angular position in degrees from plane of rotation.

It will be noted that the counterweight effect is independent of r , and therefore the counterweights may be attached at any radial point along the blade without affecting their action. Owing to vibration they are usually attached as close to the center of rotation as possible. Note also that the counterweight torque is a maximum when the angle δ is 45° . Hence, to obtain the most benefit the counterweight is set so that δ is 45° when the blade is at the angle of maximum centrifugal blade torque. If the counterweight torque equals the centrifugal blade torque at this position they will then be equal at all rpm and blade angles, since both quantities vary as the square of the rpm and as $\sin \delta \cos \delta$.

Variation of Blade Stress with RPM

At any given V/nD and blade angle the thrust coefficient C_T is constant.

Since

$$T = C_T \rho n^2 D^4$$

the thrust bending moment $M_T \sim n^2 D^5$. Also

$$\text{C.F.} = (2\pi n)^2 \cdot \frac{\delta}{g} \int_0^R A \cdot r \, dr \sim n^2 D^4$$

and the centrifugal restoring moment $M_{\text{C.F.}} \sim n^2 D^5$. Therefore the net bending moment

$$M_{\text{net}} = M_T - M_{\text{C.F.}} \sim n^2 D^5$$

$$f_b = \frac{M_{\text{net}}}{D^4} \sim \frac{n^2 D^5 \cdot D}{D^4} \sim n^2 D^2$$

$$f_{\text{C.F.}} = \frac{\text{C.F.}}{A} \sim \frac{n^2 D^4}{D^2} \sim n^2 D^2$$

It may therefore be said that for any given V/nD with geometrically similar propellers of the same material, the steady stress is proportional to the square of the tip speed.

Allowable Steady Stresses

The relationship between steady stress and vibratory stress will be discussed later. Steady stress margins of safety are usually computed on the basis of the fatigue strength of the material because of their close relationship in propeller work. Reference may be made to the material at the beginning of this chapter for the fatigue strength of common blade materials. Figure 3-19 gives

$$\text{Margin of safety} = \frac{14,000}{7,800} - 1 = 79.5\%$$

The maximum allowable rpm for this design would then be: $2000\sqrt{1.795}$ or 2680 under the design conditions.

Gyroscopic Loads

Gyroscopic loads are imposed on the propeller when the airplane is in curvilinear flight. The propeller disk tends to resist rotation of the air-

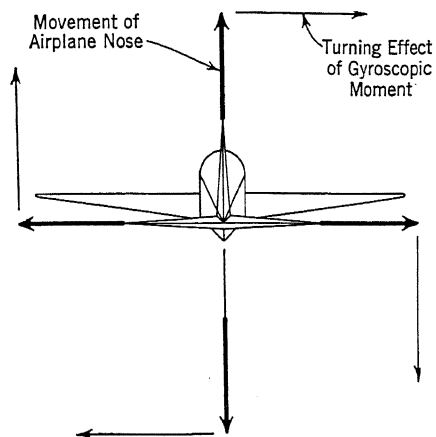


FIG. 3-24. Gyroscopic action.

plane, and thereby it imposes a bending moment on both the blade shank and the propeller shaft. The action of the propeller is to attempt to align its plane of rotation with that of the airplane. Thus, for a right-hand propeller¹³ one may obtain a diagram of forces acting as in Fig. 3-24, which shows the tendency of the gyroscopic moment to swing the

¹³ Rotating clockwise when viewed from the cockpit.

nose of the airplane when the nose is moved in any one of the four directions indicated. This diagram refers to motion as viewed from the airplane cockpit.

For the blade shank the gyroscopic bending moment follows a sinusoidal variation, making a complete cycle once each revolution. For the propeller shaft, the nature of the gyroscopic moment depends upon the type of propeller: for a two-bladed propeller, the moment varies from zero to a maximum twice each revolution whereas for three-bladed and four-bladed propellers the moment is constant. The maximum shaft bending moment is the same for both two- and four-bladed propellers. The maximum gyroscopic bending moment at the blade shank may be formulated as follows.¹⁴

$$M = 2I\Omega\omega \quad [4]$$

where M = gyroscopic moment in foot-pounds.

I = propeller blade mass moment of inertia about the center of rotation in slugs-ft².

ω = angular velocity of propeller about its shaft in radians per second.

Ω = angular velocity of airplane in yaw or pitch in radians per second.

For a conventional solid aluminum-alloy propeller blade, the radius of gyration is approximately 55 per cent of the radius. Hence, for a 12-ft diameter propeller having a blade weighing 60 lb and rotating at 1440 rpm, the blade root bending moment may be calculated directly for a given airplane rate of rotation.

$$\text{Radius of gyration} = 0.55 \times 6 = 3.30 \text{ ft}$$

$$I = \frac{60}{32.2} \times 3.30^2 = 20.3 \text{ slug-ft}^2$$

$$\frac{1440 \times 2\pi}{60} = 151 \text{ rad/sec}$$

Assume $\Omega = 1$ rad/sec yawing velocity in a flat spin, then

$$\begin{aligned} M &= 2 \times 20.3 \times 151 \times 1 \\ &= 6,130 \text{ ft-lb or } 73,600 \text{ in.-lb} \end{aligned}$$

blade root bending moment with a frequency of 1440 cycles per min.

¹⁴ Development of this formula may be found in most books on dynamics. See Younger and Woods, "Dynamics of Airplanes," John Wiley and Sons (1931), p. 32.

It will be seen from the preceding example that the gyroscopic bending moment can become appreciable on both the blade shank and propeller shaft during such maneuvers as power-on spinning, quick-turns, push-overs, etc. Fortunately the load is of short duration and occurs when the steady stresses are ordinarily not at their peak so that a propeller blade designed to withstand the maximum normal steady loads is usually satisfactory under the momentary gyroscopic loads, although certain flight maneuvers may be prohibited by this loading condition.

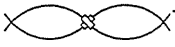
Vibratory Stresses

Torque impulses from the engine, motion of the engine on its elastic mounts, aerodynamic excitation from the blades passing near the fuselage or wing—all these and many more disturbances set up vibration in the propeller blade. Whenever the frequency of the forcing function coincides with one of the natural frequencies of the blade there is the possibility of a dangerous resonance condition arising which may result in a blade failure from fatigue due to excessive vibratory stresses, even though the steady stresses may be very low.

The many variables existing in both the disturbing forces and in the blade design make it exceedingly difficult to attempt a rigorous mathematical analysis of the vibration problem although some work has been done along this line.¹⁵

The natural frequencies may be readily determined experimentally by suspending the propeller horizontally on a shock cord or similar low-frequency support and mounting a variable speed vibrator on the hub. If sawdust or a like material is sprinkled over the blade it will collect at the nodal points when the vibrator runs at a resonant frequency. Electric contacts may be used at the blade tips to determine whether they are in phase.¹⁶ Observations are made over a range of blade angles.

There are a great many natural frequencies of a propeller, and they may be divided into three classes shown in the accompanying table.

TYPE	DESCRIPTION	BLADE MOTION	SYMBOL
Symmetrical	In phase		1L, 2L, etc.
Unsymmetrical	Out of phase		1N, 2N, etc.
Torsional			

¹⁵ Ramberg, Ballif, and West, "A Method For Determining Stresses in a Non-Rotating Propeller Blade Vibrating with a Natural Frequency," *Journal of Research of the National Bureau of Standards*, Vol. 14 (1935), p. 196.

¹⁶ H. H. Couch, "Propeller-Crankshaft Vibration Problems," *Air Corps Information Circular 703* (1936).

In the symmetrical type of vibration all blades are vibrating in phase, the hub being an anti-node or loop. In the unsymmetrical type the blades are out of phase, and the hub is a nodal point. The symmetrical and unsymmetrical vibration frequencies usually group in pairs and are referred to as 1L, 1N, 2L, 2N, etc., where the number represents the harmonic and N signifies a node and L a loop at the hub. The natural frequency in torsion leaves a sawdust pattern approximating a straight

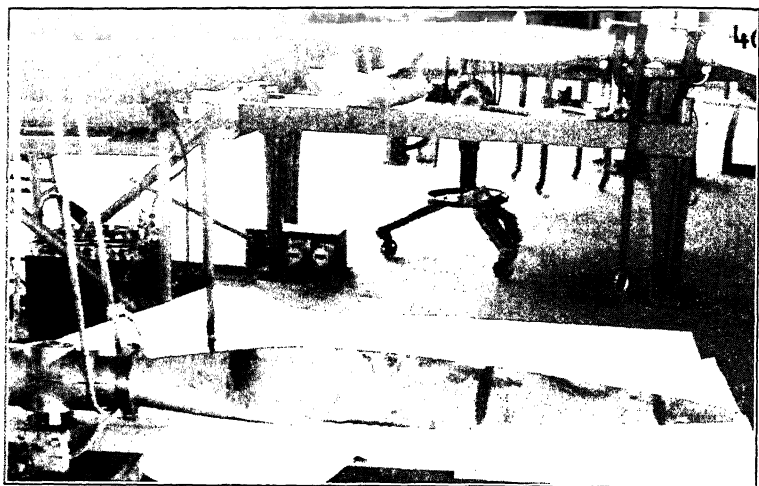


FIG. 3-25. Three-node-per-blade vibration pattern in static resonance. (Official photograph, U.S. Army Air Force.)

line parallel to the blade axis, and it usually occurs near the fourth harmonic. A pattern of the three-node-per-blade type is shown in Fig. 3-25.

The natural frequency of the propeller at rest will increase in operation because of the stiffening effect of centrifugal force on the rotating blade, and this effect may be evaluated by use of the following formula.¹⁷

$$f_R = \sqrt{f_0^2 + cN^2} \quad [5]$$

where f_R = frequency under rotation in cycles per minute.

f_0 = frequency at rest in cycles per minute.

N = rate of rotation in revolutions per minute.

c = coefficient depending on the mode of vibration and the blade shape.

¹⁷ Theodorsen, "Propeller Vibrations and the Effect of Centrifugal Force," *NACA Tech. Note 516* (1935).

The values of c given below are recommended for conventional metal blade designs.

TYPE OF VIBRATION	c
1L and 1N	1.7- 2.0
2L and 2N	6.0- 6.2
3L and 3N	12.0-12.2

With the preceding corrections, the natural frequencies for a given blade angle may be plotted versus engine rpm and the known forcing functions superimposed, as in Fig. 3-26. The engine forcing functions are for a nine cylinder, single-row, direct-drive radial engine.¹⁸ The various intersection points are all possible danger points and should be carefully investigated. The critical conditions may be definitely checked by means of blade vibration stress pickups.

Vibration Stress-Measuring Equipment

Since 1933 experiments have been carried out on various forms of vibration indicators for determining the frequency, amplitude, and types of vibration occurring in the propeller in actual operation on the engine. The difficulty has been to obtain a light-weight pickup that could be mounted on the propeller blade and give accurate readings of the preceding quantities. Early types included Rochelle salts crystals fastened to the blade so that bending of the blade under vibration varied the pressure on the crystal. The resulting electrical output from the crystal was then carried through fine wires in to a slip ring on the propeller hub and out to a stationary amplifier and oscillograph where a record was obtained. A magnetic-type pickup was also used in which the gap between a permanent magnet and a set of pickup coils with a soft-iron core varied under blade bending and generated a current in the coils. Both of these early types were relatively complicated and subject to various sources of error. A modified carbon pile pickup has been developed in recent years in which an insulated flat carbon strip is cemented to the blade surface and the change in resistance, due to a change in pressure caused by blade bending, is measured on an electric circuit. The circuit consists essentially of a battery, the pickup and a matching resistance, an amplifier, and recording oscillograph.¹⁹ Fine wires soldered to the ends of the pickup run along the blade to the hub where they connect to slip rings and out to the stationary recording equipment. The

¹⁸ F. W. Caldwell, "Vibration Problem in Aircraft Propeller Designing," *SAE Journal* (August, 1937), pp. 372-380.

¹⁹ F. W. Caldwell, "Vibration Problem in Aircraft Propeller Designs," *SAE Journal* (August, 1937), pp. 372-380. Also "Propellers for Aircraft Engines of High Power," *Journal of the Aeronautical Sciences*, Vol. 5, No. 2 (December, 1937), p. 37.

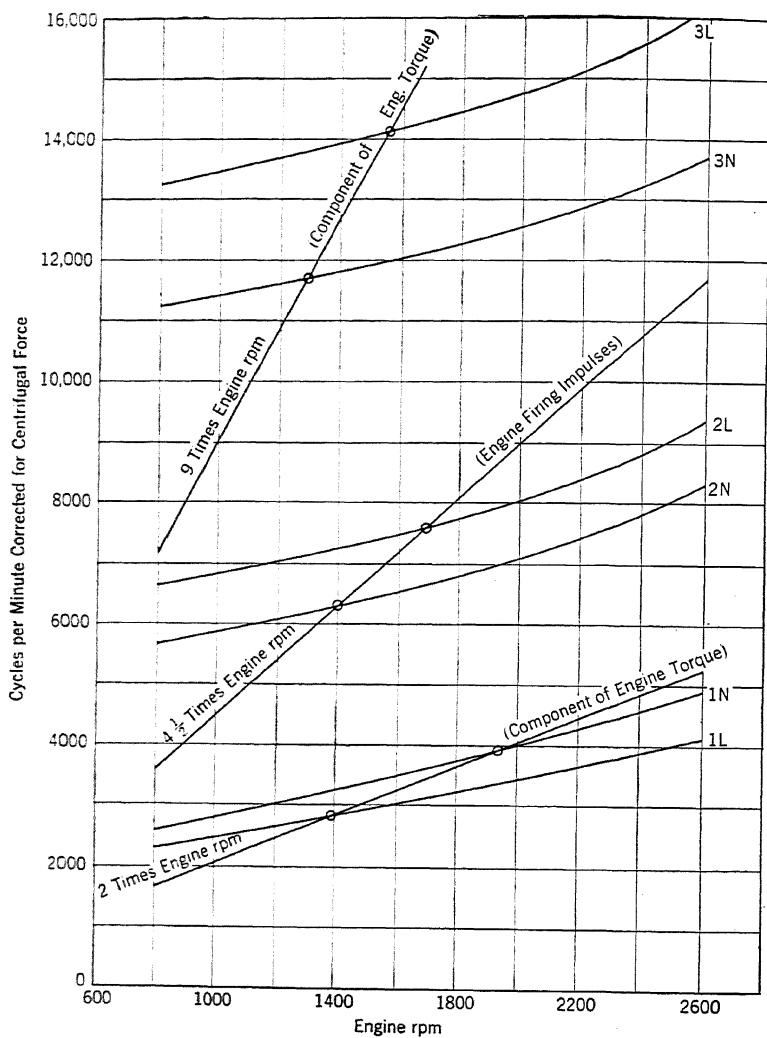


FIG. 3-26. Predicted resonance speeds for engine-propeller combination.

pickups must be mounted with their axes parallel to the direction of the stress to be measured. An oscillograph record might approximate the trace shown in Fig. 3-27.

The pickup, amplifier, and oscillograph combination may be calibrated by mounting the pickup on a cantilever beam of the blade material and vibrating it with a known frequency and amplitude. The amplitude of the oscillograph record may then be converted to pounds per square inch of stress, and the distance between critical peaks on the record establishes the frequency.

In any vibration analysis several pickups are mounted on each blade—both near the tip and around the shank—as these points are critical. The entire range of engine speeds is usually checked at 50-rpm intervals at constant-manifold pressure. The individual records are then analyzed for critical stresses and frequencies, and a composite picture is obtained, such as given by Fig. 3-28.²⁰ Definite peaks in this curve indicate a resonant condition.

Resonant conditions, if they are of dangerous proportions, must either be eliminated or avoided. Dynamic dampers on the engine crankshaft tuned to the proper frequency have helped to eliminate some very bad conditions in recent designs. Sometimes a change in blade diameter, if permissible, will help. A change in the elastic engine mount system may be helpful. If the condition cannot be eliminated it must then be avoided. It has sometimes been necessary to issue operating limitations on engine cruising rpm with a specific blade design. In addition to blade vibration stress measurements, records are also taken of engine motion along its three axes and of engine crankshaft torsional vibration because of the interrelationship of these three items.

Further isolation of the propeller from engine vibrations by means of an extension shaft or an elastic driving system may make possible an appreciable weight reduction because the most critical stresses are vibration stresses. Aluminum-alloy blades in particular are comparatively easy to nick in service, and this may result in a lowering of the fatigue strength to one-half of its original value. The nick acts as a stress concentration point, and photographs of failed blades show constantly widening circles of material failure centered around the nick as shown in item 7 of Fig. 3-29. The loss of an appreciable portion of the blade in flight may cause an unbalance sufficient to pull the engine from its mount with serious consequences.

²⁰ F. W. Caldwell, "Propellers For Aircraft Engines of High Power," *Journal of the Aeronautical Sciences*, Vol. 5, No. 2 (November, 1937), p. 51.

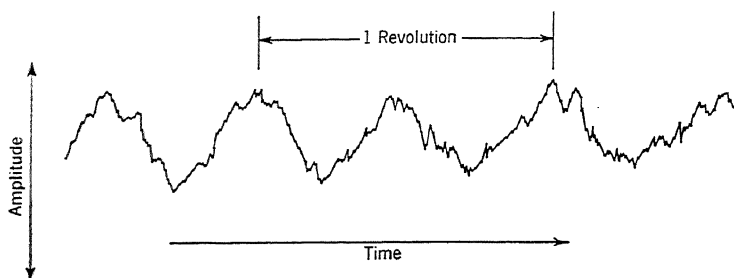


FIG. 3-27. Oscillograph record.

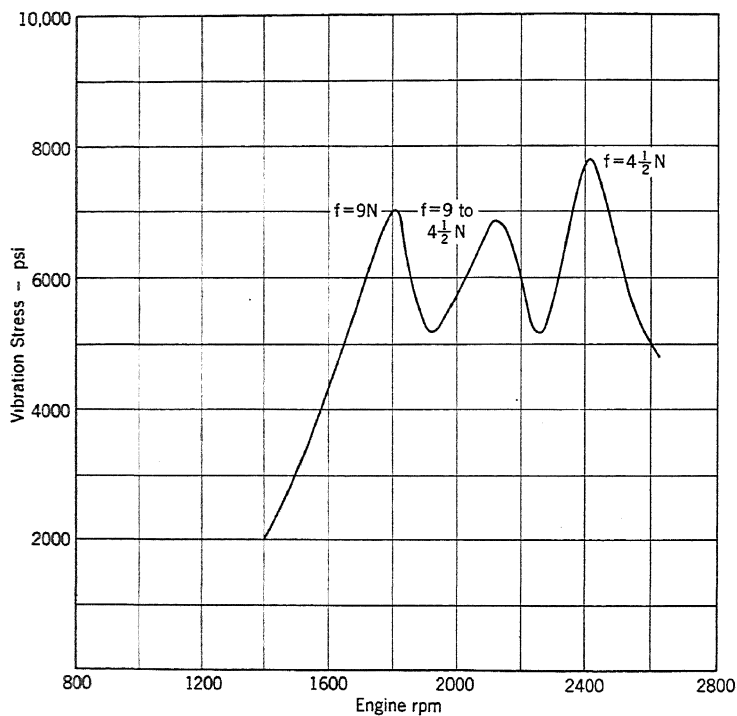


FIG. 3-28. Composite vibration stress curve for blade tip.

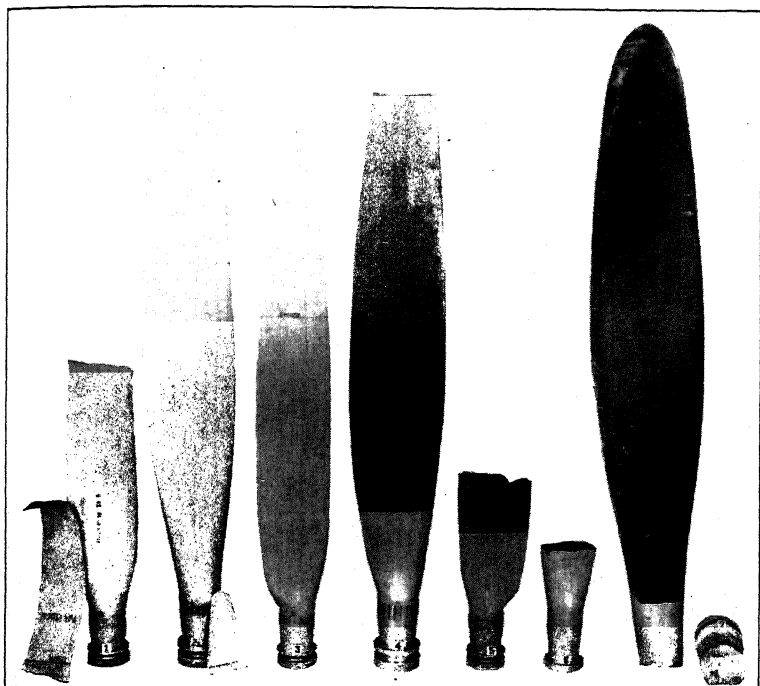


FIG. 3-29. Typical propeller vibration blade failures. (*Official photograph, U.S. Army Air Force.*)

Relation between Steady Stress and Vibration Stress

Extensive fatigue tests have indicated a general relationship between steady and vibration stresses which may be expressed in the form of a Goodman diagram. Such a diagram is drawn up for aluminum alloy 17ST in Fig. 3-30.²¹ The linear relationship between maximum alternating stress and tensile strength is an approximation to the available test data. Locate the point of steady stress along the steady stress line and read vertically the maximum and minimum fatigue limits.

On the basis of this type of diagram it would seem that fairly exact margins of safety could be computed from the steady stress analysis and vibration stress measurements. Actually, service conditions distort this picture somewhat. Vibration stresses must not become excessive owing to the adverse effect of scratches and nicks which may occur in operation. The various blade manufacturing processes may lower the fatigue strength appreciably below that of the virgin metal. The fatigue

²¹ Battelle Memorial Institute, "Prevention of Fatigue of Metals," John Wiley and Sons (1941), pp. 130-135, Fig. 113.

strength of a welded steel blade joint, for example, may be one-half that of the virgin metal.

Aluminum-alloy blade tip vibratory stresses of $\pm 5,000$ lb per sq. in. have been considered satisfactory, and steel blade tip stresses are held

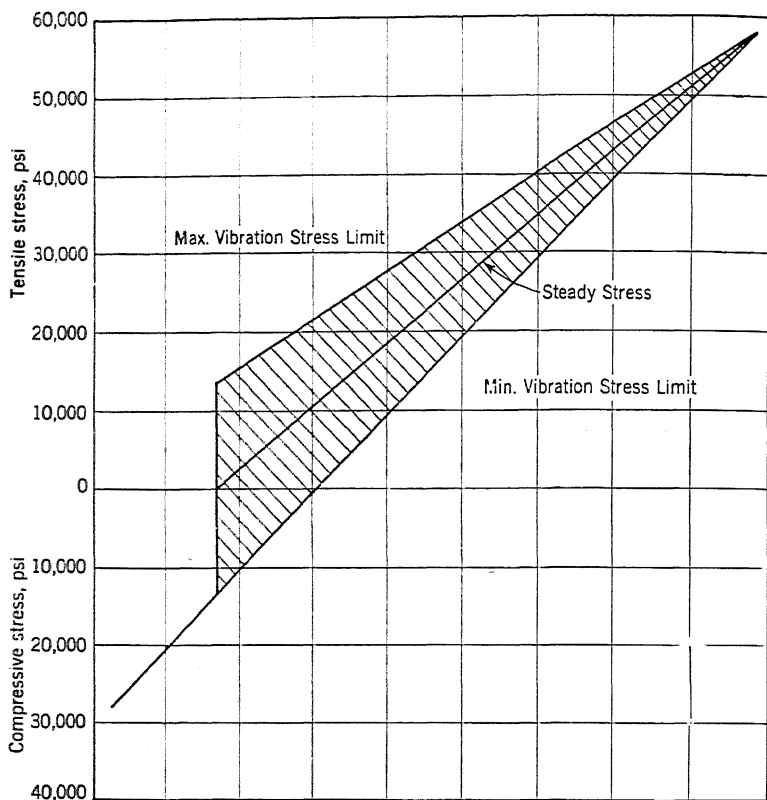


FIG. 3-30. Modified Goodman diagram for 17ST aluminum alloy for direct tension-compression tests.

to a maximum of $\pm 12,000$ lb per sq in. Shank stresses are kept to approximately one-half this amount. Steady stresses for steel blades are usually below 25,000 lb per sq in. and for aluminum-alloy blades below 14,000 lb per sq in. One may visualize the steady stress analysis as a method of proportioning the blade material while vibration stress measurements serve to define danger points in operation.

Propeller Strength Tests

Fixed-pitch wood propellers are used chiefly on small airplanes under private ownership and as such are licensed by the Civil Aeronautics

Administration. This agency requires completion of a ten-hour endurance block test run at the desired rpm on an internal-combustion engine

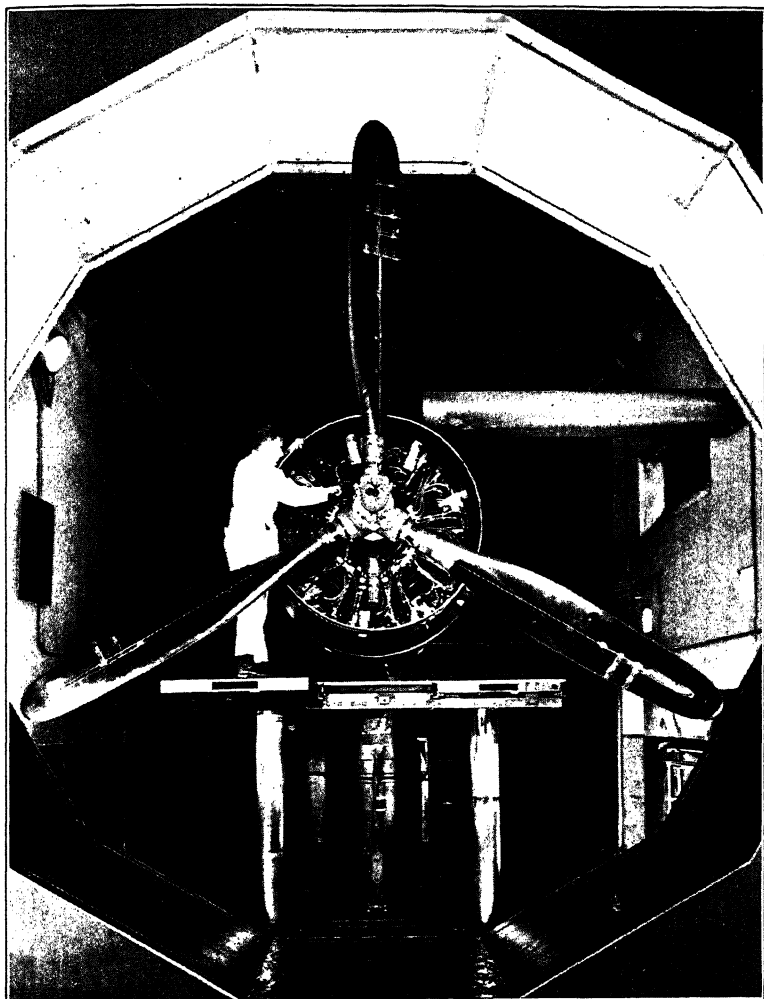


FIG. 3-31. Engine-propeller test stand. (Courtesy Curtiss Propeller Division, Curtiss-Wright Corp.)

with the propeller at maximum pitch.²² Such a test subjects the propeller to the maximum centrifugal and thrust loading in addition to heavy vibratory loads due to engine torque impulses. Any signs of

²² Fifty-hour flight test may be substituted.

cracks, loose tipping, elongated hub bolt holes, etc., are causes for rejection.

Metal propellers are approved by both the Civil Aeronautics Administration and the military services. At the present time this type of propeller is subjected to tests of the following nature:

a. 50–100 hour endurance test on the propeller and engine at rated engine power and rpm.

b. Short-time endurance test on engine at takeoff engine power and rpm.

c. Electric whirl rig test at 200 per cent takeoff engine power.

d. Electric whirl rig test at 140 per cent rated engine rpm.

e. Additional engine and propeller testing, if necessary, at points shown to be critical by vibration stress measurements.

Although propellers are not approved on the basis of a steady stress analysis, such an analysis is essential to the designer. Owing to the critical nature of the vibratory loads and also in order to determine the soundness of the propeller construction, it is necessary to obtain sufficient actual test data for final approval. Tests of the propeller and engine combination are run in special test cells equipped to reduce the noise of testing and to make accurate measurements of engine power and rpm. Note the vibration stress pickups mounted on each blade in Fig. 3-31.

PROBLEMS

1. Based upon a uniform pitch distribution, calculate the blade angle at 12-in. intervals on a 10-ft diameter propeller for 120 mph and an engine rpm of 3000 (geared 16 : 11).

2. Calculate and plot a p/D curve for the propeller of Fig. 1-10, set at a blade angle of 35° at 0.75 radius.

3. Analyze the aluminum-alloy propeller blade of Fig. 1-10 as a controllable-pitch design, and determine the margin of safety, with a static thrust of 510 lb per blade and 2200 engine rpm (direct drive).

4. Design a pair of counterweights to counterbalance the centrifugal blade torque of the propeller of problem 3 at all blade angles, keeping the counterweight arm length at 5 in. Give weight and index angle of $180^\circ - \beta - \delta$.

5. Calculate the blade root bending moment for the propeller of Fig. 1-10, rotating at 2000 rpm in a loop at a rate of 2 rad/sec.

6. Using the Goodman diagram of Fig. 3-30, determine the allowable vibrating stress for the face of the propeller of Fig. 1-10 under the critical steady stress of Fig. 3-19.

7. The Luscombe airplane uses a fixed-pitch wood propeller of 45-in. pitch (based on 0.75 radius) and 76-in. diameter. With 2150 engine rpm at a cruising velocity of 90 mph calculate the angle of attack at 0.75 radius and check to see if it falls within the maximum L/D range of Fig. 1-5.

CHAPTER 4

HUB DESIGN AND STRESS ANALYSIS

Propeller hub design has become increasingly complex on modern, high-performance aircraft. To the primary hub function of blade retention has been added the necessity for blade rotation during flight. In addition, some suitable means of governing the engine-propeller combination must be provided. A discussion of the various designs grouped under the three main propeller classifications follows.

Fixed-Pitch Propellers

Fixed-pitch propellers made of wood have a steel hub which is bolted to the propeller boss and splined (or tapered and keyed) to the engine crankshaft. The design shown in Fig. 4-1 is typical. It employs a front

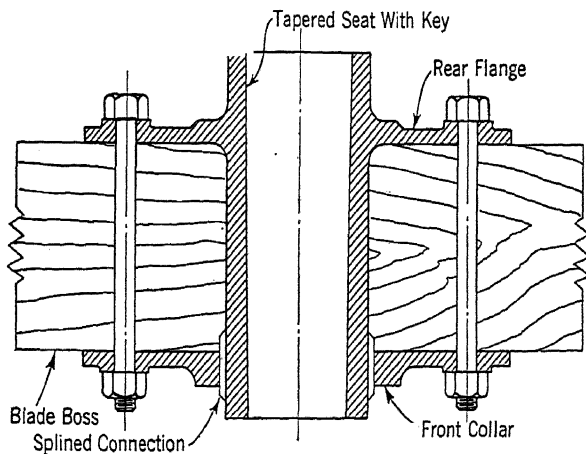


FIG. 4-1. Liberty hub for fixed-pitch wood propeller.

collar which is splined to the hub. The rear flange is forged integral with the shank, and a circle of bolts connect the front collar and rear

Curtiss-Reed one-piece forged aluminum-alloy propellers have a steel insert at the boss which is splined into the aluminum and internally tapered or splined to mate with the engine crankshaft.

Adjustable-Pitch Propellers

Adjustable-pitch propellers have a split hub, machined in two halves with an external clamping ring for clamping the hub shoulder securely around the blade shank (refer to Fig. 1-1). The aluminum-alloy, steel, and impregnated-wood blades use a steel forging for the hub whereas the lighter wood blades use an aluminum-alloy forging. A typical hub for use with aluminum-alloy blades is shown in Fig. 4-2. This hub is splined to the engine crankshaft, and therefore it requires a front and rear cone for positioning and seating on the crankshaft. The front cone

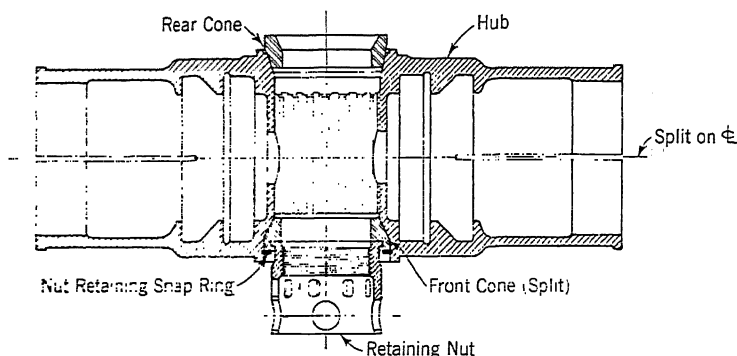


Fig. 4-2. Adjustable-pitch propeller hub assembly.

is split so that the hub nut rotates within it. After the hub nut is tightened a snap ring is inserted. This arrangement allows the hub nut to pull the front cone first when it is loosened. It then bears against the snap ring and finally pulls the hub from the rear cone. The dimensions for this type of hub and the mating blade shank dimensions have been fairly well standardized and may be found in the *SAE Handbook*.

Controllable-Pitch Propellers

Controllable-pitch propellers have a variety of hub designs, dependent primarily upon the type of pitch control used. Hydraulic, electric, and mechanical motivation are all possibilities and have been developed.

This type of hub is best discussed according to the manufacturer. The Aeroproducts Division of the General Motors Corporation, Curtiss Propeller Division of the Curtiss-Wright Corporation, and Hamilton Standard Division of the United Aircraft Corporation are all producers of controllable-pitch hubs in this country.

Aeroproducts Division

The Aeroproducts propeller is in military service alone at the present time and may therefore be discussed only in general terms. The center

of rotation is clear to allow the installation of a cannon firing through the propeller shaft. The hollow steel blades (refer to Fig. 3-6) are retained in the hub by a stack of angular contact ball bearings. The hub is a one-piece steel forging. The pitch-change mechanism is located within each hollow blade shank and consists of a cylinder which is dowelled to the blade and a piston which moves radially within the cylinder. These two members are splined together, and the internal spline of the piston mates with a fixed spline member which is dowelled to the hub. The helical spline arrangement is such that an outward movement of the piston causes an increase in blade angle. Bevel gears on each blade shank mesh with a master bevel gear so that all blades are kept at the same angle. High-pressure oil forces the piston in the blade cylinder in or out as necessary to change blade angle, thereby maintaining a constant engine rpm.

A cast-aluminum housing is mounted on the rear of the hub and forms an oil reservoir in which a gear pump and constant-speed governor operate. The gear pump revolves with the casting and rotates with its gear drive meshed with a stationary ring gear positioned on the engine nose. The pump furnishes a source of high-pressure oil which passes through a pressure relief valve to a centrifugal governor which then meters or drains the oil as needed to the piston in each blade shank.

This type of hub requires no modification of the airplane engine. The only connection to the cockpit is a cable control which adjusts the governor to maintain the desired engine rpm. A diagrammatic sectional view of the assembly is given in Fig. 4-3, showing the governor in a decrease-pitch position, corresponding to an underspeed condition.

Curtiss Propeller Division

The Curtiss pitch-changing mechanism consists essentially of a small, reversible electric motor mounted ahead of the hub and operating through a two-stage, planetary speed reducer (approximately 15,000 : 1) to rotate a master bevel gear which meshes with the blade bevel gears to increase or decrease the blade angle as needed. Four slip rings at the rear of the hub transfer electric current from the airplane power supply to the hub motor. The motor is equipped with a solenoid brake to prevent slipping under vibration. The blades are retained in the hub barrel by a set of angular-contact ball bearings held in by a retaining nut. The hub is a one-piece steel forging. Hub and blade assembly are lubricated through Alemite fittings mounted on the speed reducer housing. The complete propeller assembly is shown in Fig. 4-4.

Constant-speed control is accomplished by a fly-ball type of governor mounted on the engine nose. A diagrammatic sketch of this unit is

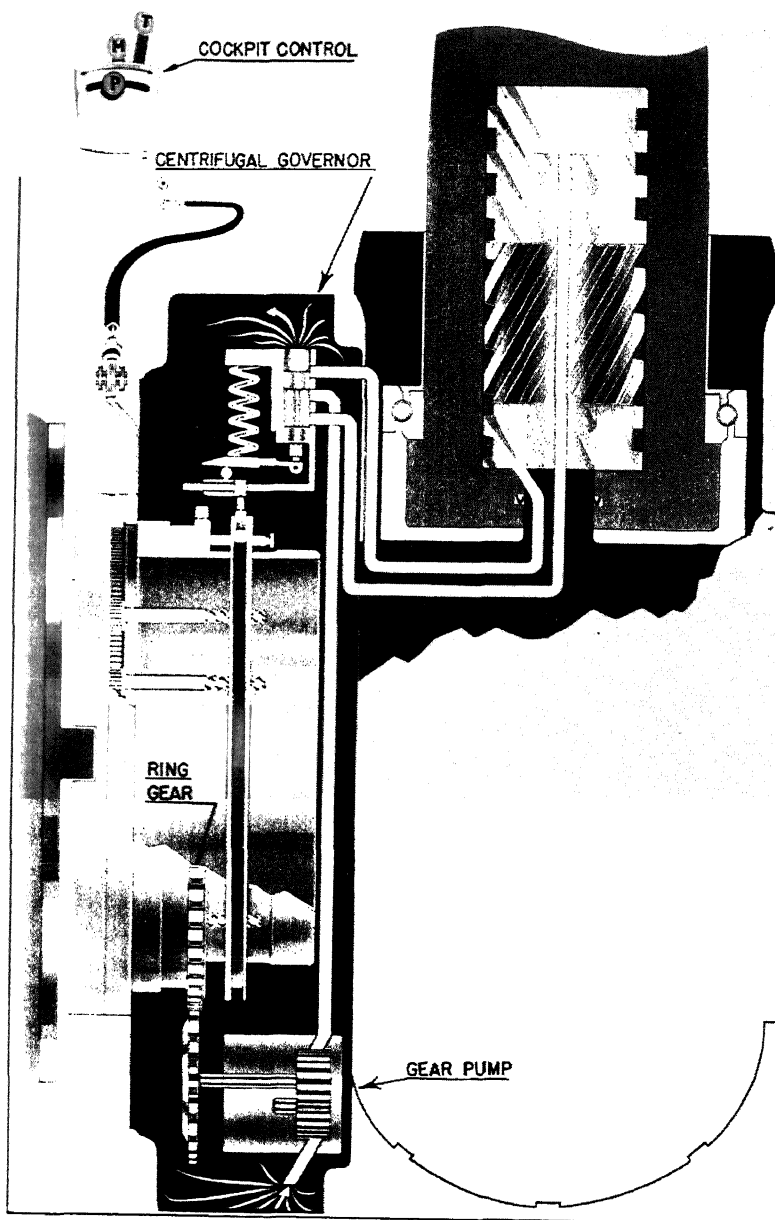


FIG. 4-3. Aeroproducts schematic assembly drawing. (Courtesy Aeroproducts Division, General Motors Corp.)

given in Fig. 4-5. The fly weights are driven directly by the engine and any variation in engine rpm changes their position thereby actuating a hydraulic valve which controls the position of the center contact of the double-throw switch. The outer two contacts of this switch are in a constant state of oscillation, resulting in a proportionalizing type of pitch control. Governor spring tension is controlled by a cable con-

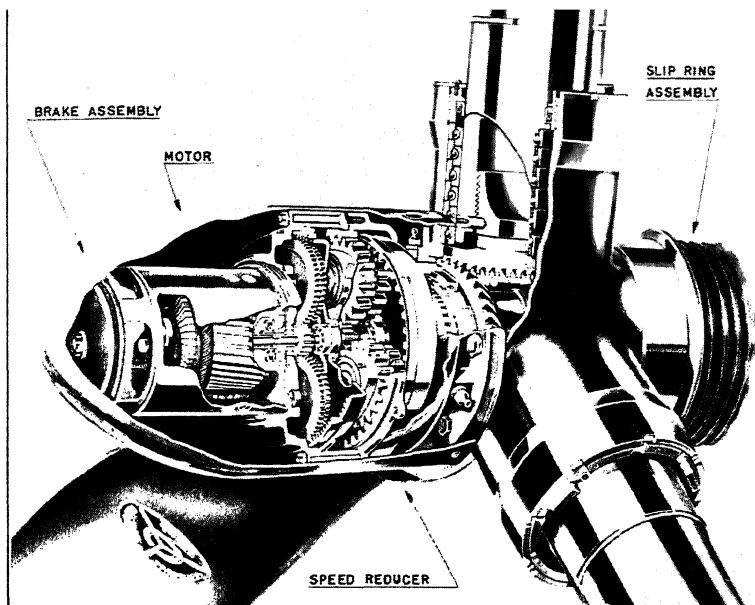


FIG. 4-4. Curtiss propeller assembly. (Courtesy Curtiss Propeller Division, Curtiss-Wright Corp.)

nection to the cockpit which operates through a rack and pinion gear on the governor. With this control the pilot selects the desired engine rpm, and the governor automatically maintains it.

This type of hub will permit a blade angle range from a feathered position of approximately 90° blade angle down to a negative pitch. The latter condition is ordinarily used for the maneuvering of large multi-engine flying boats on the water. A voltage booster is provided which will allow quick feathering in 10 to 12 sec from low pitch. The pilot may also disconnect the governor and increase or decrease pitch manually, using the propeller as a fixed-pitch unit at any setting desired. This has some advantage in that the tachometer will then reflect any loss in engine power when the fuel mixture control is being adjusted or the magnetoes checked.

Feathering a propeller consists in turning the blade chord approximately parallel to the line of flight, which stops the rotation of the engine and reduces the drag considerably. This results in greatly improved airplane performance in the event of a single engine failure at takeoff and at cruising altitudes. Disintegration of the engine under the wind-

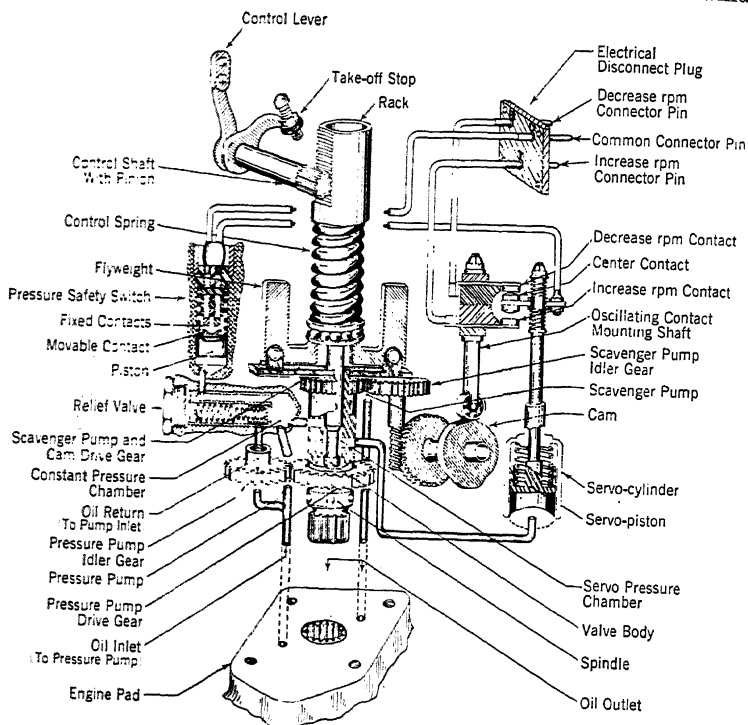


FIG. 4-5. Curtiss governor schematic drawing. (Courtesy Curtiss Propeller Division, Curtiss-Wright Corp.)

milling action of the propeller is also avoided in the event of an engine structural failure.

The complete propeller must be balanced to close limits prior to installation. This operation in the Curtiss plant is shown in Fig. 4-6.

Hamilton Standard Division

The Hamilton Standard constant-speed hub is one of two different controllable-pitch designs in operation. The other is termed the Hydro-matic design.

The Hamilton Standard constant-speed propeller assembly is shown in Fig. 4-7. A fly-ball governor driven by the engine and mounted on

the engine nose meters oil from a booster pump at 180 psi through a transfer gland to the engine crankshaft and then out to a hydraulic cylinder mounted ahead of the hub. The cylinder has a bearing shaft extending radially outward to a counterweight cam assembly attached

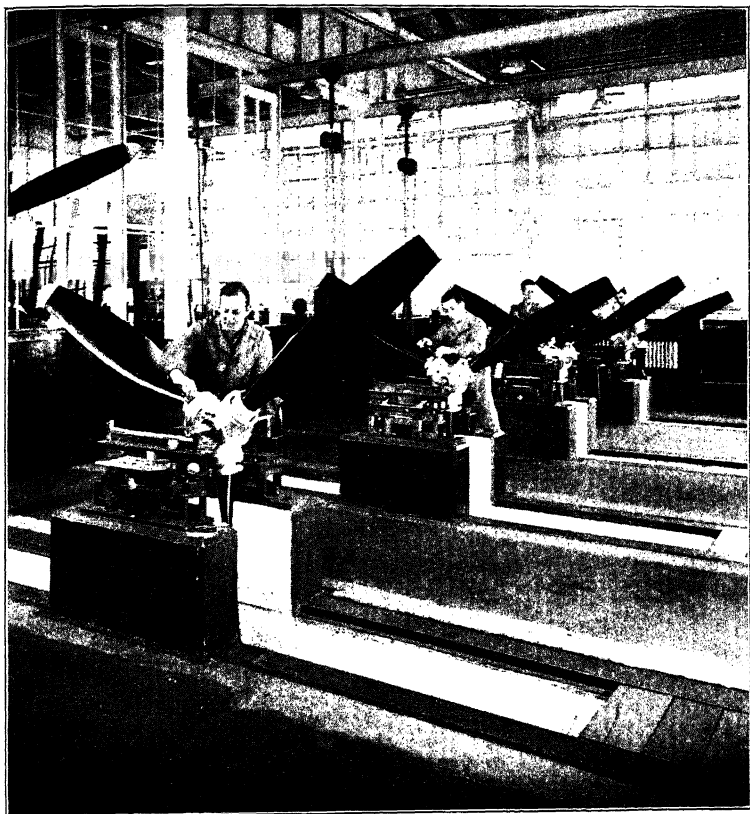


FIG. 4-6. Balancing complete propeller assembly. (Courtesy Curtiss Propeller Division, Curtiss-Wright Corp.)

to each blade shank. The blades are over-counterweighted so their normal tendency is to fly into high pitch, corresponding to the extreme aft position of the cylinder. When a lower pitch is needed, oil is admitted to the cylinder and forces it forward. The governor action is diagrammed in Fig. 4-8.

This type of propeller is also in service as a controllable-pitch design in which the governor is replaced by a three-way control valve and only the two positions of high pitch and low pitch are possible. Engine oil

pressure is used to force the cylinder forward for low pitch. The three-way valve drains this oil back into the crankcase for high-pitch operation.

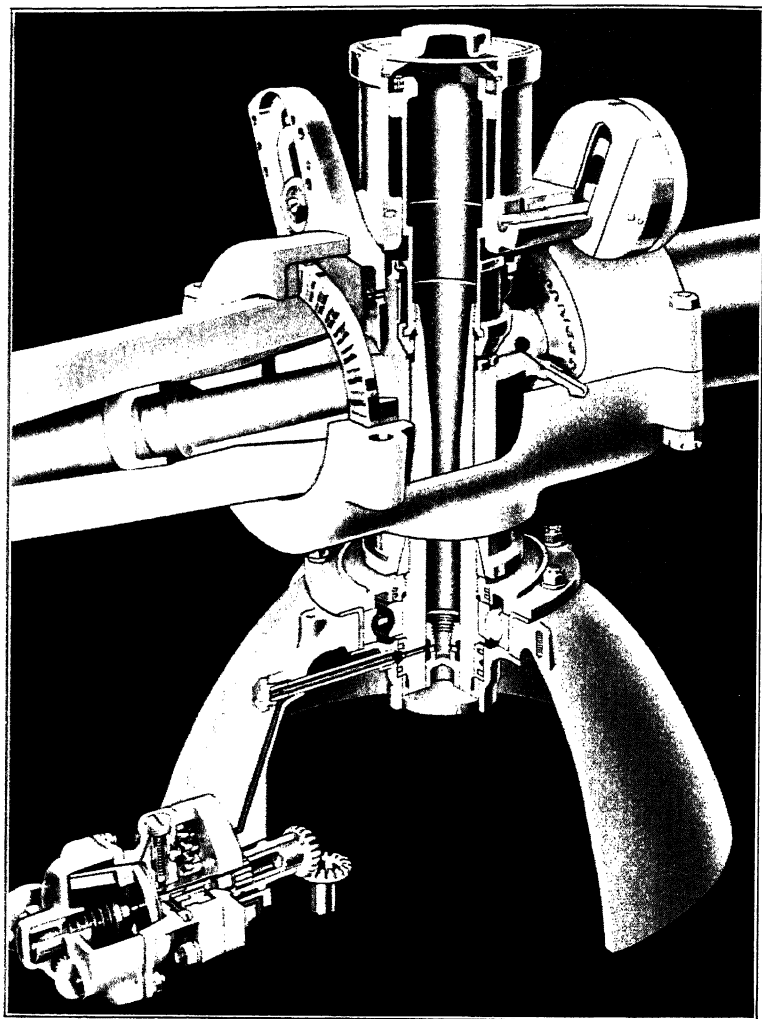


FIG. 4-7. Hamilton Standard constant-speed propeller assembly. (Courtesy Hamilton Standard Division, United Aircraft Corp.)

The hub construction is well brought out in Fig. 4-9. An internal forged steel member, called the spider, is splined to the engine crankshaft and has fingers projecting outward into each blade shank. The spider therefore transmits the engine torque loads and the propeller

thrust and torque loads. The hub spider and blade assembly is enclosed with a two-piece forged steel shell, termed the barrel, which is bolted

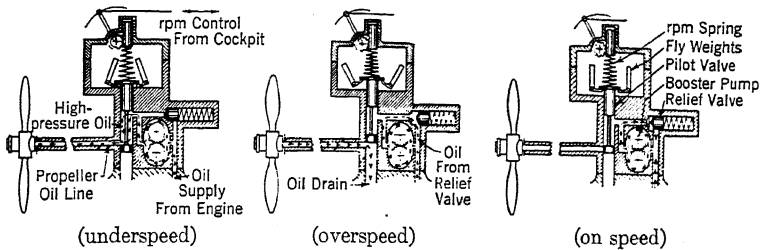


FIG. 4-8. Hamilton Standard constant-speed governor action. (Courtesy Hamilton Standard Division, United Aircraft Corp.)

together between the blade shanks. This barrel carries the radial centrifugal tension loads from each blade. A race of roller bearings acts between the hub shell and the upset blade shank to permit rotation of the blade. The hub is lubricated through Alemite fittings.

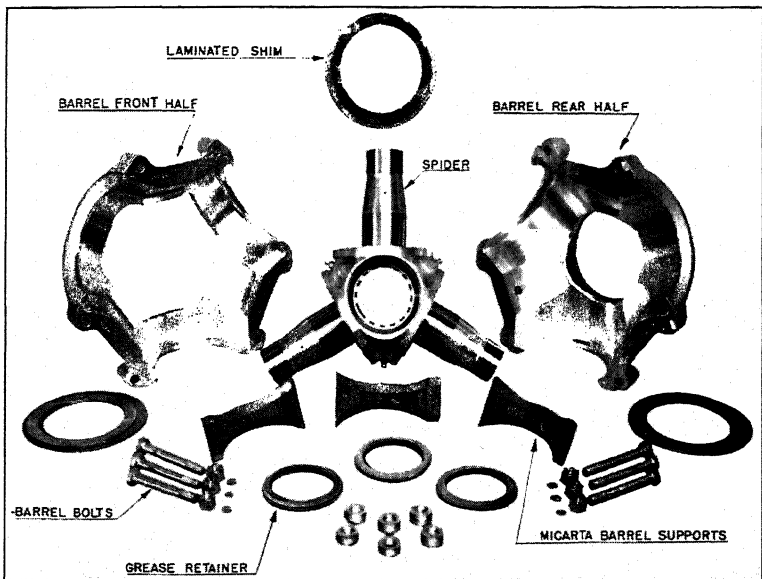


FIG. 4-9. Hamilton Standard hub construction. (Courtesy Hamilton Standard Division, United Aircraft Corp.)

The Hamilton Standard Hydromatic hub employs the same basic hub construction and governor as the older constant-speed design hub but replaces the blade counterweight and cam assembly with a different unit.

A hydraulic piston is mounted ahead of the hub and operates in a fore-and-aft direction (see Fig. 4-10). The cylinder in this design is stationary. The motion of the piston is transformed into rotary motion by means of several cam rollers which act on a pair of coaxial helical cams of opposite pitch slope. The outer cam is fastened to the hub proper and does not rotate. The inner rotates a master bevel gear which meshes with a bevel gear attached to each blade shank. Thus a forward movement of the piston causes an increase in blade angle and vice versa. The following basic forces are acting upon the pitch control mechanism in normal constant-speed operation.

- a. Centrifugal blade torque tending to reduce the blade angle.
- b. Blade bearing and cam roller friction tending to resist motion in either direction.
- c. Engine oil under normal engine pressure (60-100 psi), supplementing the centrifugal blade torque and always acting on the forward face of the piston to force the blades into low pitch.

d. Engine oil under boosted pressure from the governor (300 psi), acting on the rear face of the piston to force the blades into high pitch.

The governor then functions as in the previous design to maintain a constant rpm by metering the oil as needed to increase or decrease pitch. Note that the helical cam in front of the hub has two different slopes. For the normal pitch range the cam follows a steep helical angle, and the piston operates with a high mechanical advantage. For feathering operation it is therefore necessary to employ a greatly increased oil pressure (600-800 psi) to overcome the reduced cam slope. This means that an auxiliary source of high-pressure oil must be tapped by the pilot. A separate electric pump or a bleed into the airplane hydraulic system is used for this purpose. The object of changing the cam slope is to provide a definite high-pitch limit for normal operation and to prevent the propeller from flying into a feathered position because of malfunctioning of the mechanism. The lower cam slope for feathering also results in a rapid rotation for quick feathering. The feathering operation is given in the schematic diagram of Fig. 4-11. Unfeathering is accomplished, using a slightly higher oil pressure which causes the distributor valve to connect the high-pressure oil to the forward side of the piston.

The hub barrel in this design is held together by four bolts between each blade socket and is sealed completely so that the entire hub and blade bearing assembly is lubricated with engine oil under pressure.

Mechanical Hub Operation

Several hub designs have been developed based upon a purely mechanical operation of the pitch-control mechanism. Of these the Lycoming-

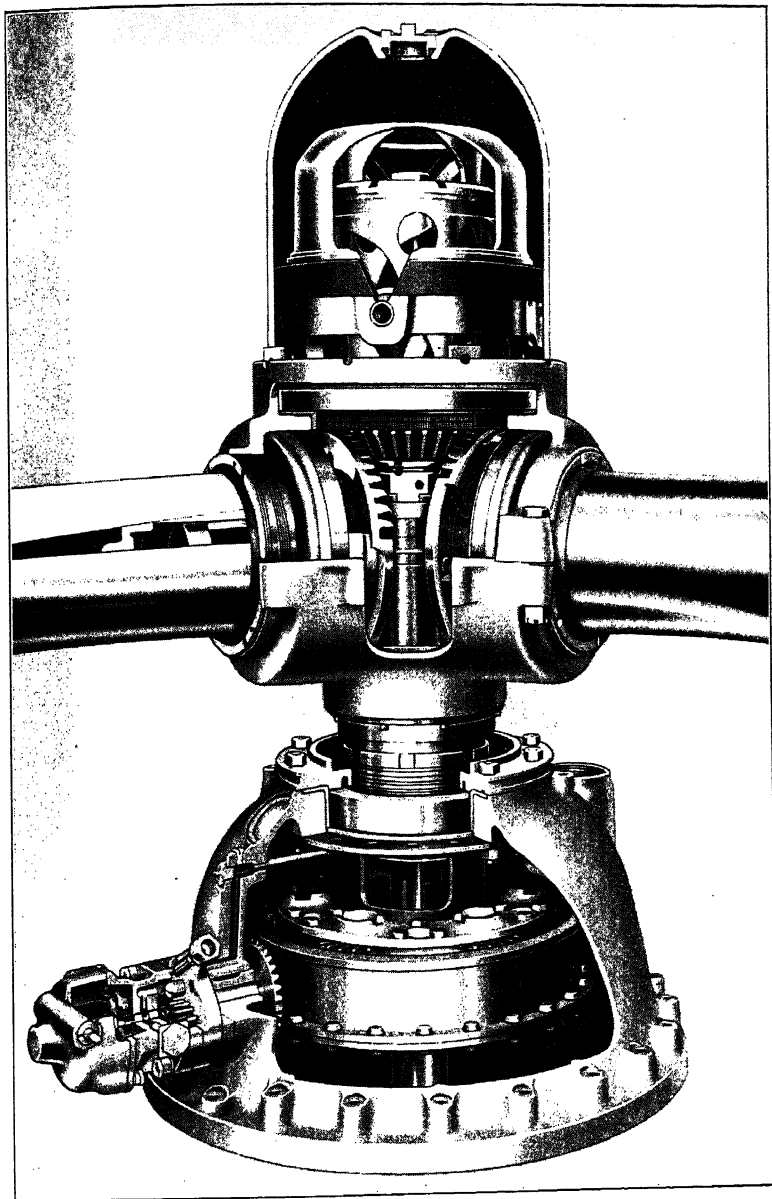


FIG. 4-10. Hamilton Standard Hydromatic assembly. (Courtesy Hamilton Standard Division, United Aircraft Corp.)

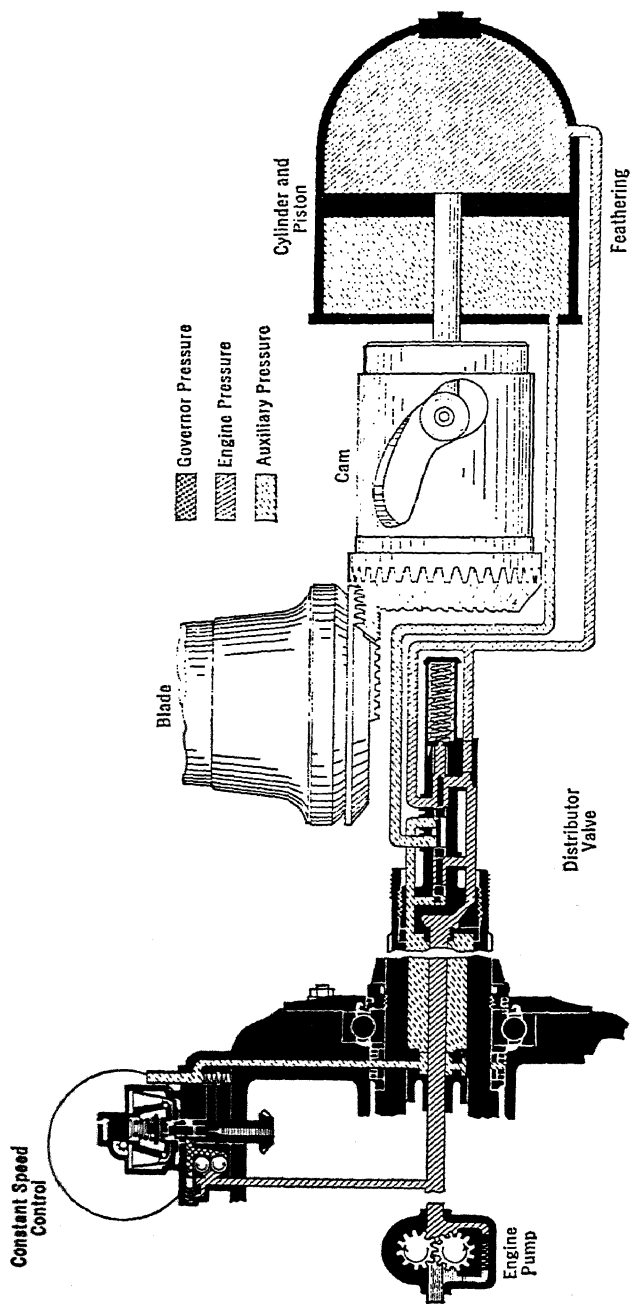


FIG. 4-11. Hamilton Standard Hydromatic feathering operation. (Courtesy Hamilton Standard Division, United Aircraft Corp.)

Smith propeller has enjoyed the widest usage. It employs a stationary sleeve mounted on the engine nose which may be shifted fore and aft by a solenoid control. In either extremity a worm thread on the sleeve meshes with a blade stop gear mounted on the hub and rotates the gear left or right. This gear operates a worm gear drive, terminating in a blade gear mounted on the blade shank and causing the blade to increase or decrease pitch as needed. The solenoid control is ordinarily attached to the airplane throttle knob so that rotation of the knob causes a pitch change.

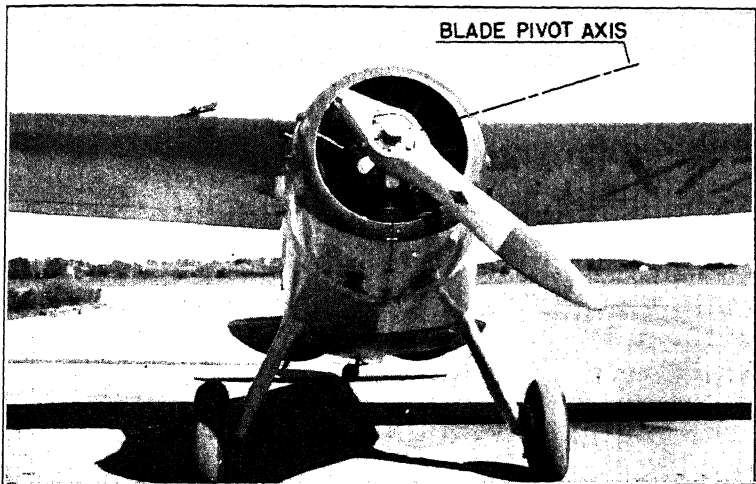


FIG. 4-12. Everel single-blade propeller. (Courtesy Western Flying.)

Automatic Pitch Control

Various types of automatic pitch control requiring no attention from the pilot have been devised. Several early designs employed a sliding hub moving forward on splines against a spring pressure so that the increased thrust of the blades at low forward velocities pulled the hub forward and rotated the blades to a low-pitch position. This idea was also developed in 1937 on the DiCesare propeller.

Several automatic pitch designs for light airplanes have been brought out by the Everel Propeller Corporation. The single-blade Everel propeller consists of one blade mounted on inclined bearings at the hub and free to rock fore and aft. This blade is statically balanced by a concentrated mass. An inclined axis of rotation is employed on the hub bearings so that rotation of the blade forward under the action of increased thrust at low velocities reduces the blade angle. When correctly designed

for a given installation a condition approximating constant-speed operation will result. A later design uses a normal two-bladed assembly with each blade mounted on an inclined axis to obtain the same results. Figure 4-12 shows the single-blade design installed on a Cessna airplane.

European Types of Controllable-Pitch Hubs

Designs comparable to the United States models previously discussed are also being developed in Europe. In Germany the Argus, Junkers, and VDM (Vereinigte Deutsche Metallwerke) are three basic types which utilize mechanical, hydraulic, and electric control energy respectively. The French Ratier design has an electric motor drive mounted on the hub. The British construct the DeHaviland propeller under Hamilton Standard license and also a hydraulic propeller known as the Rotol.

Dual Rotation

A dual-rotation propeller operating on two concentric engine drive shafts, with one hub and blade assembly rotating opposite to the other, has been under development for some time by the Army Air Force. The problem of providing a suitable driving mechanism had to be met by the engine manufacturers. Such a propeller with adjustable-pitch hubs was tested by the Matériel Division of the Air Corps at Wright Field in 1938. Recently the Curtiss, Hamilton Standard, and Aero-products Divisions have announced dual-rotation propellers with a constant-speed control. The Curtiss design is shown in Fig. 4-13. Such a design must include a pitch-change mechanism which connects front and rear hubs and allows a different rate of pitch change for each hub, dependent upon the flight range.¹

The advantages of a dual-rotation propeller lie in: (a) its neutralization of the engine torque reaction on airplanes of the pursuit type with high wing loadings and large engines; (b) increased propeller efficiency at speeds in excess of 350 mph by converting the rotational energy loss in the slipstream of the forward propeller into useful thrust on the rear propeller; (c) high solidity factor for installations where the diameter is restricted and the disk loading is high.

General Design Considerations

It is desired at this point to introduce a brief discussion of the basic considerations and aims in controllable-pitch hub design.

Propellers such as the Hamilton Standard and Curtiss, which are in use on multi-engine airplanes, must have a sensitivity of control within

¹H. M. McCoy, "Counter-Rotating Propellers," *Journal Royal Aeronautical Society* (June, 1940), pp. 481-498.

the range of $\pm 2-5$ rpm in order to accomplish synchronization of all engines and to prevent the beat which would otherwise occur. Such a noise is very disturbing to the pilot and passengers.

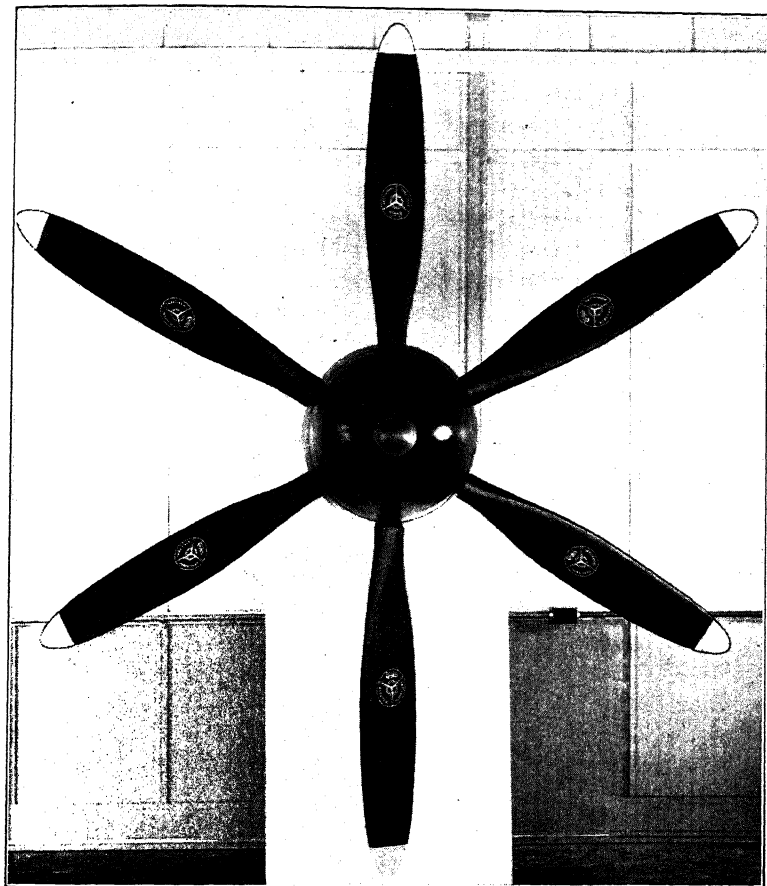


FIG. 4-13. Dual-rotation propeller. (Courtesy Curtiss Propeller Division, Curtiss-Wright Corp.)

The pitch-change mechanism must have a rate of pitch change ample to respond to normal airplane maneuvers, turbulent air, etc. This rate must not be excessive, or hunting will occur and the off-speed condition will not die out. Extensive flight tests have shown that 5° per sec is adequate for constant-speed operation. The rate of pitch change for feathering operation should be much faster in order to assume the optimum position as quickly as possible. The voltage booster in the

Curtiss design and the reduced cam slope with increased hydraulic pressure in the Hamilton Standard design accomplish this higher rate of rotation.

The blade angle travel in the normal operating range should be ample to cover all flight conditions. With the high velocities and high-altitude operation of current designs this may require a limiting high-pitch blade angle of approximately 60° at the 0.75 radius.

The hub design must be such as to provide a flyable propeller in the event of failure of the mechanism. A failure of the power supply for the Curtiss hub would convert it to a fixed-pitch propeller set at the blade angle at which failure occurred. A failure of the hydraulic system of the Hamilton Standard constant-speed design might allow the blades to fly into the high-pitch position. Positive stops are provided for both the high- and low-pitch positions so that a usable blade angle will be maintained. In the Hamilton Standard Hydromatic design a hydraulic failure might allow the blades to rotate to the low-pitch position, and stops are provided for a usable blade angle in this condition. The change in cam slope provides a high-pitch limitation.

The hub mechanism must have sufficient power to overcome the maximum operating loads. The calculations for a 12-ft diameter, three-bladed propeller suitable for a 1200-hp engine with a design rpm of 1550 follow.

Weight per blade = 60 lb.

Center of gravity of blade = 25.9 in.

Centrifugal force per blade = 105,800 lb.

Blade bearing friction torque per blade = $105,800 \times 0.014 = 1480$ in.-lb.

Centrifugal blade torque per blade = 7000 in.-lb (maximum).

Rate of pitch change = 5° per sec.

Power required = $\frac{2\pi \times \frac{5}{6} \times 3 \times 8480}{33,000 \times 12} = 0.336$ hp.

Assuming a 50 per cent efficiency for the pitch-changing mechanism, the power required = 0.672 hp.

The difficulty of transmitting this amount of power from a non-rotating body is obvious. The slip rings of the Curtiss hub and the oil transfer glands of the Hamilton Standard hub are examples of this power transfer problem.

Hub Stress Analysis

The main steady loads on the hub structure are the centrifugal radial tension load of the blades combined with the bending moment on each

blade socket due to the thrust and torque load of the blades. Centrifugal blade torque is the critical load for the pitch-change mechanism.

The stress analysis procedure naturally varies greatly with the type of hub construction. For example, the hub barrel of the Hamilton Standard design absorbs very little blade bending, but it does take all the centrifugal tension loads whereas the blade sockets in a single-piece hub construction must take a portion of the blade-bending load in addition to the centrifugal tension. With the angular-contact ball bearing arrangement employed by Curtiss and similar designs, a hoop tension load is also imposed upon the blade sockets which acts at right angles to the centrifugal load.

Threaded sections in the blade socket are critical in shear created by the radial tension loads, and sufficient thread length must be used to meet the allowable shear stress of the material. Allowable stresses in shear, tension, and bearing for the various materials may be found in ANC-5 "Strength of Aircraft Elements."

The centrifugal blade torque load is augmented by the bearing friction torque. This may be evaluated for ball bearing installations by the following formula.

$$Q = fRL \quad [1]$$

where Q = the bearing friction torque in inch-pounds.

f = the friction coefficient (0.0073 as a first approximation).

R = the ball center radius of the bearings in inches.

L = the radial load in pounds.

The number of bearing races necessary in a hub such as the Curtiss design is found by dividing the total radial load by the rated load per race multiplied by a distribution factor of 1.2. The high precision necessary in producing a stack of bearings such as these in which the load distribution is approximately equal is truly an achievement.

The splined connections between the hub and engine crankshaft have been standardized in various sizes and will be found in the *SAE Handbook*. Front and rear cone dimensions have also been standardized. The engine specification will give the engine shaft size.

Care must be taken to avoid rapid changes in cross section with a resulting stress concentration. The interior profile of the hub is carefully checked to avoid excess weight and a poor stress distribution. A thread relief of ample curvature must be provided at such points as the blade nut threads on the blade sockets. Surface finish is critical in such a highly stressed part, and all surfaces must be free from tool marks. Normally the exterior surface is ground and polished to a smooth finish, after which it is cadmium plated.

A hub working under severe operating conditions may show signs of galling on the cone seats, blade bearings, gear teeth, etc. Problems of this type must be solved for each installation. Obviously, if the blades are in a bad state of resonance because of disturbances originating in the engine the hub will suffer as the connecting link in the assembly.

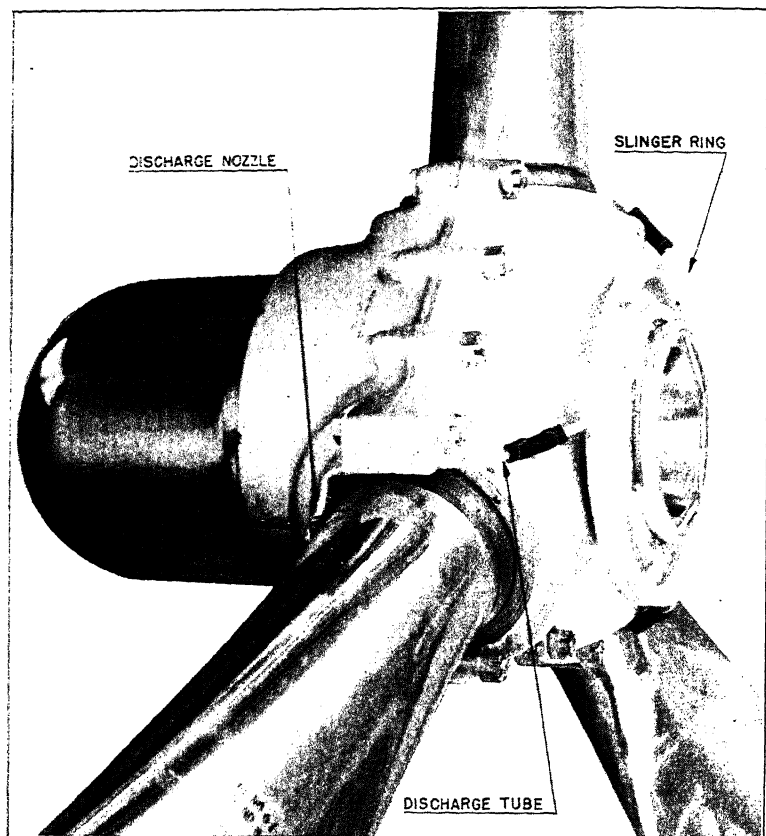


FIG. 4-14. Hamilton Standard Hydromatic de-icer installation. (Courtesy Hamilton Standard Division, United Aircraft Corp.)

Hub Accessories

Suitable provision must be provided for prohibiting the accumulation of ice on the propeller blades, and this is accomplished by feeding a mixture of 85 per cent alcohol and 15 per cent glycerin to the blade shank from a "slinger ring" and tube assembly. The fluid is pumped into the slinger ring from a tank mounted behind the engine. It is then picked up in the ring and flows outward to the blade shank under the action of

centrifugal force. Once on the blade the fluid moves radially outward under action of centrifugal force and back over the blade because of aerodynamic forces. A typical installation on the Hamilton Standard Hydromatic propeller is shown in Fig. 4-14.

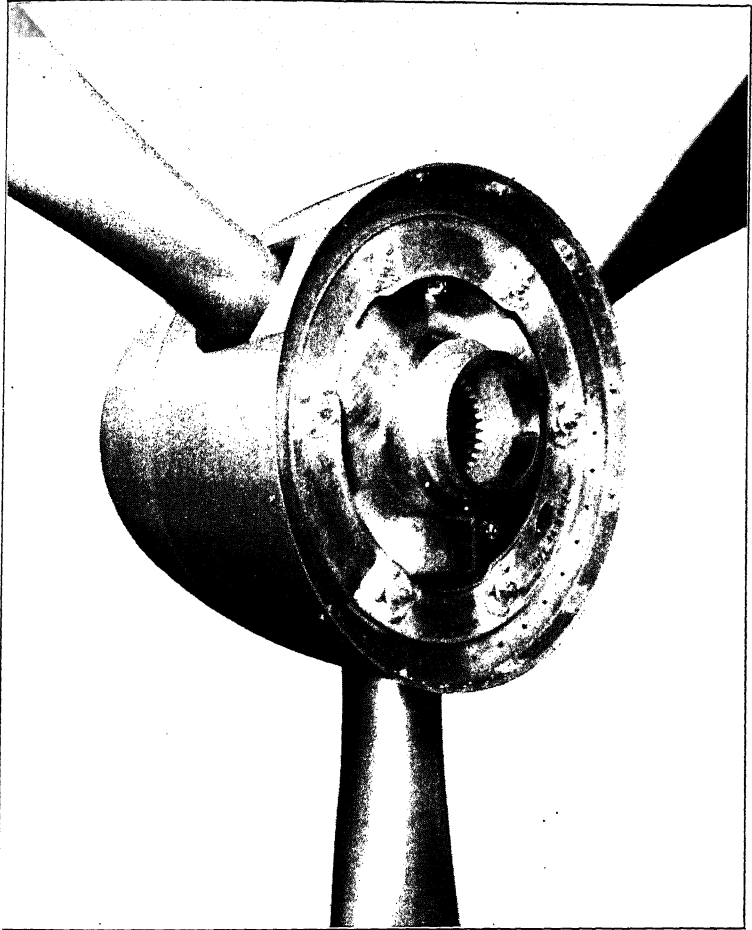


FIG. 4-15. Rear view of spinner assembly. (*Courtesy Hamilton Standard Division, United Aircraft Corp.*)

The fluid used prohibits ice accumulation and loosens existing ice layers which are then thrown off radially. An application of approximately two pints per hour per blade is usually sufficient.

Another accessory which is mounted on the hub is the spinner. The size and shape of the spinner varies according to the installation. They

are usually spun from aluminum alloy, accurately balanced, and securely mounted at the back to a bulkhead or bracket support aft of the blades. Figure 4·15 is a rear view of a Hamilton Standard spinner assembly for the Lockheed Constellation. The six bolts on the rear bulkhead clamp it securely to the hub assembly.

PROBLEMS

1. Determine the power required to operate the propeller blade of Fig. 1·10 as a two-bladed constant-speed propeller, using the critical condition as 2000 rpm and a rate of pitch change of 6° per sec. Assume ball bearing races in the blade socket with a ball center diameter of 4.375 in. and a mechanical efficiency for the mechanism of 40 per cent.

CHAPTER 5

EFFECT OF THE PROPELLER ON AIRPLANE PERFORMANCE

General Considerations

The functioning of the propeller is inextricably combined with the airplane engine operation. Optimum performance of the powerplant unit demands the most favorable operating conditions for both engine and propeller. Unfortunately, this combination is not easily obtainable. It is, moreover, dependent upon another variable, the performance of the complete airplane.

Reference to Fig. 2-9 will clarify some points in propeller performance. Keeping in mind that each of the blade angle curves is a plot of thrust versus velocity for a given propeller and throttle setting, note the decided increase in thrust with decrease in blade angle throughout the entire flight range. It would seem that a general rule of utilizing the lowest blade angle possible would provide maximum thrust, and therefore the maximum propulsive efficiency for any given velocity. The only limitation to this decrease in blade angle lies in the engine rpm. As the blade angle decreases the engine rpm increases but it must not be allowed to exceed its maximum rated value for safe operation.

A fixed-pitch or adjustable-pitch propeller must therefore be pitched high enough to prevent the engine from dangerously overspeeding at the condition of maximum velocity for the airplane. Reference to the blade element relationship of Fig. 1-8 will show that this condition determines the reference blade angle at which the blade must be set. At all lower velocities the engine is held to a lower speed owing to the increase in angle of attack of each blade element, which in turn increases the aerodynamic torque of the blades and slows the engine down. In terms of test coefficients the previous explanation implies that the power coefficient C_p must increase with decreasing V/nD for a given blade angle. Such a relationship exists in the test data of Fig. 2-7 and similar data.

As airplane velocities increased it became necessary to increase the blade angle setting to compensate. This increase in blade angle caused a decided drop in thrust at the lower velocities and particularly during takeoff because of a stalled condition existing over a large portion of the blade as shown in Fig. 2-4. The advent of the two-position, controllable-

pitch propeller then made it possible to obtain an optimum blade angle for both takeoff and maximum velocity, resulting in greatly increased takeoff and climb performance.

With constantly increasing airplane velocities and high-altitude operation due to engine supercharging, it became necessary to extend the blade angle range between low and high pitch and to provide intermediate settings. This range of blade angle settings in a modern, high-performance airplane must adapt the propeller to the following conditions:

- a. Takeoff.
- b. Cruising and maximum velocity at low altitude.
- c. Climb to rated power altitude.
- d. Cruising and maximum velocity at the rated power altitude.
- e. Flight at service ceiling.

Of all the various possibilities of providing the essential range of blade angle settings for the propeller the scheme of increasing or decreasing the blade angle as needed to maintain a constant engine rpm has evolved as the most satisfactory to date. The propeller diameter may be selected from a design chart to favor the most critical condition and the blade angle is then automatically adjusted by one of the various governing methods discussed previously to provide a selected engine rpm under all other conditions. Thrust and torque forces, centrifugal force, aerodynamic and centrifugal blade torque are all potential motivators in a control mechanism, but thus far centrifugal force as created by the crankshaft rotation and used in a fly-weight governor has been employed predominantly. With constant-speed control the engine is protected from overspeeding, and the maximum amount of brake horsepower is released for a given throttle setting even though the actual propulsive efficiency is not the maximum possible under all conditions.

Performance Analysis

To illustrate a method of propeller performance calculation and to point out the basic differences between the preceding propeller types, a hypothetical airplane will be equipped with a fixed-pitch, two-position, and constant-speed propeller installation, and the airplane power required and available curves will be compared. The following airplane characteristics are assumed:

Bimotor, low-wing, transport monoplane.

Pratt & Whitney Wasp, Jr., SB motors, each rated 400 bhp at 2200 rpm to 5000 ft.

Gross weight 12,000 lb.

Wing area 500 sq ft, aspect ratio 7.

Airplane efficiency factor, $e = 0.90$.

$C_{D_p} = 0.0230$.

Three-bladed, aluminum-alloy propeller with Clark-Y section.

The horsepower required curve is plotted versus velocity in Fig. 5-1 for sea level.¹

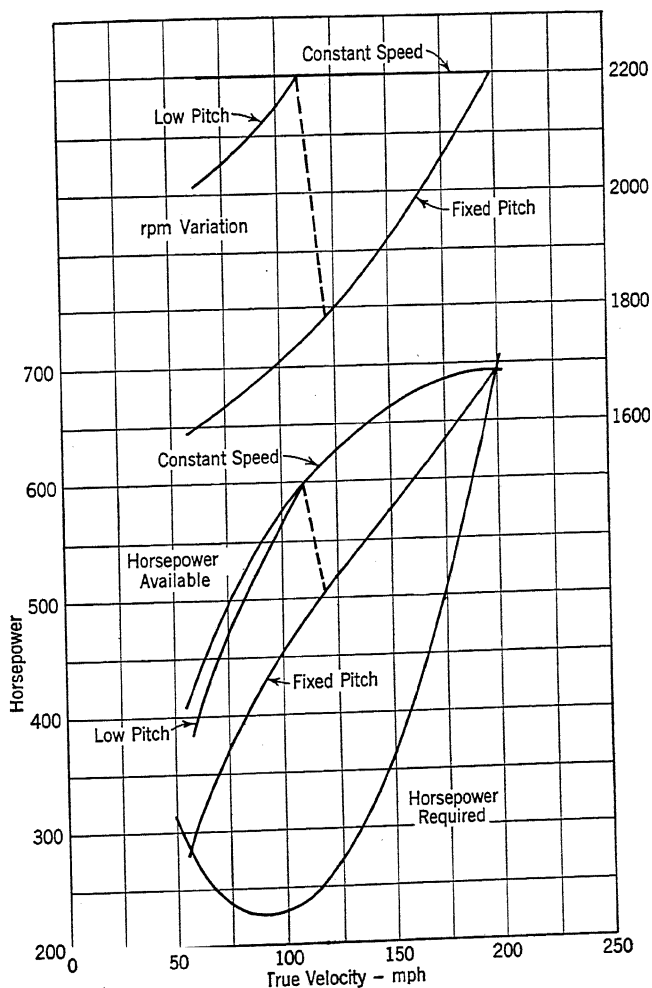


FIG. 5-1. Power available and rpm relationships.

¹ For a discussion of the power required relationship see Millikan "Aerodynamics of the Airplane," John Wiley and Sons (1941), Chapter 3.

Propeller Selection

The propeller is selected for maximum efficiency at sea-level maximum velocity. An estimated value of propulsive efficiency is used to obtain an approximate thrust horsepower which yields an approximate value for maximum velocity on the horsepower required curve. This velocity is then used in the propeller selection. If the efficiency does not closely approximate the estimated value the process is repeated. In this case the design chart of Fig. 5-7 will be used. The assumption is made that this test data with a liquid-cooled engine nacelle will apply to a radial engine nacelle. The calculations follow.

Assume $\eta = 0.86$ from Fig. 5-7.

$V_{\max} = 198$ mph from Fig. 5-1.

$$C_s = \frac{0.638 \times 198 \times 1}{(400)^{1.5} (2200)^{2.5}} = \frac{0.638 \times 198 \times 1}{3.32 \times 21.7} = 1.75.$$

$\beta = 25^\circ$ at 0.75 radius from Fig. 5-7, using line of maximum efficiency for C_s .

$$\frac{V}{nD} = 1.02 \text{ from Fig. 5-7.}$$

$$D = \frac{198 \times 1.467 \times 60}{2200 \times 1.02} = 7.76 \text{ ft (7 ft 9 in.).}$$

Check. Actual η with propeller selected = 0.86, which checks the assumed value. Tip speed is 893 ft per sec, which is below the critical value given by Fig. 2-10.²

Fixed-Pitch Analysis

Fixed-pitch propeller performance may be evaluated by several different methods.³ The approach discussed in the Appendix of *NACA Tech. Rept. 640* and based upon the use of power coefficient curves will be used herein because of its adaptability to published data and the relatively high degree of accuracy which it insures. The procedure follows.

By using the subscript 0 to denote the design condition, $(V/nD)_0$ and β_0 determine C_{T_0} and C_{P_0} from Fig. 5-. At even values of V/nD

² A minimum tip clearance of 9 in. from the ground, 18 in. from the water, and 1 in. from the fuselage will also limit the diameter selected.

³ See E. P. Warner, "Airplane Design," McGraw-Hill (1936), Chapter XIV.

pick off C_T and C_P for a constant β_0 . Compute C_{P_0}/C_P and calculate the engine rpm using the relationship ⁴ $n/n_0 = \sqrt{C_{P_0}/C_P}$. Then

$$\text{Brake horsepower} = bhp_0 \left(\frac{n}{n_0} \right)$$

for the condition of full throttle. Also

$$\eta = \frac{C_T}{C_P} \left(\frac{V}{nD} \right)$$

and

$$\text{Thrust horsepower} = \text{Brake horsepower} (\eta)$$

The velocity may be determined from V/nD and the rpm. Propeller thrust at any velocity may also be computed, if needed, using the relationship

$$T = T_0 \left(\frac{C_{P_0}}{C_P} \right) \left(\frac{C_T}{C_P} \right) = k \left(\frac{C_T}{C_P} \right)$$

However, thrust calculations are avoided at this point in order to emphasize engine performance and propulsive efficiency variations.

By using $\beta_0 = 25^\circ$ and $(V/nD)_0 = 1.02$, values of $C_{T_0} = 0.057$ and $C_{P_0} = 0.067$ are obtained from Fig. 5-8. A tabular summary of the calculations follows. Slide rule accuracy is used throughout.

FIXED-PITCH PROPELLER

SEA-LEVEL HORSEPOWER AVAILABLE CALCULATION

$\beta = 25^\circ$ at 0.75 radius

7 ft 9 in. diameter

V/nD	C_T	C_P	C_{P_0}/C_P	n/n_0	rpm	bhp	η	thp	mph
0.4	0.152	0.127	0.527	0.725	1593	580	0.479	278	56
0.5	0.149	0.122	0.549	0.740	1628	591	0.610	360	72
0.6	0.136	0.117	0.572	0.756	1662	605	0.697	421	88
0.7	0.120	0.110	0.610	0.781	1720	625	0.764	477	106
0.8	0.101	0.101	0.664	0.815	1792	651	0.800	521	127
0.9	0.080	0.086	0.780	0.884	1942	706	0.836	590	154
1.00	0.060	0.070	0.958	0.978	2150	782	0.856	670	190
1.02	0.057	0.067	1.000	1.000	2200	800	0.866	693	198

Note that the total brake horsepower of both engines is used in the bhp and thp calculations whereas C_T and C_P apply only to each propeller unit. C_{P_0} may be checked by direct calculation for the design condition

⁴ This follows from equation 6, Chapter 2, assuming constant engine torque for a fixed throttle position.

and has a computed value of 0.0668. The variation of power available and engine rpm is plotted versus velocity in Fig. 5-1. The decrease in bhp along with the drop in propulsive efficiency has accounted for the reduced power available at the low velocities. Climb in feet per minute at any velocity may be calculated by multiplying the excess horsepower by 33,000 and dividing by the airplane gross weight.

Note that the pilot with a fixed-pitch propeller installation may control his engine rpm in level flight only by adjusting the throttle and therefore a fixed relationship exists between manifold pressure and rpm.⁵

Two-Position Analysis

When a two-position propeller is available, the low-pitch position may be selected to favor climb and takeoff. In the present instance the low-pitch blade angle will be selected for a climbing velocity of 110 mph at sea level.

$$\frac{V}{nD} = \frac{110 \times 1.467 \times 60}{2200 \times 7.76} = 0.566$$

$$C_P = \frac{400 \times 550}{\rho n^3 D^5} - 0.002378(36.7)^3(7.76)^5 = 0.0668$$

The previous analysis may now be repeated for velocities below 110 mph, using the new design condition $(V/nD)_0 = 0.566$ combined with $C_{P_0} = 0.0668$. From Fig. 5-8, we obtain $\beta = 19^\circ$ at 0.75 radius and $C_{T_0} = 0.088$.

TWO-POSITION PROPELLER

SEA-LEVEL HORSEPOWER AVAILABLE CALCULATION

$\beta = 19^\circ$ at 0.75 radius

7 ft 9 in. diameter

V/nD	C_T	C_P	C_{P_0}/C_P	n/n_0	rpm	bhp	η	thp	mph
0.35	0.128	0.080	0.835	0.914	2010	731	0.560	410	62
0.40	0.120	0.078	0.856	0.925	2035	740	0.615	455	72
0.45	0.112	0.075	0.891	0.945	2080	756	0.672	508	83
0.50	0.100	0.072	0.928	0.964	2120	771	0.695	536	94
0.566	0.088	0.0668	1.000	1.000	2200	800	0.746	596	110

The preceding two-position analysis is essentially that for two fixed-pitch propellers of the same diameter but with different blade angles. The large increase of excess power at the low-pitch angle will result in

⁵ For part throttle operation refer to Weick, "Aircraft Propeller Design," McGraw-Hill (1930), p. 172.

greatly improved climb. In addition there will be a substantial increase in thrust during takeoff. The results are plotted in Fig. 5.1 for comparison with the fixed-pitch analysis.

Constant-Speed Analysis

The same propeller will now be considered as a constant-speed unit, based on the previous design condition of 7 ft 9 in. diameter, favoring maximum velocity at sea level. The power coefficient chart of Fig. 5.8 is again used but the procedure is modified. The power coefficient C_P is now a constant and equals 0.0668 at all velocities at sea level. At even values of V/nD interpolated values of C_T are obtained.

$$\eta = \frac{C_T}{C_P} \left(\frac{V}{nD} \right)$$

Thrust horsepower = Brake horsepower (η) = 800 (η)

The velocity is calculated from V/nD . The thrust may also be calculated from the relationship $T = C_T \rho n^2 D^4 = k C_T$. A tabular summary of the calculations follows.

CONSTANT-SPEED PROPELLER SEA-LEVEL HORSEPOWER AVAILABLE CALCULATION
2200 rpm $C_P = 0.0668$ 7 ft 9 in. diameter

V/nD	C_T	β	η	thp	mph
0.3	0.118	17.0°	0.530	424	58
0.4	0.106	17.5°	0.635	508	78
0.5	0.095	18.3°	0.711	570	97
0.6	0.086	19.4°	0.772	618	116
0.7	0.077	20.5°	0.807	645	136
0.8	0.070	21.0°	0.838	670	155
0.9	0.064	23.2°	0.862	690	175
1.00	0.058	24.6°	0.868	694	194
1.02	0.057	25.0°	0.870	695	198

Note that the propulsive efficiency is sustained at fairly high levels. The lower blade angles at velocities below the maximum tend to increase the efficiency whereas the lower V/nD values decrease the efficiency so that the final value depends upon the relative effect of these conflicting tendencies. The large increase in thrust horsepower, however, is due to the maximum brake horsepower being available from the engine under all conditions. The results are plotted in Fig. 5.1 for comparison with the previous examples.

The pilot with a constant-speed propeller control may select any combination of engine rpm and manifold pressure necessary to meet his requirements inasmuch as the control of these two items is now completely independent. Dangerous engine resonance condition may be avoided by proper rpm selection. Operating economy of the engine may be increased by cruising at reduced rpm and increased manifold pressure. On the airlines a cruising descent at cruising horsepower without overspeeding the engine may be accomplished, resulting in improved schedules.

However, for sea-level performance it is apparent that no appreciable gain may be derived from constant-speed operation when compared to two-position control. The benefits of constant-speed control become much more important with supercharged engine operation.

Supercharged Engines

To emphasize the effect of supercharging it will be assumed that the engines of the present example are supercharged to 10,000 ft altitude. The constant-speed calculations follow.

$$C_P = \frac{400 \times 550}{\rho n^3 D^5} = \frac{0.0668}{0.738(0.002378)(36.7)^3(7.76)^5} = \frac{0.0668}{0.738} = 0.0906$$

CONSTANT-SPEED PROPELLER 10,000-FT HORSEPOWER AVAILABLE CALCULATION

2200 rpm $C_P = 0.0906$

7 ft 9 in. diameter

V/nD	C_T	β	η	thp	mph
0.3	0.143	20.5°	0.474	379	58
0.4	0.133	20.8°	0.588	470	78
0.5	0.122	21.2°	0.675	540	97
0.6	0.111	22.0°	0.736	590	116
0.7	0.100	22.8°	0.774	619	136
0.8	0.092	24.0°	0.814	650	155
0.9	0.083	25.3°	0.825	660	175
1.0	0.770	26.5°	0.850	680	194
1.1	0.070	27.8°	0.850	680	214

Horsepower required at altitude is obtained by multiplying the sea-level values of horsepower and velocity by $1/\sqrt{\sigma}$. The constant-speed analysis for both sea-level and 10,000-ft operation is plotted in Fig. 5-2. Note that the propulsive efficiency holds up very well at altitude

although an appreciably higher blade angle is required. Both fixed-pitch and two-position propellers would require the pilot to throttle back at altitude with a supercharged engine to prevent the engine from overspeeding. This would result in a large loss of engine power, and the altitude performance for a fixed-pitch propeller would not be much better than that for sea level at the same power output.⁶

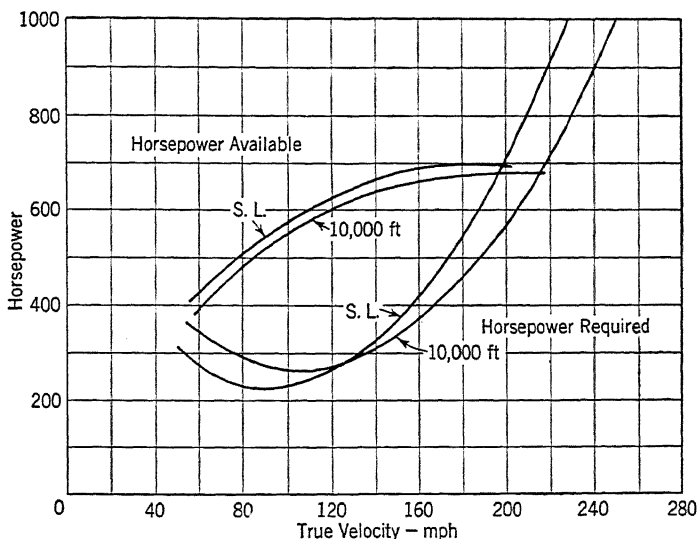


FIG. 5-2. Constant-speed propeller performance at sea level and altitude with supercharged engine.

Thrust During Takeoff

During the takeoff period the concept of propulsive efficiency is not applicable because the efficiency diminishes to zero as the velocity approaches zero. A direct evaluation of thrust is necessary as it alone is the accelerating force acting upon the airplane. Several methods of computing airplane takeoff performance are available,⁷ and will not be discussed here. It is obvious that the takeoff performance will always be optimum for the propulsive unit yielding the highest amount of thrust, all other factors being equal.

A comparison of propeller sea-level thrust for the three previous cases will be of interest and may be readily calculated from the previous data.

⁶ For a more detailed discussion of performance and supercharging effects refer to E. P. Warner, "Airplane Design," McGraw-Hill (1936), Chapter XIV.

⁷ W. S. Diehl, "The Calculation of Take-Off Run," *NACA Tech. Rept. 450* (1933).
M. Schrenk, "Take-Off and Propeller Thrust," *NACA Tech. Mem. 703* (1933)

For the fixed-pitch propeller,

$$T = T_0 \left(\frac{C_{P_0}}{C_{T_0}} \right) \frac{C_T}{C_P} = 664 \left(\frac{0.0668}{0.0570} \right) \frac{C_T}{C_P} = 778 \frac{C_T}{C_P}$$

V/nD	C_T	C_P	C_T/C_P	$T_{(lb)}$	mph
0	0.161	0.149	1.080	840	0
0.10	0.158	0.143	1.102	857	13
0.20	0.156	0.138	1.130	879	27
0.30	0.154	0.132	1.168	907	42
0.40	0.152	0.127	1.198	930	56
0.50	0.149	0.122	1.220	949	72
0.60	0.136	0.117	1.162	905	88
0.70	0.120	0.110	1.090	847	106

For the low-pitch position of the two-position propeller,

$$T = T_0 \left(\frac{C_{P_0}}{C_{T_0}} \right) \frac{C_T}{C_P} = 1025 \left(\frac{0.0668}{0.0880} \right) \frac{C_T}{C_P} = 778 \frac{C_T}{C_P}$$

V/nD	C_T	C_P	C_T/C_P	$T_{(lb)}$	mph
0	0.155	0.084	1.845	1435	0
0.10	0.152	0.083	1.830	1422	17
0.20	0.145	0.082	1.768	1372	35
0.30	0.135	0.081	1.668	1298	53
0.40	0.120	0.078	1.538	1196	72
0.45	0.112	0.075	1.492	1162	83
0.50	0.100	0.072	1.390	1080	94
0.566	0.088	0.0668	1.318	1024	110

For the constant-speed propeller:

$$T = C_T \rho n^2 D^4 = C_T (0.002378) (36.7)^2 (7.76)^4 = 11,620 C_T$$

mph	V/nD	C_T	$T_{(lb)}$
0	0	0.148	1722
20	0.103	0.141	1640
40	0.206	0.130	1512
60	0.309	0.117	1360
80	0.412	0.105	1220
100	0.515	0.093	1082
110	0.566	0.088	1024

A plot of thrust versus velocity is given in Fig. 5-3 for the three examples. Note the decided loss in thrust at low velocities for the fixed-pitch propeller because of the stalled condition of a large portion of the blade. The two-position propeller results in a 71 per cent increase in static thrust, which will be reflected in a substantial increase in takeoff performance. The constant-speed propeller will also give an improved takeoff. It should be realized at this point that as the maximum velocity

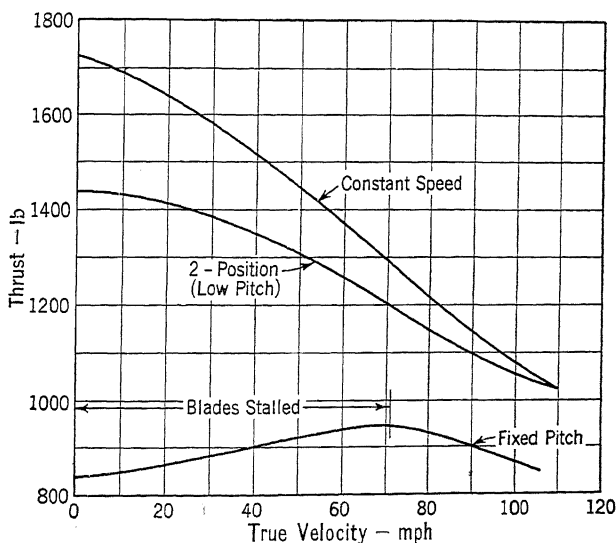


FIG. 5-3. Propeller thrust during takeoff.

of the airplane increases, the constant-speed installation will show a constantly increasing margin over the two-position.

Note that propeller thrust in general is inversely proportional to the airplane velocity, making the conventional propeller inherently a low-velocity device. A jet propulsion system becomes theoretically attractive for high velocities owing to its freedom from compressibility effects and its development of a thrust force which is independent of forward velocity.

Engine Gearing

The reduction of propeller rpm by means of a gear reduction drive on the engine crankshaft has come into extensive use within recent years. Such an arrangement allows the engine to operate under more favorable

conditions without penalizing the propeller with tip losses due to excessive tip speeds. The increased V/nD ratio likewise improves the propulsive efficiency. Typical gear ratios employed are 16 : 11, 16 : 9, 16 : 7, and 3 : 2. The high rpm of current engine designs combined with critical tip speeds at altitude and takeoff have resulted in continued increases in the gear reduction drive ratio. No general comparison may be made between airplanes, and each case must be considered individually to determine the best solution.

Power Coefficient Curves and Design Charts

In order to facilitate performance calculations and propeller selection for different designs, seven additional sets of power coefficient curves and design charts are included in Figs. 5·5 to 5·18 which are reproduced from *NACA Tech. Rept. 640*. The blade form curves are given in Fig. 5·4. The test series may be classified as follows.

Airfoil Sections	Number Blades	Reference Propeller Number	Figure Numbers
Clark Y	2	5868-9	5·5, 5·6
Clark Y	3	5868-9	5·7, 5·8
Clark Y	4	5868-9	5·9, 5·10
RAF-6	2	5868-R6	5·11, 5·12
RAF-6	3	5868-R6	5·13, 5·14
RAF-6	4	5868-R6	5·15, 5·16
RAF-6	2	37-3647	5·17, 5·18

All the propellers tested were of 10-ft diameter and had the same plan-form, thickness, width, and pitch distribution except 37-3647 which had a 50 per cent greater width than the two-bladed 5868-R6 propeller. All were tested on the liquid-cooled engine nacelle of Fig. 2·2.

For small changes in blade width on similar propellers the power and thrust may be assumed to vary directly with blade width. Hence in C_s and C_P calculations the power should be multiplied by the ratio b/b' where b is the blade width at 0.75 radius for the tested propeller and b' is the same quantity for the propeller under consideration. The thrust obtained from the charts should then be divided by b/b' to obtain the actual thrust.

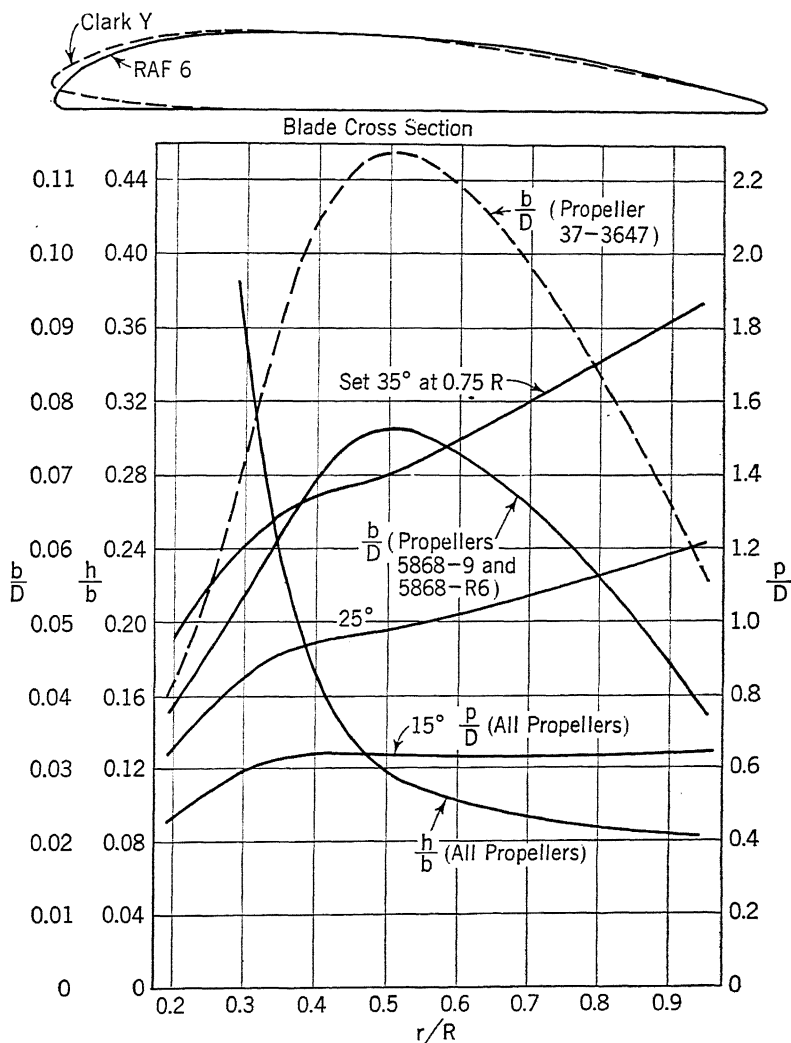


FIG. 5-4. Blade form curves. (NACA Tech. Rept. 640.)

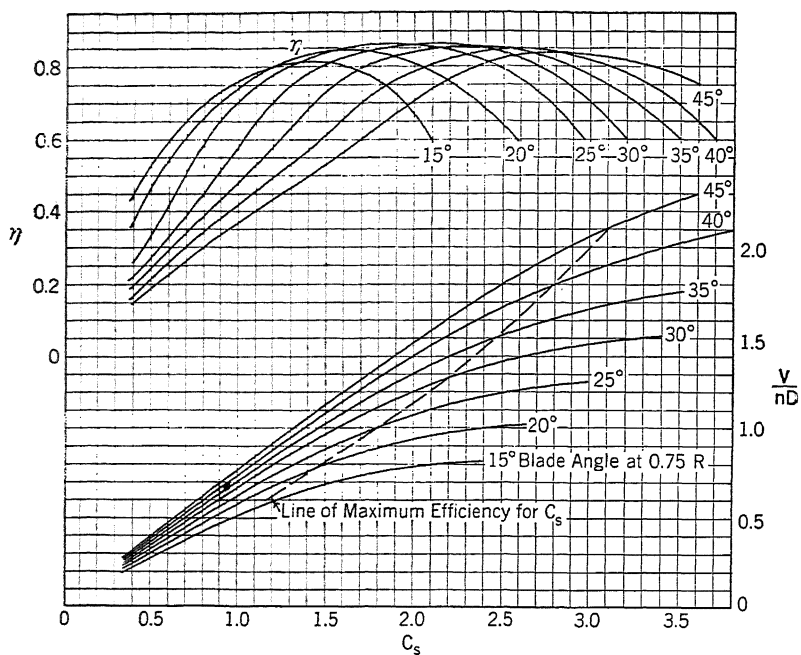


FIG. 5-5. Design chart for propeller 586S-9, Clark-Y section, two blades.
(NACA Tech. Rept. 640.)

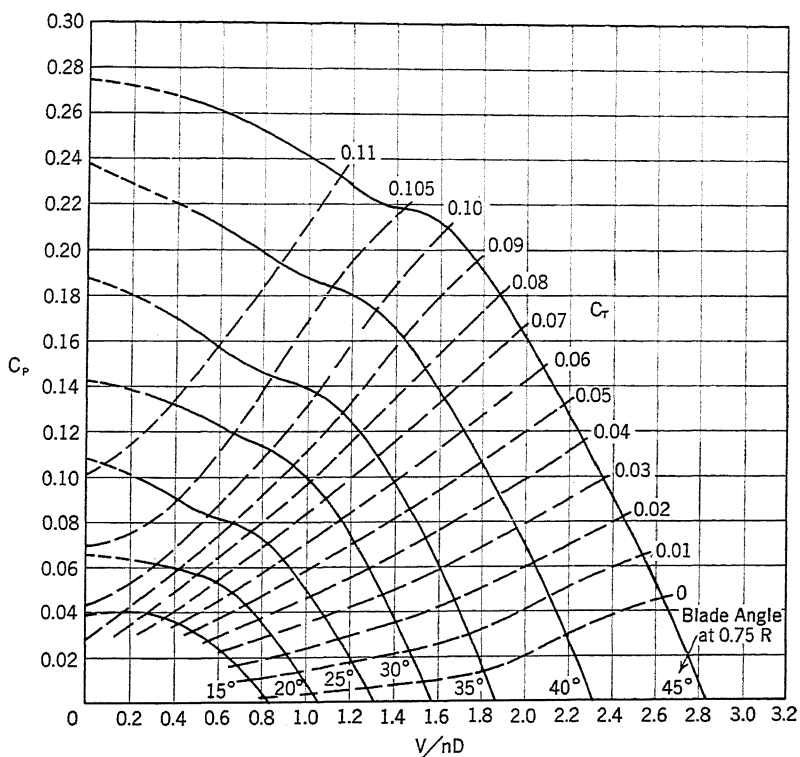


FIG. 5-6. Power coefficient curves for propeller 586S-9, Clark-Y section, two blades.
(NACA Tech. Rept. 640.)

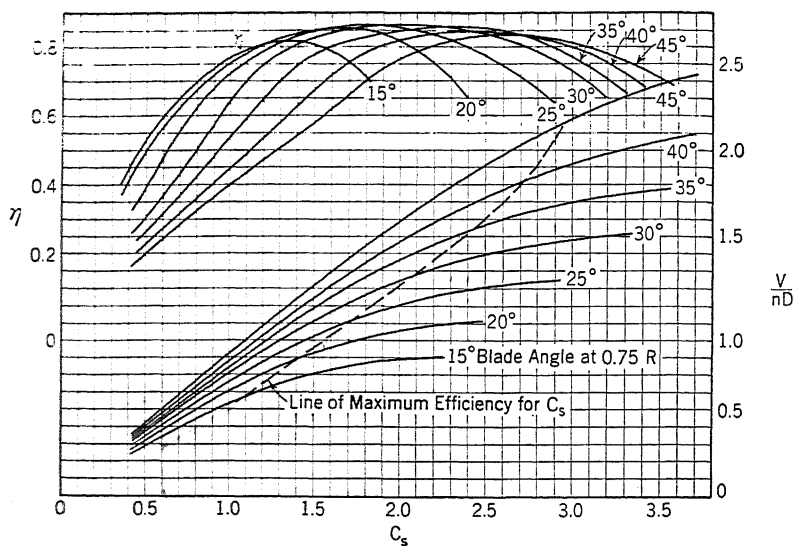


FIG. 5-7. Design chart for propeller 5868-9, Clark-Y section, three blades.
(NACA Tech. Rept. 640.)

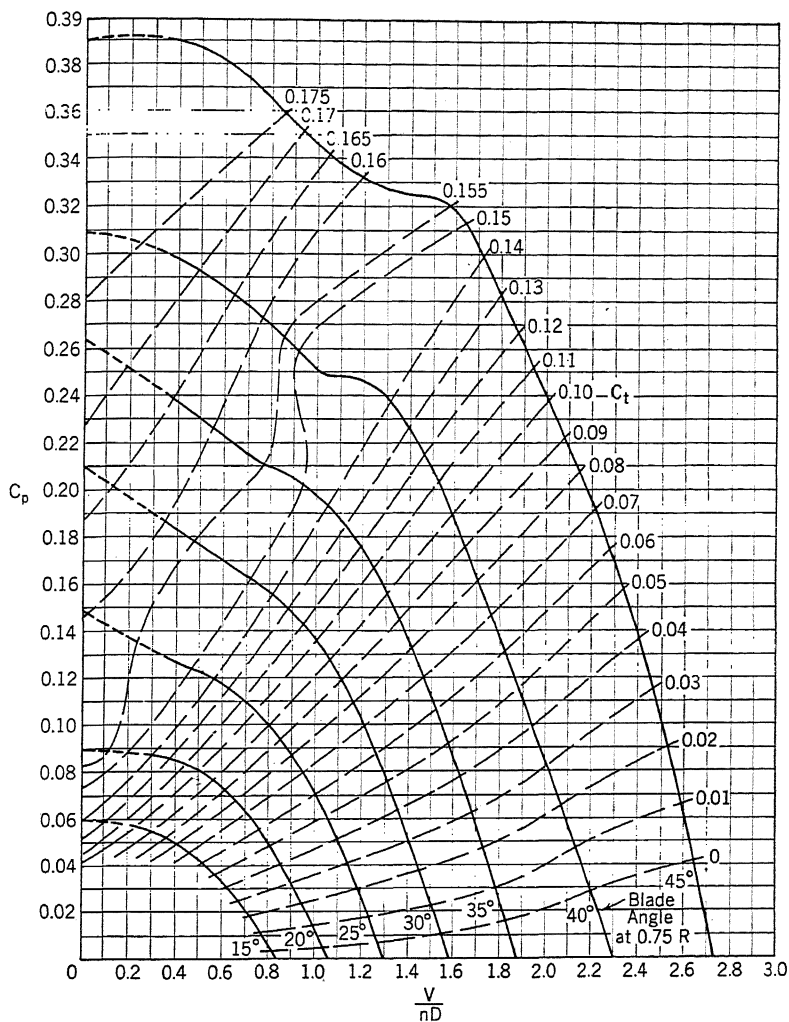


FIG. 5-8. Power coefficient curves for propeller 5868-9, Clark-Y section, three blades. (NACA Tech. Rept. 640.)

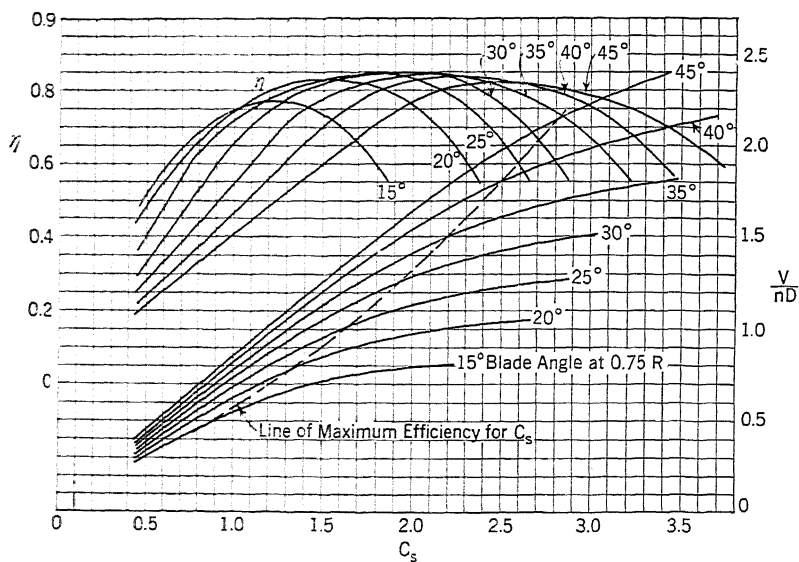


FIG. 5-9. Design chart for propeller 5868-9, Clark-Y section, four blades.
(NACA Tech. Rept. 640.)

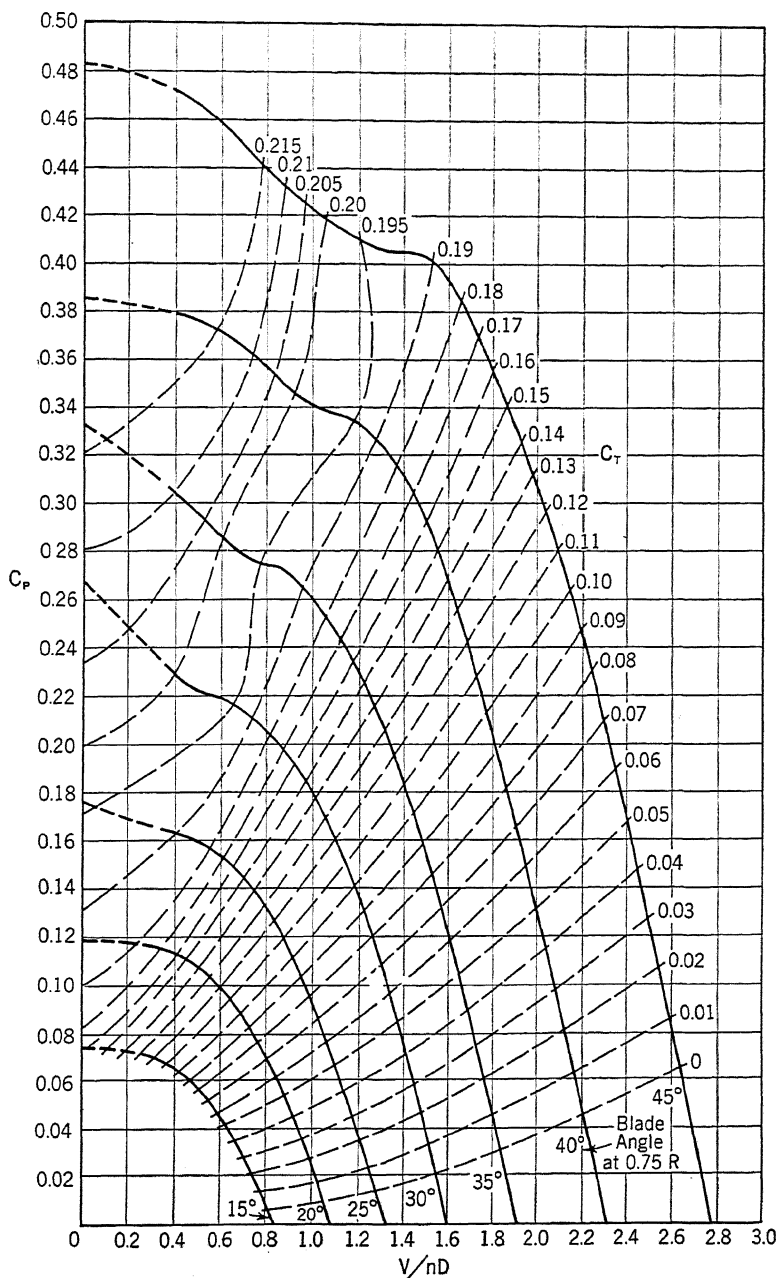


FIG. 5-10. Power coefficient curves for propeller 5868-9, Clark-Y section, four blades. (NACA Tech. Rept. 640.)

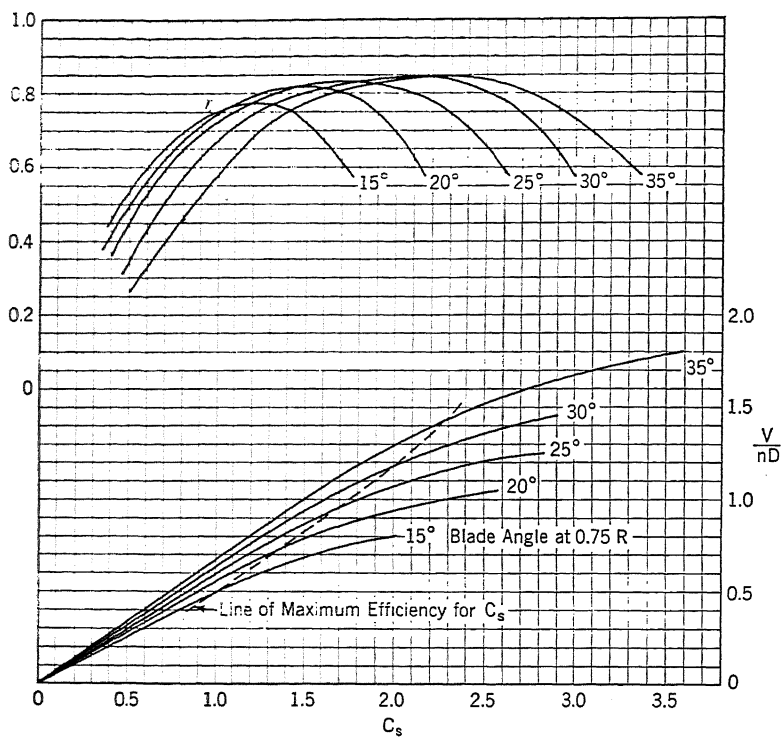


FIG. 5-11. Design chart for propeller 5868-R6, RAF-6 section, two blades. (NACA Tech. Rept. 640.)

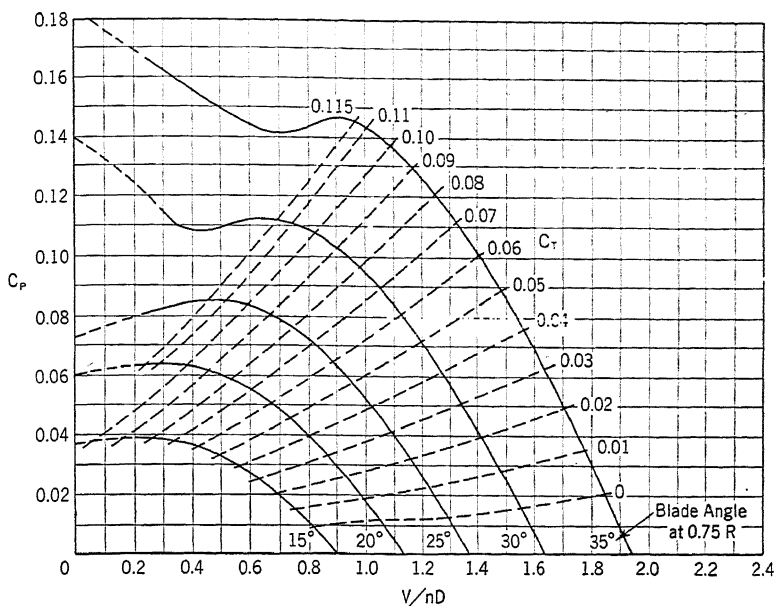


FIG. 5-12. Power coefficient curves for propeller 5868-R6, RAF-6 section, two blades. (NACA Tech. Rept. 640.)

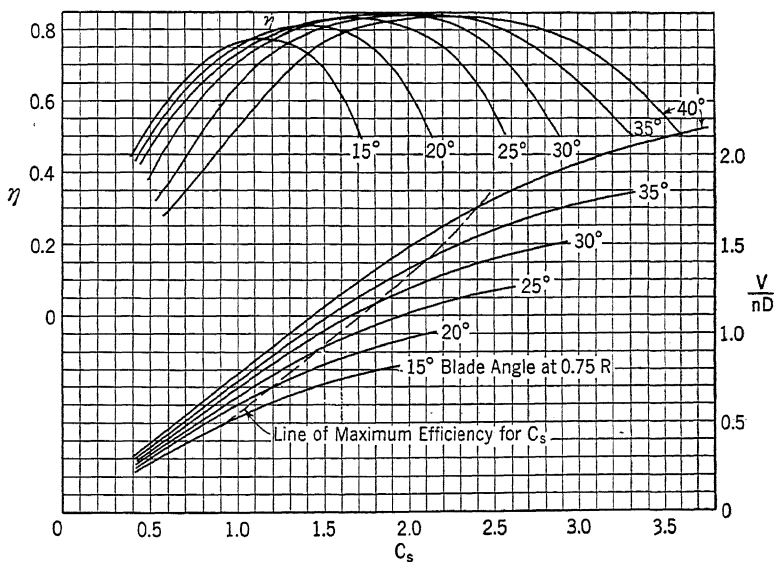


FIG. 5-13. Design chart for propeller 5868-R6, RAF-6 section, three blades. (NACA Tech. Rept. 640.)

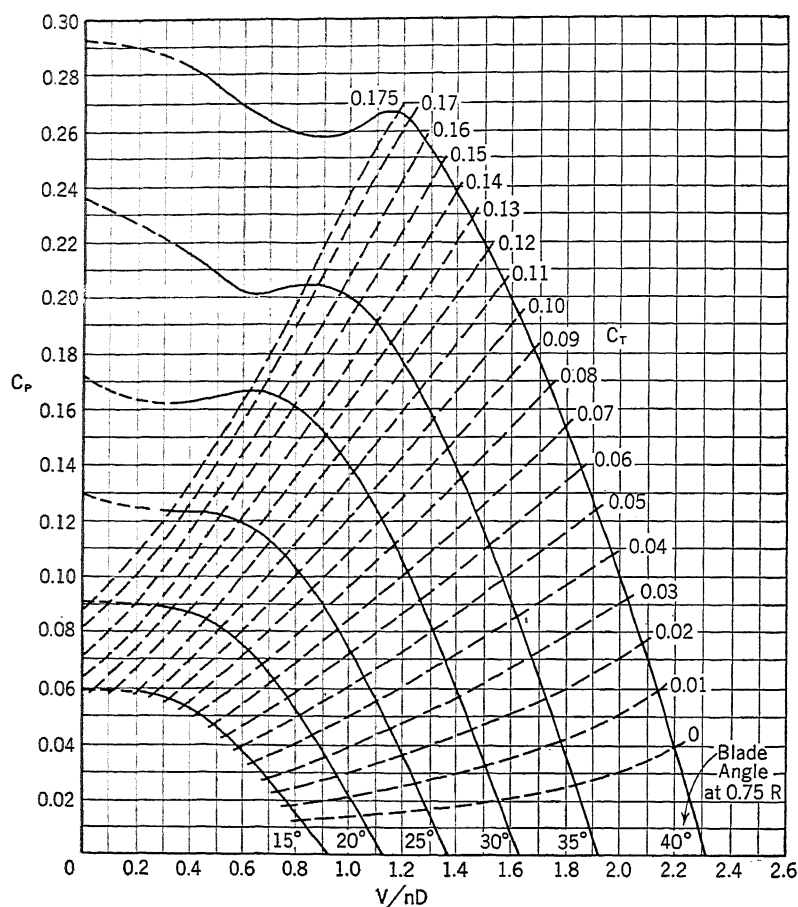


FIG. 5-14. Power coefficient curves for propeller 5868-R6, RAF-6 section, three blades. (NACA Tech. Rept. 640.)

PROBLEMS

1. Calculate and plot the thrust and propeller blade angle variation during sea-level takeoff (0–100 mph) on the Douglas DC-3 airplane equipped with Wright Cyclone GR-1820G-102 engines rated 1100 bhp at 2350 rpm (16 : 11) and three-way, constant-speed propellers of Clark-Y section and 11 ft 6 in. diameter. Assume that test data of Figs. 2·7 and 2·8 apply.

2. Calculate and plot the sea-level power available and propeller blade angle variation for the airplane, engine, and propeller of problem 1, with the engine operating at its normal rating of 900 bhp at 2200 rpm (16 : 11). Use a velocity range of 60 to 220 mph.

3. Repeat problem 2 for the critical altitude of the engine, 6000 ft.

4. Select a propeller diameter for the airplane of problem 1 for maximum efficiency at a cruising velocity of 165 mph at sea level with an engine output of 900 bhp at 2200 rpm (16 : 11), using the data of Figs. 2·7 and 2·8. Assume that the fuselage tip clearance limits the diameter of the propeller to 11 ft 6 in. Check for compressibility losses, and give the corrected chart efficiency.

5. Calculate and plot the sea-level power available for a Cessna airplane equipped with a Warner Super Scarab engine rated 145 bhp at 2050 rpm. Propeller installation is a Curtiss single-piece design of Clark-Y section selected for maximum efficiency at rated power at 135 mph at sea level. Assume test data of Figs. 5·5 and 5·6 apply. Use a velocity range of 40 to 150 mph.

6. A constant-speed propeller is to be installed in an airplane and engine with the following characteristics:

$V_{\max} = 300$ mph at 12,000 ft.

Pratt & Whitney Twin Wasp SC-G engine rated 900 bhp at 2550 rpm.

Engine critical altitude 12,000 ft.

Engine gear ratio available 2 : 1, 3 : 2, 16 : 9.

Assuming that the propeller tip ground clearance limits the diameter to 11 ft 0 in. and the only blade available is 10 ft 10 in. diameter, select the proper engine gear ratio to favor maximum efficiency at V_{\max} , including compressibility losses. Assume the installation is identical with that given in Figs. 2·7 and 2·8.

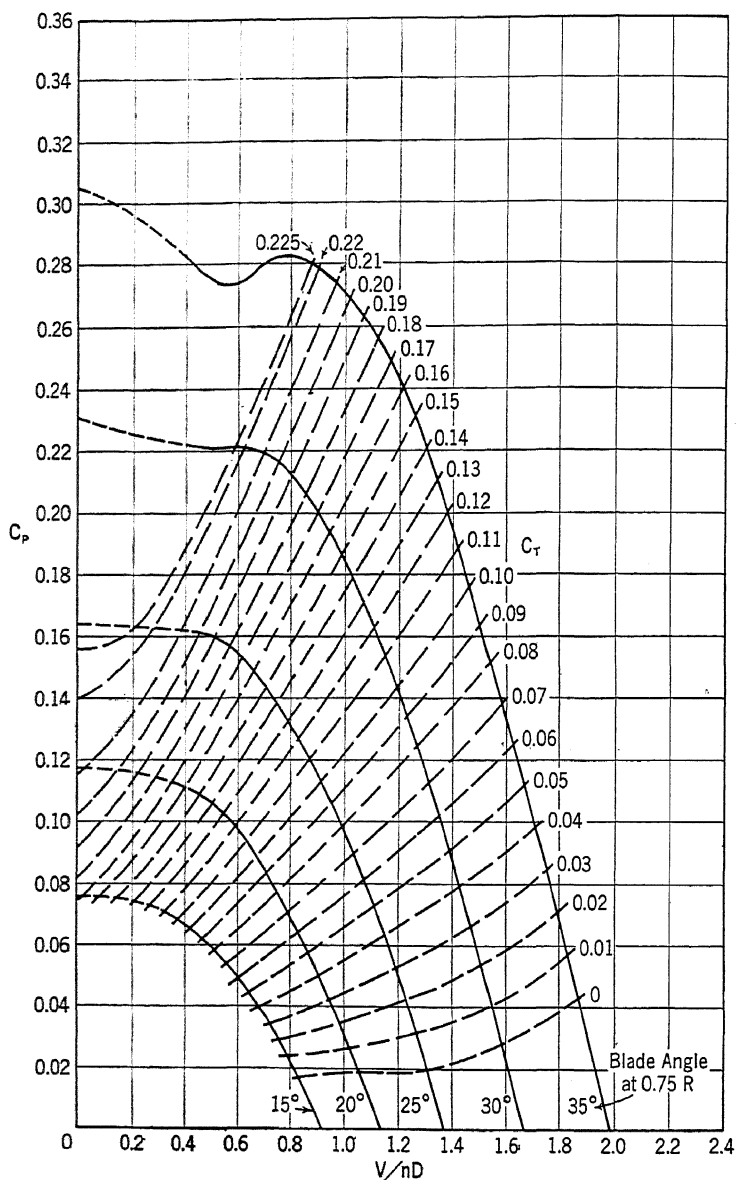


FIG. 5-16. Power coefficient curves for propeller 5868-R6, RAF-6 section, four blades. (NACA Tech. Rept. 640.)

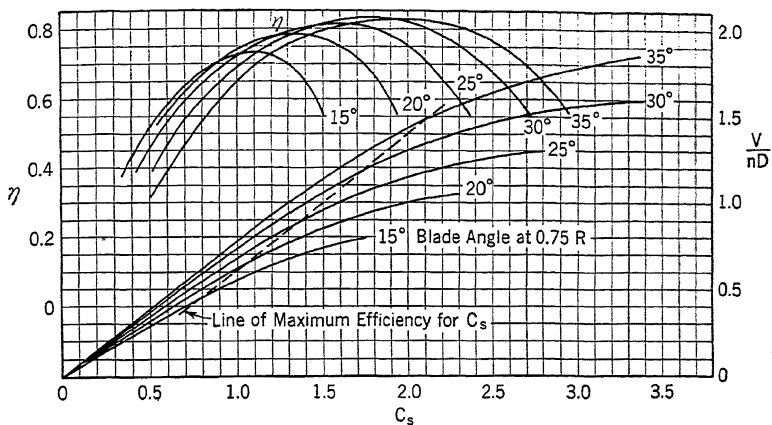


FIG. 5-17. Design chart for propeller 37-3647, RAF-6 section, two blades. (NACA Tech. Rept. 640.)

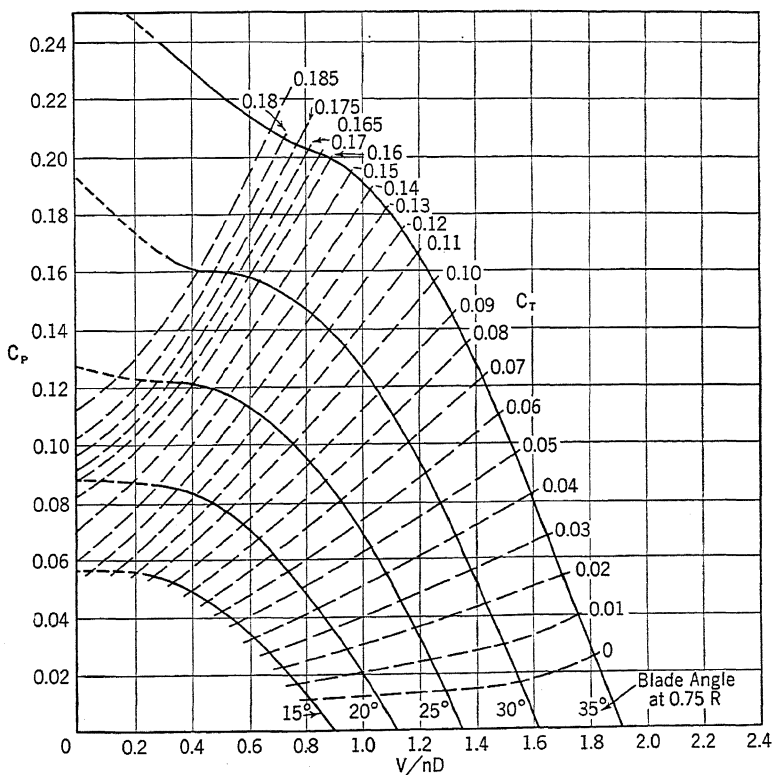


FIG. 5-18. Power coefficient curves for propeller 37-3647, RAF-6 section, two blades. (NACA Tech. Rept. 640.)

PROBLEMS

1. Calculate and plot the thrust and propeller blade angle variation during sea-level takeoff (0–100 mph) on the Douglas DC-3 airplane equipped with Wright Cyclone GR-1820G-102 engines rated 1100 bhp at 2350 rpm (16 : 11) and three-way, constant-speed propellers of Clark-Y section and 11 ft 6 in. diameter. Assume that test data of Figs. 2·7 and 2·8 apply.

2. Calculate and plot the sea-level power available and propeller blade angle variation for the airplane, engine, and propeller of problem 1, with the engine operating at its normal rating of 900 bhp at 2200 rpm (16 : 11). Use a velocity range of 60 to 220 mph.

3. Repeat problem 2 for the critical altitude of the engine, 6000 ft.

4. Select a propeller diameter for the airplane of problem 1 for maximum efficiency at a cruising velocity of 165 mph at sea level with an engine output of 900 bhp at 2200 rpm (16 : 11), using the data of Figs. 2·7 and 2·8. Assume that the fuselage tip clearance limits the diameter of the propeller to 11 ft 6 in. Check for compressibility losses, and give the corrected chart efficiency.

5. Calculate and plot the sea-level power available for a Cessna airplane equipped with a Warner Super Scarab engine rated 145 bhp at 2050 rpm. Propeller installation is a Curtiss single-piece design of Clark-Y section selected for maximum efficiency at rated power at 135 mph at sea level. Assume test data of Figs. 5·5 and 5·6 apply. Use a velocity range of 40 to 150 mph.

6. A constant-speed propeller is to be installed in an airplane and engine with the following characteristics:

$V_{\max} = 300$ mph at 12,000 ft.

Pratt & Whitney Twin Wasp SC-G engine rated 900 bhp at 2550 rpm.

Engine critical altitude 12,000 ft.

Engine gear ratio available 2 : 1, 3 : 2, 16 : 9.

Assuming that the propeller tip ground clearance limits the diameter to 11 ft 0 in. and the only blade available is 10 ft 10 in. diameter, select the proper engine gear ratio to favor maximum efficiency at V_{\max} , including compressibility losses. Assume the installation is identical with that given in Figs. 2·7 and 2·8.

Definitions

(Reference, *NACA Tech. Rept. 474*)

Angle

Blade angle. The acute angle between the chord of a section of a propeller, or of a rotary wing system, and a plane perpendicular to the axis of rotation.

Coning angle. The average angle between the span axis of a blade or wing of a rotary wing system and a plane perpendicular to the axis of rotation.

Effective helix angle. The angle of the helix described by a particular point on a propeller blade as the airplane moves forward through air otherwise undisturbed.

Area, projected propeller. Projected blade area times the number of blades.

Area, projected propeller-blade. The projection of the propeller-blade area on a plane perpendicular to the axis of rotation of the propeller.

Area, propeller. Blade area times the number of blades.

Area, propeller-blade. The developed area of the blade face exclusive of the boss and the root, i.e., exclusive of that portion the thrust of which is negligible in comparison with the total thrust of the blade.

Area, propeller-disk. The total area swept by a propeller, i.e., the area of a circle having the same diameter as the propeller.

Aspect ratio, propeller-blade. The ratio of the tip radius to the maximum blade width. (Obsolete.)

Blade back. The side of a propeller blade that corresponds to the upper surface of an airfoil.

Blade element. A portion of a propeller blade contained between the surfaces of two cylinders coaxial with the propeller cutting the propeller blades.

Blade face. The surface of a propeller blade that corresponds to the lower surface of an airfoil. Sometimes called thrust face or driving face.

Blade section. A cross section of a propeller blade made at any point by a plane parallel to the axis of rotation of the propeller and tangent at the centroid of the section to an arc drawn with the axis of rotation as its center.

Blade-width ratio. The ratio of the chord of a propeller blade section to the diameter of the propeller.

Mean blade-width ratio. The ratio of the mean blade width to the diameter of the propeller.

Dynamometer, hub. A device built into a propeller hub for measuring the engine thrust and/or torque.

Inflow. The flow of air into a propeller.

Leading edge. The foremost edge of an airfoil or propeller blade.

Nacelle. An enclosed shelter for personnel or for a powerplant. A nacelle is usually shorter than a fuselage and does not carry the tail unit.

Pitch of a propeller

Effective pitch. The distance an aircraft advances along its flight path for one revolution of the propeller.

Geometrical pitch. The distance an element of a propeller would advance in one revolution if it were moving along a helix having an angle equal to its blade angle.

Zero-thrust pitch. The distance a propeller would have to advance in one revolution to give no thrust. Also called experimental mean pitch.

Pitch ratio (propeller). The ratio of the pitch to the diameter.

Propeller. Any device for propelling a craft through a fluid, such as water or air; especially a device having blades which, when mounted on a power-driven shaft, produce a thrust by their action on the fluid.

Propeller rake. The mean angle which the line joining the centroids of the sections of a propeller blade makes with a plane perpendicular to the axis.

Propeller root. That part of the propeller blade near the hub.

Propeller thrust. The component of the total air force on the propeller which is parallel to the direction of advance.

Propeller thrust, effective. The net driving force developed by a propeller when mounted on an aircraft, i.e., the actual thrust exerted by the propeller, as mounted on an airplane, minus any increase in the resistance of the airplane due to the action of the propeller.

Propeller thrust, static. The thrust development by a propeller when rotating without translation.

Propeller tipping. A protective covering of the blade of a propeller near the tip.

Propulsive efficiency. The ratio of the product of the effective thrust and flight speed to the actual power input into the propeller as mounted on the airplane.

Slip. The difference between the geometrical pitch and the effective pitch of a propeller. Slip may be expressed as a percentage of the mean geometrical pitch, or as a linear dimension.

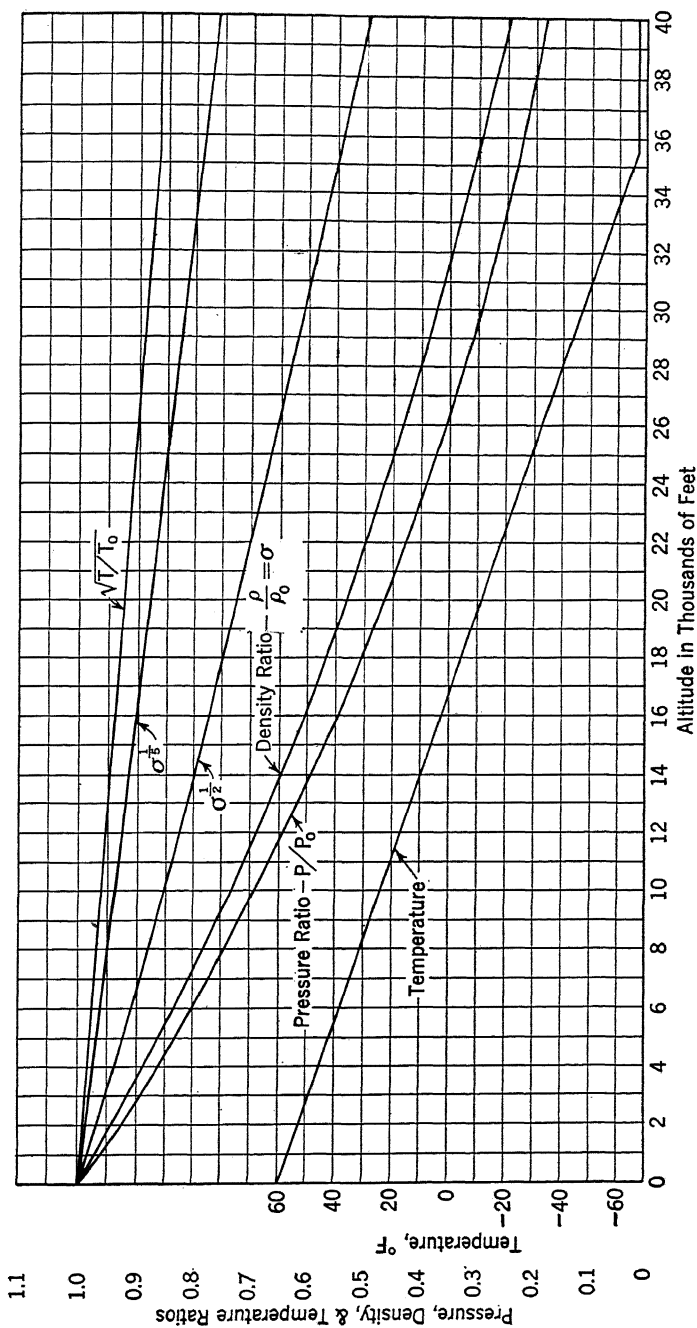
Slip function. The ratio of the speed of advance through the undisturbed air to the product of the propeller diameter and the number of revolutions per unit time, i.e., V/nD .

Slipstream. The current of air driven astern by a propeller.

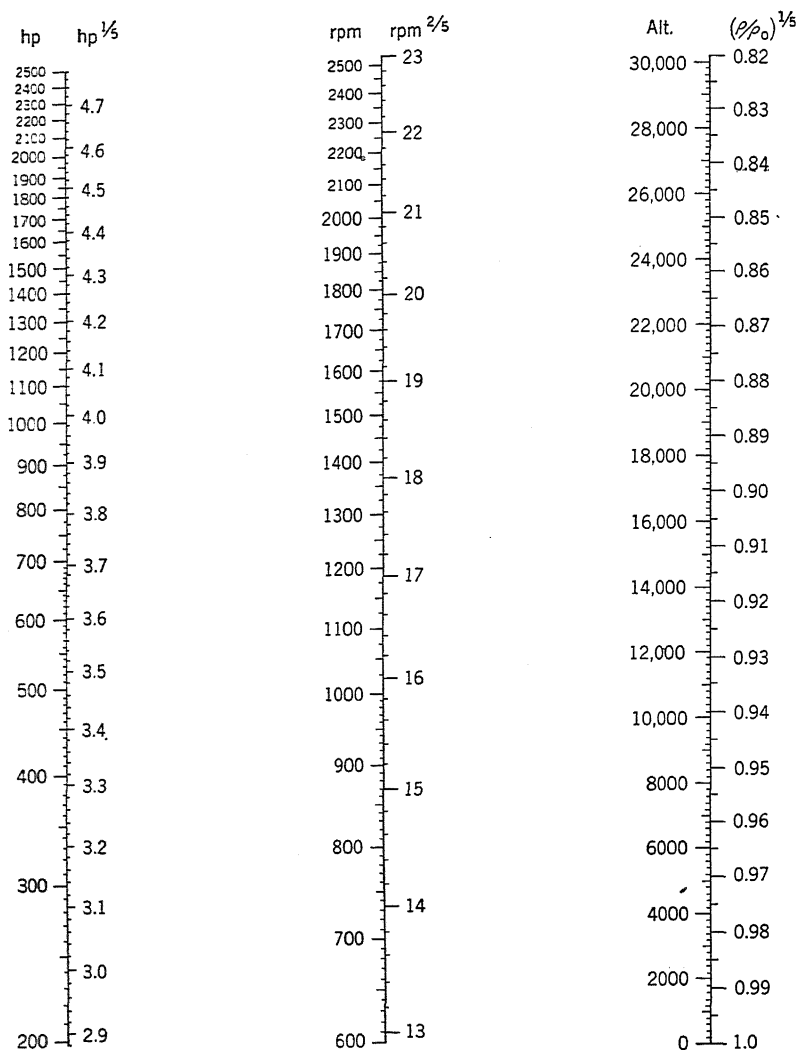
Spinner. A fairing of approximately conical or paraboloidal shape, which is fitted coaxially with the propeller hub and revolves with the propeller.

Tip radius (or propeller radius). The distance of the outermost point of a propeller blade from the axis of rotation.

Trailing edge. The rearmost edge of an airfoil or of a propeller blade.



Variation of density, pressure, and temperature of standard atmosphere with altitude. (NACA Tech. Rept. 218.)



$$C_s = \frac{0.638 \text{ (mph)} (\rho/\rho_0)^{1/5}}{(\text{bhp})^{1/5} (\text{rpm})^{2/5}}$$

Speed-power coefficient chart.

INDEX

A

Activity factor, 34
Aeroproducts Division, 78
Airfoil sections, blade, 46
Airfoil test data, 9
Airplane performance, propeller effect on, 97
Altitude effect on propeller, 33, 104
Aluminum-alloy propellers, 38
Area, blade section, 49
Assumptions, blade bending, 58
Axis, neutral, 57

B

Balance, blade, 41
 hub and blade assembly, 82
Bearing friction torque, 92, 93
Bending stress, 52
Blade angle range, controllable-pitch, 97
Blade counterweight action, 61
Blade element efficiency, 13
Blade element theory, 9
Blade form curves, 46
Blade number, 43
Blade planform, 44
Blade section, 46
Blade tilt, 59
Blade torque, aerodynamic, 48, 60
 centrifugal, 60
Blade width, 43
Body interference, 29
Brake state, 22

C

Center of gravity, blade section, 49
Clark-Y airfoil, 46
Coefficient, airfoil drag, 7
 airfoil lift, 7
 power, 24
 speed-power, 27
 thrust, 23
 torque, 23
 torque-speed, 30

Compressibility effect, 30
Correction of test data, 33
Counterweight, blade, 61
Cuff, blade, 45
Curtiss Propeller Division, 79

D

Deflection, blade, 54
 torsional, 59
De-icer, 94
Design chart, 27, 108
Disk loading, 43

E

Efficiency, apparent, 29
 ideal, 6
 net, 29
 propulsive, 28
 simple blade element, 13
Engine, supercharged, effect of, 104
 requirements of, 44
Engine gear reduction, 107
Everel propeller, 89

F

Fan state, 21
Fatigue failures, 71
Flight tests, 20
Force, centrifugal, 50
Frequencies, natural, 67

G

Gear reduction, engine, 107
Goodman diagram, 73
Governor, Aeroproducts, 79
 Curtiss, 79
 Hamilton Standard, 82
Gyration, blade radius of, 66
Gyroscopic loads, 65

H

Hamilton Standard Division, 82
Hub, adjustable-pitch, 1, 78
 controllable-pitch, 4, 78

- Hub, controllable-pitch, Aeroproducts, 78
 - Curtiss, 79
 - European models, 90
 - Hamilton Standard, 82
 - fixed-pitch, 77
 - general design considerations of, 90
 - stress analysis of, 92
 - Hub accessories, 94
- I
- Inertia, blade section moments of, 49
 - Interference, body, 29
- L
- Loads, critical operating, 49
 - gyroscopic, 65
 - main steady, 48
 - Lycoming-Smith propeller, 89
- M
- Magnesium propellers, 40
 - Materials, blade construction, 36
 - Micarta propellers, 41
 - Moment, centrifugal restoring, 53, 56
 - Moment, thrust bending, 52
 - Momentum theory, 3
- O
- One-piece forged propellers, 38
 - Oscillograph record, 71
- P
- Performance analysis, fixed-pitch, 100
 - two-position, 102
 - constant-speed, 103
 - Performance curves, propeller, 20
 - Pickup, blade vibration stress, 69
 - Pitch, adjustable, 1
 - controllable, 1
 - effective, 3
 - fixed, 1
 - geometric, 3
 - Pitch control, automatic, 89
 - Pitch change, rate of, 91
 - Pitch distribution, 42
 - uniform geometric, 43
 - Power available, fixed-pitch, 100
 - two-position, 102
 - constant-speed, 103
 - Power coefficient, 24
 - Power coefficient curves, 26, 108
 - Power required, controllable-pitch hub, 92
 - Propeller state, 22
- R
- RAF-6 airfoil, 46
 - Rotation, dual, 90
 - RPM variation, fixed-pitch, 101
 - two-position, 102
 - constant-speed, 103
- S
- SAE hub standards, 93
 - Safety, margin of, 65
 - Selection of propeller, 27, 100
 - Sensitivity of speed control, 91
 - Solidity factor, 43
 - Sound, variation of velocity of, 33
 - Speed-power coefficient, 27
 - Spinner, 29, 95
 - Standards, SAE hub, 93
 - Steel propellers, 39
 - Strength tests, 74
 - Stress, allowable, 65, 74
 - bending, 52
 - centrifugal, 51
 - combined, 58
 - steady, 48, 65
 - vibratory, 67, 74
 - Stress analysis, blade, 47
 - hub, 92
 - Stress-measuring equipment, vibratory, 69
 - Stress variation with rpm, 64
- T
- Takeoff thrust, 105
 - Terminology, 1
 - Test data, application of, 33
 - Tests, aerodynamic, 18
 - flight, 20
 - strength, 74
 - wind tunnel, 18
 - Thickness ratio of blade section, 45
 - Thrust, effective, 28
 - takeoff, fixed-pitch, 106
 - two-position, 106
 - constant-speed, 106
 - variation of, 30, 97